



UNIVERSITY
OF TURKU

A large, stylized sunburst or fan-like graphic in a lighter shade of teal, positioned on the left side of the cover. It consists of a central vertical stem with multiple curved, radiating segments that resemble the petals of a flower or the rays of a sun.

MODIFYING UPCONVERTING NANOPARTICLES WITH POLYELECTROLYTE MULTILAYERS

Emilia Palo



UNIVERSITY
OF TURKU

MODIFYING UPCONVERTING NANOPARTICLES WITH POLYELECTROLYTE MULTILAYERS

Emilia Palo

University of Turku

Faculty of Science and Engineering
Department of Chemistry
Laboratory of Materials Chemistry and Chemical Analysis
University of Turku Graduate School
Doctoral Programme in Physical and Chemical Sciences

Supervised by

Adjunct Professor Mika Lastusaari, PhD
Department of Chemistry
Laboratory of Materials Chemistry and
Chemical Analysis
University of Turku
Turku, Finland

Adjunct Professor Mikko Salomäki, PhD
Department of Chemistry
Laboratory of Materials Chemistry and
Chemical Analysis
University of Turku
Turku, Finland

Reviewed by

Maria Sammalkorpi, PhD
Department of Chemistry and
Materials Science
Aalto University
Espoo, Finland

Thomas Hirsch, PhD
Institut für Analytische Chemie,
Chemo- und Biosensorik
Universität Regensburg
Regensburg, Germany

Opponent

Professor Darja Lisjak, PhD
Department for Materials Synthesis
Jožef Stefan Institute
Ljubljana, Slovenia

The originality of this thesis has been checked in accordance with the University of Turku quality assurance system using the Turnitin Originality Check service.

ISBN 978-951-29-7572-3 (PRINT)
ISBN 978-951-29-7573-0 (PDF)
ISSN 0082-7002 (Print)
ISSN 2343-3175 (Online)
Grano Oy - Turku, Finland 2019

“It's vital to remember who you really are. It's very important. It isn't a good idea to rely on other people or things to do it for you, you see. They always get it wrong.”

- *Terry Pratchett, Sourcery*

CONTENTS

Contents	4
List of original publications	6
Abbreviations	7
Abstract	9
Tiivistelmä	10
1 Introduction	11
2 Review of the literature	13
2.1 Upconverting nanoparticles	13
2.1.1 Upconversion mechanisms.....	13
2.1.2 Composition of host materials.....	15
2.2 Luminescence properties of upconverting nanoparticles	19
2.2.1 Enhancement of upconversion luminescence.....	22
2.3 Applications for upconverting nanoparticles	24
2.3.1 Reporters in assays.....	25
2.3.2 Sensors.....	27
2.3.3 Bioimaging.....	30
2.4 Surface properties of upconverting nanoparticles	31
2.4.1 Surface modifications.....	32
2.4.2 Bioconjugation.....	36
3 Aims of the study	37
4 Summary of materials and methods	38
4.1 Preparation of UCNPs	38
4.1.1 Surface modifications of UCNPs.....	39
4.2 Characterization	41
4.2.1 Particle structure, size, morphology and uniformity.....	41
4.2.2 Surface properties and elemental composition.....	42
4.2.3 Luminescence properties.....	42
4.2.4 Disintegration of the UCNPs.....	43
5 Summary of results and discussion	45
5.1 Structure and uniformity of UCNPs	45

Contents

5.1.1	Crystal structure and phase purity	45
5.1.2	Particle size and morphology	46
5.2	Surface modification of UCNPs.....	47
5.2.1	Removal of OA capping ligands	48
5.2.2	Layer-by-layer assembly on UCNP surface	48
5.3	Upconversion luminescence properties of UCNPs.....	54
5.3.1	As prepared UCNPs	55
5.3.2	Surface modified UCNPs	56
5.4	Disintegration studies of UCNPs	60
5.4.1	Optical detection.....	60
5.4.2	Fluoride ion selective detection.....	62
6	Conclusions and future prospects	65
	Acknowledgements.....	67
	References	70
	Original publications.....	87

LIST OF ORIGINAL PUBLICATIONS

The experimental part of this thesis is based on the following original publications and supplementary unpublished results. The original publications are referred to in the text by their Roman numerals (I–IV).

- I** Emilia Palo, Minnea Tuomisto, Iko Hyppänen, Hendrik C. Swart, Jorma Hölsä, Tero Soukka and Mika Lastusaari, Highly uniform up-converting nanoparticles: Why you should control your synthesis even more, *J. Lumin.* **185** (2017) 125–131.
- II** Emilia Palo, Mikko Salomäki, and Mika Lastusaari, Surface modification of upconverting nanoparticles by layer-by-layer assembled polyelectrolytes and metal ions, *J Colloid Interface Sci.* **508** (2017) 137–144.
- III** Emilia Palo, Satu Lahtinen, Henna Päckilä, Mikko Salomäki, Tero Soukka, and Mika Lastusaari, The effect of the polyelectrolyte length on the layer-by-layer assembled surface structures and properties of NaYF₄:Yb³⁺,Er³⁺ upconverting nanoparticles, *Langmuir* **34** (2018) 7759–7766.
- IV** Emilia Palo, Mikko Salomäki, and Mika Lastusaari, Restraining fluoride loss of NaYF₄:Yb³⁺,Er³⁺ upconverting nanoparticles in aqueous environments using crosslinked poly(acrylic acid)/polyallylamine hydrochloride multilayers, *J Colloid Interface Sci.* **538** (2019) 320–326.

The original publications have been reproduced with the permission of the copyright holders; **I, II, IV** – Elsevier and **III** – American Chemical Society.

ABBREVIATIONS

AFM	atomic force microscopy
AIBN	2,2'-azobisisobutyronitrile
AMPS	1-acrylamido-2-methylpropane sulphonic acid
ANDBS	4-((4-(2-aminoethylamino)naphtalen-1-yl)diazenyl)benzenesulfonic acid
BET	back energy transfer
BHMT	bis(hexamethylene)triamine
BSA	bovine serum albumin
BsAb	bispesific antibody
BTB	bromothymol blue
CCD	charge coupled device
CET	co-operative energy transfer
CT	X-ray computed tomography
DSC	differential scanning calorimetry
ESA	excited state absorption
EDC	1-ethyl-3-(3-dimethylaminopropyl)-carbodiimide
EDTA	ethylenediaminetetraacetic acid
EMU	energy migration upconversion
ETU	energy transfer upconversion
FT-IR	Fourier transform infrared
FRET	Förster –type resonance energy transfer
GSA	ground state absorption
GSH	gulthatione
IgG	immunoglobulin G
IR	infrared
LbL	layer-by-layer
LFA	lateral flow assay
LIR	luminescence intensity ratio
LRET	luminescence resonance energy transfer
MAEP	monoacryloxyethyl phosphate
MRI	magnetic resonance imaging
MWCO	molecular weight cut-off
NIR	near infrared
OA	oleic acid
ODE	1-octadecene
OEGA	oligo(ethylene glycol) methyl ether acrylate
PAA	poly(acrylic acid)
PAH	poly(allylamine hydrochloride)
PEG	polyethylene glycol
PET	positron emission tomography
PMAO	poly(maleic anhydride- <i>alt</i> -1-octadecene)
PMT	photomultiplier tube

Abbreviations

PP	polyphosphate
PSS	poly(sodium-4-styrenesulfonate)
RhB	rhodamine B
RET	resonance energy transfer
SPECT	single-photon emission computed topography
Sulfo-NHS	N-hydroxysulfosuccinimide
TEM	transmission electron microscope
TEOS	tetraethyl ortosilicate
TGA	thermogravimetric analysis
TPPS	tetraphenylporphyrin tetrasulfonic acid hydrate
TSPP	meso-tetra(4-sulfonatophenyl)porphine dihydrochlorid
UC	upconversion
UCL	upconversion luminescence
UCNP	upconverting nanoparticle
XRD	X-ray diffraction / X-ray powder diffraction
XRF	X-ray fluorescence spectroscopy

ABSTRACT

Upconversion luminescence where visible light can be obtained through low energy near-infrared radiation is an interesting research topic especially within the scope of biomedical applications using optical detection. The benefits of using upconverting nanoparticles are low background due to low autofluorescence and narrow bandwidth of lanthanide luminescence. However, their use is still being hampered by the challenges arising from the water based biological matrices. The research for creating hydrophilic nanoparticle surfaces for aqueous environment and simultaneously preventing the quenching of the upconversion luminescence is still ongoing.

The aim of the study conducted in this thesis was to produce uniform and highly luminescent upconverting $\text{NaYF}_4:\text{Yb}^{3+},\text{Er}^{3+}$ nanoparticles suitable for biomedical applications accounting for the challenges of water based matrices. To produce such nanoparticles a synthesis route was modified and selected parameters affecting the nanoparticle structure, size and uniformity were studied and their upconversion luminescence behaviors were measured.

To make the upconverting nanoparticles biocompatible, a layer-by-layer approach was chosen for the surface modification method as it has not been studied with upconversion nanoparticles in detail. Two types of bilayer structures in the surface modifications were used, one combining negative polyelectrolytes and positive metal ions and one where both components were polyelectrolytes that could be crosslinked to produce a more rigid bilayer structure. The layer deposition conditions affecting the bilayer structure formation such as polyelectrolyte length, polyelectrolyte concentration, and ionic concentration were studied. The formation of the coating by the layer-by-layer method was confirmed for both bilayer structures and their effect on the upconversion luminescence was studied. It was observed that with the selected coatings and the number of bilayers the obtained upconversion luminescence could be enhanced. The enhancement could be maintained even with five bilayers of coating using additional fluoride during the layer formation.

In addition, studies to observe the possible disintegration of the coated upconversion nanomaterials were conducted by both optical and solution concentration methods. It was found that in polyelectrolyte/metal ion coated nanoparticles prepared with selected conditions the emission was maintained in pure water for 24 hours. Crosslinking of the two polyelectrolyte coatings was successful in effectively hindering the fluoride loss from the core nanomaterial. This study demonstrates the usefulness of a widely modifiable layer-by-layer method in the surface modification of upconverting nanoparticles. It offers possibilities to create surface structures where the luminescence and the core particle can be shielded from the deleterious environmental effects while rendering the nanoparticles with functionality for further biomodifications.

TIIVISTELMÄ

Matalaenergisien lähi-infrapunasäteilyn pinoamisen kautta saatava näkyvä valo, eli käänteisviritteinen luminesenssi (upkonversio), on mielenkiintoinen tutkimuskohde optista luentaa käyttävien biolääketieteellisten sovellusten kannalta. Matala mittaustausta sekä lantanidien luminesenssille ominaiset kapeat emissioviivat ovat tällaisten nanokokoisten loisteaineiden suurimmat hyödyt. Paljon vettä sisältävä biologinen ympäristö aiheuttaa kuitenkin merkittäviä haasteita. Luminesenssin sammumisen sekä partikkelien hajoamisen estäminen ovat toistaiseksi ongelmia, joiden ratkaiseminen auttaisi materiaalien laajemmassa hyödyntämisessä.

Väitöskirjatyön tarkoituksena oli valmistaa muodoltaan yhtenäisiä ja hyvin loistavia käänteisviritteisiä $\text{NaYF}_4:\text{Yb}^{3+}, \text{Er}^{3+}$ nanopartikkeleita joita voitaisiin hyödyntää biolääketieteellisissä sovelluksissa niiden haasteet huomioiden. Partikkeleiden valmistamista varten muokattiin synteessimenetelmä, jonka valikoituja ominaisuuksia sekä niiden vaikutusta partikkelien rakenteeseen, kokoon ja yhdenmukaisuuteen sekä loisteominaisuuksiin tutkittiin.

Kerroskasvatusmenetelmä valittiin pintamuokkausmenetelmäksi koska sillä voitaisiin samaan aikaan tutkia loisteominaisuuksien säilyttämistä, partikkelin hajoamista sekä niiden muokkaamista vesiympäristöön sopivaksi. Menetelmä on myös verrattain vähän käytetty käänteisviritteisten loisteaineiden pintamuokkauksessa. Kerroksia kasvatettiin kahdella tavalla, joko käyttäen negatiivista polyelektrolyyttiä ja positiivista metalli-ioniä tai hyödyntäen polyelektrolyyttejä molempina komponentteina, jolloin niiden ketjut voitiin ristosita. Eri olosuhteita, kuten polyelektrolyytin pituutta ja pitoisuutta, ionikonsentraatiota sekä näiden vaikutusta kerrosten kasvuun tutkittiin. Molemmilla kerrostustavoilla saatiin kasvatettua haluttu pinta partikkelin pinnalle. Loisteominaisuuksia saatiin parannettua tiettyjä kerrostusolosuhteita käyttäen. Lisäämällä kerrostuksen aikana liuoksen fluoripitoisuutta ja tekemällä ristisidonta kahden polyelektrolyytin välille voitiin parannetut loisteominaisuudet säilyttää jopa viiden kaksoiskerroksen jälkeen.

Pinnoitettujen partikkelien hajoamista tutkittiin sekä luminesenssiin perustuvan että fluoriselektiivisen menetelmän avulla. Polyelektrolyytti/metalli-ioni – pinnoitus säilytti näytteen loisteen vedessä 24 ja fosfaattipuskurissa neljä tuntia. Fluorin irtoaminen partikkeleista voitiin tehokkaasti estää ristisitomalla kasvatettu polyelektrolyyttipinta. Tutkimus auttaa hyödyntämään laajasti muokattavaa kerroskasvatusmenetelmää ja tarjoaa aiempaa monipuolisempia mahdollisuuksia käänteisviritteisten loisteaineiden muokkaukseen. Menetelmän avulla voidaan vähentää ympäristöstä johtuvia ongelmia ja toisaalta tuoda partikkelin pinnalle funktionaalisia ryhmiä myöhempää käyttöä varten.

1 INTRODUCTION

The use of lanthanide based luminescence, where visible light is obtained by irradiating the material with ultraviolet radiation (i.e. downshifting luminescence), has over the years covered lighting, detectors, displays and biomedical research.^{1,2} The biomedical research adopted the use of lanthanide luminescence due to its long lived energy states and narrow emission lines which were beneficial in luminescent labels used in assays and imaging. To date various bioanalytical assays and detection methods are based on the optical detection of time resolved emission and the use of various specific lanthanide chelates as luminescent labels.

The conventional downshifting luminescence gained an interesting new counterpart in the 1960s when François Auzel discovered that visible emission could be obtained through near-infrared excitation.³ As the use of luminescent lanthanide chelates in biomedical research requires time resolved methods due to ultraviolet excitation which also affects the tissue used and biomolecules the use of non-interfering near-infrared radiation in producing visible light has gained much attention and research. The increasing research on producing the upconverting materials started in the late 1990s from the micrometer-sized particles which are less favorable in the use of biomedical research. However, as the synthesis research and knowledge has increased, the size of the produced upconverting materials has decreased first below 100 nm and already down to 10 nm nanomaterials which can be more applicable in the current biomedical research field aiming for more precise and smaller designs.^{4,5} The preferred size can vary with the biomolecules used as the large biomolecules are within 10-100 nm size (i.e. antibodies, viruses) but small molecules only a few nanometers.

While the small size is beneficial for the bioapplications it has its drawbacks when luminescence properties are concerned. The reduced size results in lowered upconversion luminescence emission intensity due to the increased surface-to-volume ratio of the nanoparticles. This is because the possible surface defects affect negatively the obtainable luminescence. An even greater influence on the upconversion luminescence comes from the water molecules. As water is a very important medium in biomedical research and most upconverting materials are hydrophobic, modifications have to be made on the upconversion particle surfaces to make them water dispersible. The modifications try to shield the nanoparticles from the negative effects of water molecules which both quench luminescence as well as disintegrate the nanoparticles.⁶⁻⁸ Also, surface modifications are crucial in biomedical applications because of the need for linking into target biomolecules. In addition, while the most used excitation radiation (980 nm) is transmitted completely by most of the biological matrices it is still absorbed by water. This means that the use of upconversion nanoparticles in biomedical imaging and *in vivo* studies is restricted because only low excitation powers can be used.

Several strategies in designing the upconverting nanoparticles from their very core to the outer surface have been studied for many applications. While there have been successful attempts in circumventing the problems of upconverting nanoparticles, there seems to be no thorough answer in solving all of the problems simultaneously. Surface modifications allowing good water dispersibility induce upconversion quenching through the vibrational states of the molecules. Very small and biocompatible nanoparticles typically show low upconversion luminescence intensity and bright upconversion nanoparticles are usually not water dispersible or have the desired particle size. In these aspects, the research is still ongoing and only time will tell if the methods to enhance these properties will remain in wider use of the research field.

2 REVIEW OF THE LITERATURE

2.1 Upconverting nanoparticles

When talking about upconverting nanoparticles (UCNPs in short) researchers usually refer to materials with nanosized (< 100 nm) particles able to convert low energy radiation (near infrared, NIR) into higher energy radiation such as visible light. The phenomenon was first described by François Auzel in the middle of the 1960s when he demonstrated that a sequential energy transfer resulting in visible emission was possible with lanthanide ion pairs ($\text{Yb}^{3+}\text{-Er}^{3+}$ and $\text{Yb}^{3+}\text{-Tm}^{3+}$).³ The majority of the upconversion materials up to date still rely on these first found lanthanide ion pairs and their interactions.

This thesis is focused on materials based on solid inorganic matrices where lanthanide ions are responsible for the energy transfer processes resulting in visible upconversion luminescence. In addition to these inorganic crystal structures with lanthanides also other hosts such as lanthanide coordination molecules can host upconversion luminescence. This is done via energy transfer either between lanthanide ions or molecular antennas but they are out of the scope of this thesis.⁹⁻¹¹

2.1.1 Upconversion mechanisms

The energy transfers within the upconversion processes using lanthanide ions are based on their long lived energy states which gives the energy transfer process the needed time to obtain the subsequential piling of absorbed excitation.^{3,12} The most common mechanisms to obtain upconversion luminescence are described in Figure 1 where two or more photons are absorbed and converted into one emitted photon of higher energy than the adsorbed ones. The simplest upconversion mechanism is the excited state absorption (ESA) which follows the ground state absorption (GSA) within a single activator ion such as erbium (Er^{3+}). However, the process is not very efficient, having for example a relative efficiency of *ca.* 10^{-5} in $\text{SrF}_2\text{:Er}^{3+}$.³ It needs suitable amount of activators in the structure; not too many to quench the upconversion luminescence due to cross-relaxation processes within similar ions and energy levels and not too few so that the probability of obtaining upconversion luminescence is decreased.

The most used energy transfer process in the upconversion mechanism is the energy transfer upconversion (ETU) which is common with sensitizer-activator pairs like ytterbium-erbium ($\text{Yb}^{3+}\text{-Er}^{3+}$) and ytterbium-thulium ($\text{Yb}^{3+}\text{-Tm}^{3+}$) (Figure 1.). It has a relative efficiency of 10^{-3} in e.g. $\text{YF}_3\text{:Yb}^{3+},\text{Er}^{3+}$ making it the most efficient of the processes.³ It involves a ground state absorption from the energy-transferring sensitizer ion (ytterbium) and the energy is then transferred to an energetically similar energy level of the activator (e.g. erbium). When the energy accepting level of the activator is reasonably long lived it can subsequently accept similar energy transfers

from another sensitizer ion resulting in a higher excited state which can then produce visible upconversion luminescence when relaxing.

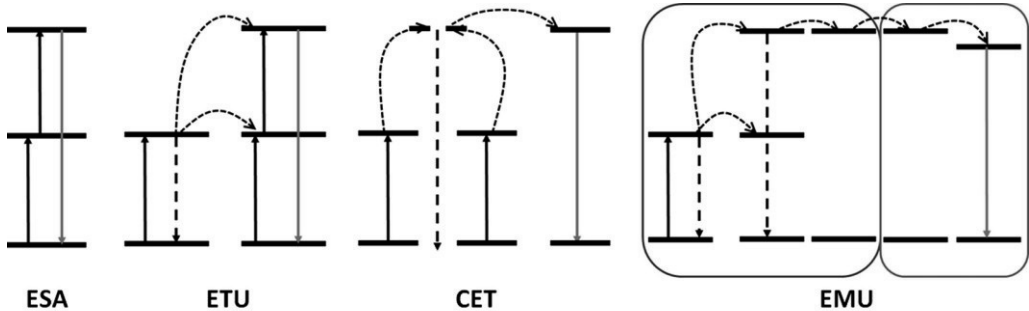


Figure 1. Simplified mechanisms of the different upconversion processes. ESA denotes energy state absorption, ETU energy transfer upconversion, CET co-operative energy transfer and EMU energy migration upconversion. Solid, dotted and dashed lines represent photon absorption, energy transfer processes and photon emission, respectively. (Modified from Dong et al.¹²)

Not as efficient as ETU but still applied energy transfer mechanism is the co-operative energy transfer (CET). Its relative efficiency is already lower (10^{-8} in YbPO_4) and the most distinguishable difference in comparison to ETU is that the two sensitizing ions are able to create a virtual intermediate energy level that does not exist in their energy structure but is able to transfer the gained energy into the real energy level of an acceptor ion. The CET mechanism can be observed with europium (Eu^{3+}) and terbium (Tb^{3+}) upconversion luminescence with Yb^{3+} as the sensitizer.^{13,14}

Energy migration upconversion luminescence (EMU) is the least efficient upconversion process of these four and its relative efficiency is not known. It is widely taken advantage of in various core-shell type upconversion materials.¹⁵⁻¹⁷ The EMU process involves sensitizers that can absorb the excitation, ions with suitable energy levels to allow energy migration while not enhancing cross-relaxation within the structure, and finally an activator with the emitting energy levels. While the process allows the possibility to create detailed energy transfer structures using ions with desired energy levels it is also heavily influenced by possible cross-relaxation processes between ions.

Cross-relaxation processes are energy transfer processes that can affect the emission of the upconversion luminescence.^{3,18} The energy transfer can occur when the energy level difference between adjacent ions is close enough. This allows the energy transfer from one ion to another thus populating a new energy level. The cross-relaxations can happen within similar or different ions. Depending on the ions and the cross-relaxation processes the process can weaken the overall upconversion luminescence intensity if the populated energy state can be easily depopulated via non-radiative transfers. If the

populated energy level is an emitting energy level the cross-relaxation processes can also enhance a specific emission of an emitting ion resulting in varying color ratios (i.e. red-to-green ratio in $\text{NaYF}_4:\text{Yb}^{3+},\text{Er}^{3+}$).¹⁸

2.1.2 Composition of host materials

To obtain efficient upconversion luminescence the choice of host material is crucial. The energy transfer processes within the lanthanide ions go through long lived intermediate energy levels which makes them greatly influenced by multiphonon relaxations in the host lattice. Currently, the most widely used host material in many upconversion nanomaterials is NaYF_4 . One reason for the wide use is that NaYF_4 has two possible structures of which the hexagonal structure ($\beta\text{-NaYF}_4$) is superior in upconversion luminescence intensity in comparison to the cubic one ($\alpha\text{-NaYF}_4$) and other upconversion host materials.¹⁹ The superiority of the NaYF_4 material is expected to rise from the low phonon frequency of the fluoride host (ca. 350 cm^{-1}).²⁰ In addition to the low phonon frequency the distance between lanthanide ions is ca. 0.4 \AA shorter in the hexagonal structure than in cubic one.²¹ It is also speculated, that cation reordering in the materials' structure plays a role on the upconversion luminescence efficiency of the fluoride materials, as the hexagonal structure has multiple cation sites; one solely for sodium ions, two which both sodium and lanthanide ions can occupy (Figure 2).^{22,23} However, during the manufacturing process the lanthanides can also invade the sodium site creating closer clusters of lanthanides which can then affect the upconversion luminescence properties.²⁴

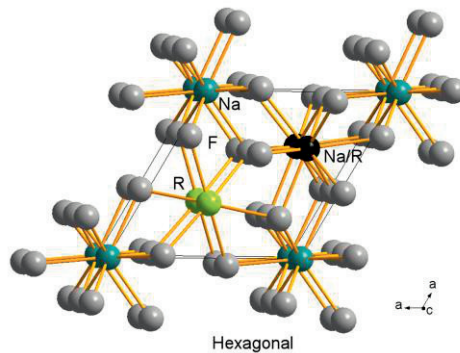


Figure 2. Hexagonal unit cell of $\text{Na}(\text{Y}_{0.80}\text{Yb}_{0.17}\text{Er}_{0.03})\text{F}_4$ structure from Harju et al.²¹

A variety of other inorganic matrices have been utilized as upconverting materials. These materials include oxides (Y_2O_3 , ZrO_2), oxysulfides ($\text{Y}_2\text{O}_2\text{S}$), oxyfluorides and –chlorides (GdOF , GdOCl), phosphates (YPO_4) and vanadates (YVO_4).⁵ However, due to their higher lattice phonon frequency (oxides $\sim 500\text{-}550$, phosphates ~ 1050 , and vanadates $\sim 890\text{ cm}^{-1}$) the obtained upconversion luminescence is not as efficient as with the fluoride based materials.^{5,25} Also other halides (chlorides, bromides, iodides) have low lattice phonon frequencies which would suggest they would be useful

upconversion host candidates but they are more hygroscopic which limits their use greatly.²⁶

Optically active ions

For the upconversion phenomena to occur, the suitable host materials needs to have optically active ions with long lived energy levels in the excited state. Commonly lanthanides (La-Lu) are harnessed due to their ladder-like energy level structure. Also transition metals with suitable 5d energy levels have been studied but they cannot be used without lanthanide ions and they are more commonly used in tuning the obtained luminescence color or enhancing the overall luminescence intensity.²⁷⁻²⁹

It is possible to obtain upconversion luminescence with only one optically active emitter ion (activator) if the ion has multiple similar energy gaps to make the process efficient. This is the case for example with Er^{3+} where the energy difference between $^4\text{I}_{11/2}$ and $^4\text{I}_{15/2}$ is similar to that between $^4\text{I}_{11/2}$ and $^4\text{F}_{7/2}$ which are both in good agreement with the 980 nm excitation energy.²⁵ In the case of one active ion the process of obtaining upconversion luminescence is ground state absorption (GSA) followed by excited state absorption (ESA), however the process is not as efficient as using sensitizer ions.

The upconversion process can be enhanced significantly by introducing additional ions into the host lattice to absorb the excitation energy (sensitizers). The process is called energy transfer upconversion (ETU). Ytterbium is a widely used sensitizer ion in the upconversion processes with multiple activators (Er^{3+} , Tm^{3+} , Ho^{3+}) because the energy gap between its ground state $^2\text{F}_{7/2}$ and excited state $^2\text{F}_{5/2}$ has a good match with the energy levels of erbium making the energy transfer process efficient without significant energy loss. Even if the energy levels of ytterbium do not match as well with Tm^{3+} and Ho^{3+} activators as with Er^{3+} the upconversion process is still efficient. While the upconversion process is the most efficient with the previously mentioned lanthanide activators, upconversion luminescence can also be obtained from other lanthanides such as Pr^{3+} , Sm^{3+} , Dy^{3+} via similar energy transfer processes through Yb^{3+} .¹² Also with Eu^{3+} , and Tb^{3+} reasonable upconversion luminescence is obtained even though the mechanism for it is much less efficient needing a co-operative energy transfer (CET) from two Yb^{3+} creating a virtual energy level to transfer the energy.^{17,30} Gd^{3+} does not have good energy levels to produce upconversion luminescence but it has been used in transferring the energy in high energy excited states through the EMU process.³¹

Nd^{3+} can also be used as a sensitizer instead of ytterbium. It is widely studied because of its 808 nm absorption that could be useful in applications where the 980 nm excitation needed for the ytterbium absorption is not as efficient due absorption by the matrix and/or water.^{17,32,33} However, Yb^{3+} is still often used alongside Nd^{3+} in the structure as an energy transfer component because the upconversion process through it to the emitter ions is much more efficient than with using only neodymium.

Synthesis methods for NaYF₄

Multiple synthesis methods have been utilized in manufacturing the upconversion particles depending on the preferred host matrices.^{5,25} While microcrystalline particles of the most widely used NaYF₄ have been known longer, the possibility to obtain small nanosized materials with narrow size distribution was only reported in the mid-2000s.³⁴⁻³⁶

Nowadays the most common pathway to produce UCNPs with a small size distribution is to use solvents with a high boiling point temperature such as oleic acid and octadecene and/or oleylamine, sometimes called high-temperature co-precipitation method or thermal decomposition. This method was first introduced in 2004 for the preparation of trifluoride nanoplates³⁷ and later 2006 for producing β -NaYF₄.³⁸ Another method with trifluoroacetate precursors in the synthesis is still used³⁹⁻⁴¹ but also variations in the precursor material such as acetates^{17,18} and lanthanide oleates formed from their oxide/chloride precursors^{42,43} have been published. The synthesis procedure usually consists of two heating periods, in which during the first one the lanthanide oleates are formed. After the first heating the sodium and fluoride precursors are added into the reaction. With the addition of sodium and fluoride, a cubic NaYF₄ structure is formed and during the second heating period the cubic nanoparticles undergo the conversion to hexagonal NaYF₄ if the temperature is high enough (usually ca. 300 °C).⁴⁴ The size and shape of the UCNPs can be controlled by the reaction temperature and time during the second heating as well as tuning the ratios of the organic solvents and capping ligands used along with the sodium and fluoride ratios.⁴⁵ Changing the dopants and their concentration can affect the size and shape of the UCNPs, too. For example, adding gadolinium to replace yttrium leads to decreasing nanoparticle size.⁴³

The obtainable size-range of UCNPs in the most used syntheses is ca. 20-30 nm, but also syntheses to produce sub 10 nm nanoparticles have been proposed.^{46,47} Ye et al. recently reported a synthesis procedure where obtaining small 10 nm hexagonal NaYF₄:Yb,Er needed only a fast heating up to a high temperature (250-300 °C) to produce the nanoparticles instead of holding the temperature for prolonged time.⁴⁸ With the second heating period ranging from 0 to 30 min a range of 7 to 11 nm β -NaYF₄:Yb,Er were obtained by using sodium oleate as a sodium source instead of sodium hydroxide. However, the synthesis for producing NaYF₄ shell on the sub-10 nm nanoparticles still needed 90 minutes in the second heating. A slightly modified synthesis procedure was published by Homann et al. where the precursor acetates were treated with acetic anhydride to reduce the water content in the synthesis. The used solvents were dried and the precursors were introduced in the fresh and dried solvents in each synthesis step to produce highly luminescent 10 nm UCNPs.⁴⁹ In addition, replacing 1-octadecene with Therminol® 66 in the synthesis produced hexagonal sub 10 nm nanoparticles with uniform morphology in much shorter reaction time (5-10 min instead of 60 min).⁵⁰

The solvothermal synthesis method using the solvent pressure as an advantage has also been used in manufacturing upconversion materials.⁵¹⁻⁵⁴ The syntheses are conducted using autoclaves where the precursors are added into a Teflon cup and heated to the desired temperature. The synthesis time can vary from a few hours up to 24 hours and the obtained materials can be controlled through changing the solvent and precursor materials as well as temperature, pressure and time. The products of solvothermal synthesis are quite often in the microscale and the uniformity of the particles is not as good as with the materials made in high boiling solvents.

Co-precipitation synthesis is one of the earliest and simplest of the upconversion materials syntheses, as it needs only mixing in the room temperature to produce cubic NaYF₄ particles. However, the products need annealing after the synthesis to produce the more luminescent hexagonal material^{35,55}. The annealing in high temperature, while resulting in the desired hexagonal structure, can also have a negative effect on the particles such as aggregation resulting in large particle size.

Ionic liquids have also been introduced into the synthesis protocols of upconverting nanoparticles with the high-boiling solvent synthesis.⁵⁶ The size-range and uniformity of the materials still leaves room for further research but it remains to be seen if ionic liquids will push their way further into the synthesis of upconversion materials.

As the reaction time to produce UCNPs is still relatively long there have been reports to make the synthesis procedure faster while still producing the desired structure, size and shape for the nanoparticles. Du et al. suggested a new fast synthesis route to produce NaBiF₄ particles where an ethylene glycol solution containing the desired nitrates (sodium, bismuth and lanthanides) was added into a solution of ammonium fluoride in ethylene glycol.⁵⁷ With adjusted fluoride amount they were able to produce the desired structure with upconversion luminescence but the particle size was still relatively large at ca. 200 nm.

Most of the syntheses used in obtaining upconverting nanoparticles make use of hydrophobic organic ligands (oleic acid, oleylamine) which control the growth of nanoparticles during the synthesis.^{5,58,59} This requires further modification of the nanoparticle surfaces when they are introduced in the aqueous environments of biological applications. It is also possible to synthesize UCNPs directly with hydrophilic surfaces so that they are directly dispersible to aqueous solutions. Ethylenediaminetetraacetic acid (EDTA)^{60,61} and citric acid⁶² can be used as a similar controlling agent in solvothermal syntheses or co-precipitation synthesis as oleic acid. Also some polymers such as poly(acrylic acid)^{63,64} and polyethylimine^{65,66} can be used in the solvothermal synthesis and polyvinylpyrrolidone in the thermal decomposition synthesis⁶⁷ as surface capping ligands. However while the dispersibility is increased with the as-prepared hydrophilic surfaces it seems that the upconversion intensity is not as good as with those prepared with hydrophobic surfaces.

2.2 Luminescence properties of upconverting nanoparticles

The obtained upconversion luminescence, its efficiency and color are greatly dependent on the lanthanide ions used and how they are paired to form sensitizer-activator combinations in their host lattice. Pairing Yb^{3+} and Er^{3+} results in strong red and green and sometimes weak blue upconversion luminescence while pairing with Tm^{3+} instead of Er^{3+} results in mostly blue upconversion luminescence in the visible range and NIR and UV radiation (Figure 3).^{3,12,68}

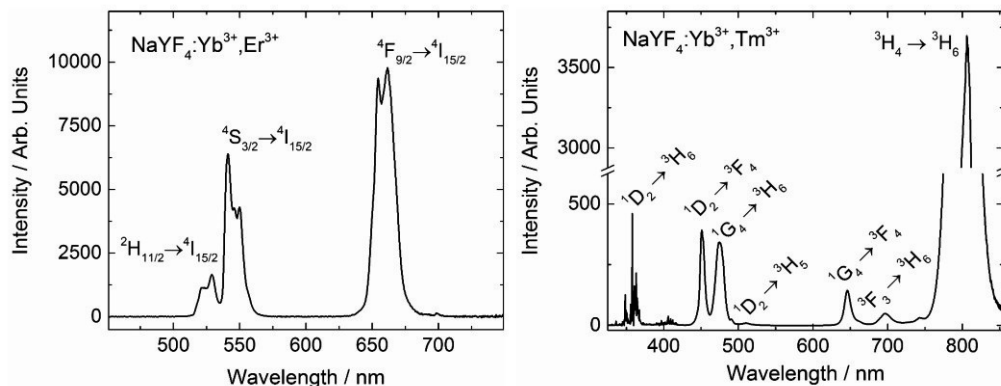


Figure 3. Upconversion luminescence spectra of $\text{NaYF}_4:\text{Yb}^{3+}$ materials co-doped with Er^{3+} (left) and Tm^{3+} (right) and their respective transitions. (Modified from Haase *et al.*²⁵)

The currently accepted energy transfer upconversion luminescence mechanism for the Yb^{3+} - Er^{3+} pair is shown in Figure 4. The energy transfer between ytterbium and erbium is efficient due to their well-matching energy levels $^2\text{F}_{5/2}$ (Yb^{3+}) and $^4\text{I}_{11/2}$ (Er^{3+}) where the energy is easily transferred without a significant energy loss. Also the second energy transfer from $^4\text{I}_{11/2}$ (Er^{3+}) to $^4\text{F}_{7/2}$ (Er^{3+}) has a similar energy gap and is likewise very efficient. For obtaining green upconversion luminescence, a two-photon process is needed through the Yb^{3+} - Er^{3+} energy transfer and this process remains similar regardless of the environment of the nanoparticles. The red upconversion luminescence process seems to be more affected by the environment. It can be obtained with a two-photon process via a relaxation from the green emitting levels $^2\text{H}_{11/2}$, $^4\text{S}_{3/2}$ to the red emitting level $^4\text{F}_{9/2}$ or it can be a result of a three photon process involving a back energy transfer (BET) between the $^4\text{G}_{11/2}$ energy level of Er^{3+} to the ground state $^2\text{F}_{7/2}$ of Yb^{3+} .^{18,69,70} It seems that the three photon process is more dominant in larger nanoparticles and when the measurements are made in organic solvents without water. However, after the nanoparticles are introduced into aqueous environments and as the surface to volume ratio is increased the two-photon process becomes more dominant. It is also very probable that in most cases the upconversion process is a combination of both population mechanisms of the red emitting state.

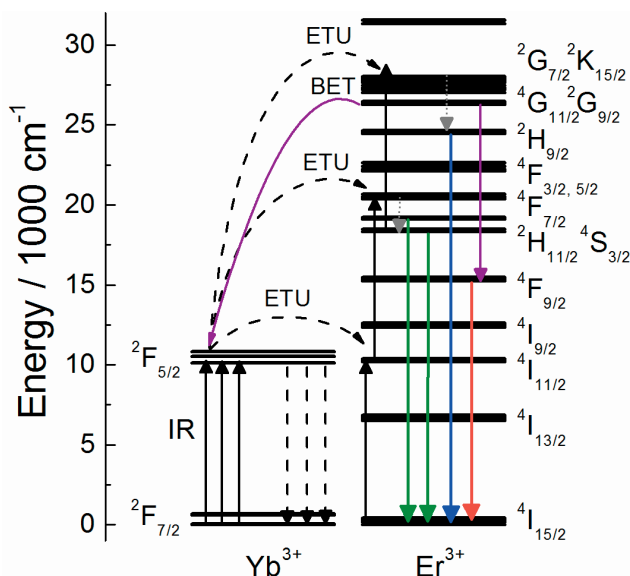


Figure 4. The upconversion mechanism between Yb^{3+} and Er^{3+} ions. Where ETU denotes energy transfer upconversion and BET back energy transfer. (Modified from Anderson et al.⁷¹ to publication II)

The upconversion luminescence efficiency and the quantum yield are greatly dependent on the environment where the materials are used and on the nanoparticle size. The quantum yield would be the simplest way to compare various upconverting materials and their efficiency but measuring it is still challenging. Currently there is no valid reference upconversion material that can be reproduced so the measurements have to be done as absolute quantum yield measurements.^{70,72,73} Absolute quantum yield measurements require well calibrated equipment with an integrating sphere and are affected by the excitation power profile.

The conditions of the upconversion luminescence measurements and the environment of the measured particles can rather easily be adjusted and their effect on the upconversion luminescence intensity evaluated. However, the local structure and the concentration of the optically active ions in the upconversion host material are difficult to control and thus not all of the aspects affecting the emission intensity can be controlled or studied in detail. For this reason the availability of easy and accessible quantum yield measurements would be beneficial. So far the quantum yields of bare $\beta\text{-NaYF}_4\text{:Yb}^{3+},\text{Er}^{3+}$ nanomaterials with a 25 nm size are *ca.* 0.5 % when measured from powders.^{73,74} In addition, a decrease in size results in an even larger decrease in the quantum yield due to surface defects and quenching through their vibrational states. Core-shell $\text{NaYF}_4\text{:Yb}^{3+},\text{Er}^{3+}@ \text{NaYF}_4$ UCNPs with a size range from 15 to 45 nm were recently manufactured by a modified synthesis procedure and their quantum yield was seen to increase significantly and the quantum yield of the 45 nm UCNPs already

approached the quantum yield of the microcrystalline upconversion materials being 9%.⁴⁹

The main reasons for a low quantum yield and upconversion luminescence quenching can be found in the energy levels of lanthanide ions and the energy transfer mechanisms between them. While the long lived energy states of lanthanide ions make the upconversion mechanism possible they also enable other possible routes for energy transfer such as non-radiative transitions and cross-relaxation processes between ions. With small nanosized particles also the increasing surface to volume ratio results in the increase of the number of surface defects and molecules (*eg.* OH⁻, H₂O, organic ligands) and their effect in quenching the upconversion luminescence.^{6,75} It has been further studied that especially the energy transfer process between Yb³⁺ and Er³⁺ is affected as the energy migration to the particle surface via various Yb³⁺ energy levels gets easier with decreasing particle size.⁷⁶ This results in draining the energy reservoir needed for the upconversion process at the near infrared (²F_{5/2} (Yb³⁺), ⁴I_{11/2} (Er³⁺)) energy levels through the surface impurities and solvent vibrations resulting in weaker upconversion luminescence and lower quantum yield.^{70,76,77} Johnson et al. also noted, that the quenching of upconversion luminescence due to concentration quenching is much less than that arising from transferred energy leaking from the surface impurities as they managed to gain significant upconversion luminescence from a pure NaErF₄ material when a thick NaLuF₄ shell was manufactured on the core particle surface.⁷⁵

Another major factor in the decrease of upconversion luminescence is the disintegration of the nanoparticles that is observed when the fluoride containing UCNPs are introduced into aqueous environments.^{7,8,54,78} The disintegration can be observed from the decrease in the upconversion luminescence intensity with time as well as the decrease in the emission decay lifetimes. It has been observed that the disintegration is enhanced with lower UCNP concentration in the solutions and especially in phosphate based buffers, where it is expected that the phosphate buffer can detach the lanthanide ions from the fluoride structure more easily and thus enhance the disintegration process. It seems, that the disintegration of the UCNPs can be hindered by introducing fluoride ions to the buffer solutions used suggesting that the driving force behind the disintegration is the fluoride imbalance in the solution used. However, even a thick silica shell⁸ or specially designed amphiphilic polymer coatings⁷⁹ are unable to block the process completely. Dukhno et al. studied the disintegration of the UCNPs by imaging the emission intensity of single particles when the particles were modified with amphiphilic N-dodecyl-polyisobutylene-alt-maleamic acid (PMA).⁸⁰ They also confirmed the fast time-scale of the disintegration in water and the favorable impact of using fluoride in the solutions to prevent disintegration.

2.2.1 Enhancement of upconversion luminescence

The most common way for upconversion luminescence quenching is the energy transfer process through the nanoparticle onto the surface.^{6,75,77} Various methods for enhancing the luminescence intensity and preventing the quenching has been proposed. This section is focused on the NaRF₄ (R: Y, Sc, La-Lu) nanoparticles, their structure and surface environment and how modifying them can affect the upconversion luminescence. The surface modifications made to ensure the compatibility in aqueous environment and biomedical applications are discussed in more detail in their respective sections.

Host lattice manipulation is the simplest route to modify and enhance upconversion luminescence efficiency as it depends greatly on the host material. Also upconversion color tuning is done by manipulating the optically active ions in the lattice. Enhancement in the upconversion luminescence intensity has been obtained by doping Li⁺, K⁺ or Sc³⁺ ions into the lattice to partly replace Na⁺ or Y³⁺, respectively.^{81,82} Similarly using transition metals such as Fe³⁺, Mn²⁺ the host lattice and obtained upconversion emission can be tuned and in some cases enhanced.^{83,84} The enhancement is believed to be due to the mismatching sizes of the dopants distorting the lattice used, which can then result in shorter distances between the lanthanides. However, tuning the host lattice still leaves the surface exposed to the environmental effects which leaves the particles needing further surface engineering.

The core-shell structure has been one of the most studied topics in enhancing the upconversion luminescence.⁸⁵ The idea of the core-shell structure is to shield the core particle and prevent the energy loss through surface ions (Figure 5.). This can be done by growing an inert and passive shell structure on top of the nanoparticle surface.^{75,86-89} This is called an active-core/inert-shell structure. Usually, the shell is grown with a similar structure to that of the active core but without the optically active ions (eg. NaYF₄, NaLuF₄ and NaGdF₄). It is also possible to grow inert shells with another crystal structure such as CaF₂.⁹⁰ The shell can be manufactured in a way that the earlier prepared core material is added into pre-heated lanthanide oleate solution before the fluoride and sodium are added.^{16,91} After the addition of the fluoride and sodium solution the fluoride structure starts to grow onto the added core material surface. One other method for shell growth is to use a so called sacrificial cubic-NaYF₄.^{75,86,92} In this method small cubic nanoparticles are prepared earlier and they are added to the synthesis of the hexagonal core particles after ca. 60 min during the second heating when the hexagonal particles have been formed. The cubic particles are then used as seeds or building blocks for the desired shell on the hexagonal particle surface.

The shell thickness plays a significant role in the upconversion luminescence enhancement and the shape of the grown shell can be altered by the injection rate and steps.⁸⁶⁻⁸⁹ It has been observed that while the upconversion emission is enhanced greatly within the formation of the first few nanometers of inert shell and continues

throughout the shell growth. However, the overall enhancement of the quantum yield does not increase after 4 nm shell growth because the rate-limiting steps in the upconversion mechanism become more important than the surface quenching.⁸⁹ A sophisticated characterization of the core-shell materials and the elemental distribution through the nanoparticle is crucial in confirming the shell formation as the growth of the shell might not be symmetric throughout the core surface.⁹³ In addition, evidence of the cation intermixing at the core – shell interface has been observed which creates questions about the energy transfer processes and if the shell is truly inert optically.⁹⁴

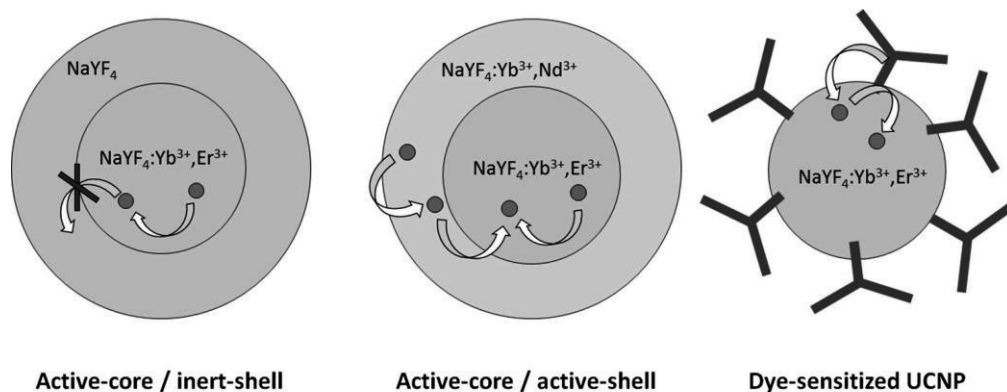


Figure 5. Methods to enhance the upconversion luminescence intensity through inert (left) or active (center) shell structures as well as sensitizing with dye molecules (right). (Modified from Resch-Genger et al.⁵⁸)

Also active-shell structures involving optically active ions can be grown on top of the nanoparticle core creating active-core/active-shell nanomaterials.^{16,17,95–98} Using an active shell the optical properties and energy transfer within the material can be controlled by combining desired active ions in the shell structure (Figure 5). The active shell can be used to enhance the obtained upconversion luminescence intensity by using emitting ions on the shell structure and varying the core ions.^{95,96} The advantage of having emitting ions at the shell is the shorter distance between emitting ions and possible acceptors on the surface which can enable efficient sensing applications and luminescence resonance energy transfer (LRET) processes.⁹⁶ The problem with the active-shell structure is how to keep the active ions separated well enough in the shell structure so that no cross-relaxation related to quenching can happen. This can be achieved by creating transition layers that have less active ions that can interfere with the energy transfer process.¹⁶ One recent aspect in the active-shell structures is to introduce Nd^{3+} ions into the structure to harvest 800 nm excitation which could be more suitable for the biomedical applications such as imaging where the heating effect of water can be a problem. By using neodymium it is possible to absorb the 800 nm excitation and then subsequently transfer the energy through Yb^{3+} ions which then can more efficiently transfer energy to the activators to obtain visible light.^{17,98} This can then enable the excitation through both Nd^{3+} and Yb^{3+} ions.³³

However, it has been discussed if the use of active-shell structures without an additional inert shell on the outer layer is as beneficial as using only an inert shell on the surface as the surface mediated quenching is again activated by the optically active ions in the shell structure.⁷⁵

While the core-shell structure can be used to host other sensitizers as Nd^{3+} for the 800 nm excitation the absorption lines of the lanthanides are relatively narrow. For this reason using spectrally broad absorbing dye molecules have been studied as an antenna structures on the nanoparticle surface.^{39,99–102} The use of dye molecules as an energy transferring antennas is based on Förster –type resonance energy transfer (FRET) between the energy levels of donor-dye and acceptor-lanthanide ion (Figure 5.). A similar kind of FRET energy transfer can also be observed into the opposite direction, from the lanthanide ions to the dyes.¹⁰³ The most common path of sensitizing through dyes is to use a 808 nm absorbing dye (such as IR-808) and transfer the energy through Nd^{3+} energy levels into Yb^{3+} and further to Er^{3+} ^{101,102} but also direct energy transfer from IR-808 to UCNPs have been observed.¹⁰⁰ One of the most recent advances has been the use of a visible emitting dye (ATTO-542) on the nanoparticle surface. The dye interacts with the surface Er^{3+} ions making them active and thus enhances the upconversion luminescence.³⁹ Especially with the small nanoparticles (diameter *ca.* 10-15 nm) the enhancement in the obtained upconversion quantum yield is significant, *ca.* $10\times$, due to the activation of the surface emitters.^{39,76}

Another method of enhancing the upconversion luminescence intensity is to take advantage of the plasmon enhancement arising from the use of noble metals in close contact with upconversion nanoparticles.^{104,105} Multiple approaches have been studied such as structures of gold nanorods¹⁰⁶ or thin silver films¹⁰⁷ below the nanoparticle assembly. In addition, structures such as nanoparticles on top of a silver-gold nanocage¹⁰⁸ and decorating the nanoparticle surface with gold particles have been proposed.¹⁰⁹ The plasmonic effect can also be used for enhancing upconversion luminescence from a single nanoparticle by using an AFM cantilever with gold coating. Such a setup could be used in sensitive imaging applications.¹¹⁰

2.3 Applications for upconverting nanoparticles

While the unique property of converting low energy radiation into higher energy is in itself a fascinating topic of research it has many advantages which drive the research focus onwards especially in the biomedical field. In addition to biomedical research upconverting nanoparticles have also gained attention in renewable energy research and photovoltaics,^{111,112} and anti-counterfeiting^{113,114} but these applications will not be further discussed in this thesis.

Biomedical research and applications can benefit from the upconversion materials in many ways. The NIR excitation can be used in background-free diagnostic assays instead of UV excited fluorescent materials while the upconversion process itself can be obtained via inexpensive continuous wavelength light sources.⁵⁸ The narrow

emission lines from lanthanide luminescence with anti-Stokes emission makes them good candidates for spectral multiplexing and the possibility of tuning the luminescence lifetime allows time-gated measurements and the use of Förster –type resonance energy transfer mediated detection. Upconversion materials do not have photobleaching in the time course as fluorescent molecules and they are also available for single-particle applications due to their non-blinking emission.

2.3.1 Reporters in assays

The research and use of upconversion materials as luminescent reporters started already before nanoscale materials were developed. The use of ground microsized upconversion materials in biomedical use was first demonstrated in heterogeneous assays by the group of Hans Tanke in 1999 in the detection of antigens and then later 2001 in lateral flow assay (LFA) in testing human papillomavirus infections.^{115,116} The first homogeneous assays exploiting the properties of upconversion luminescence were presented in 2005 simultaneously by Kuningas et al. and Wang et al.^{117,118}

The homogeneous assays can be described as an easy mix and measure type of assay without additional washing steps (Figure 6.). The detected signal (usually luminescence) is dependent on the biomolecule interactions and the binding between the labeled analyte and biomolecules.¹¹⁹ This also enables the use of homogeneous assays as biosensors. Due to the nature of the homogeneous assay it is prone to many limitations and interference such as sample autofluorescence and absorption. The use of upconversion materials can overcome some of these problems as the autofluorescence from NIR excitation is out of the measurement window and it can also enable the use of whole blood as a measurement matrix.^{120–122} However if the homogeneous assay signal detection is based on the energy transfer processes such as FRET/LRET between the UCNP and the analyte label it is distance dependent and requires much attention to the nanoparticle and energy transfer design because of the short distance needed for the energy transfer.^{103,123–125} The combination of the needed distance in addition to the aqueous measurement matrix which is known to quench luminescence makes the designing and protecting the UCNPs an important task.

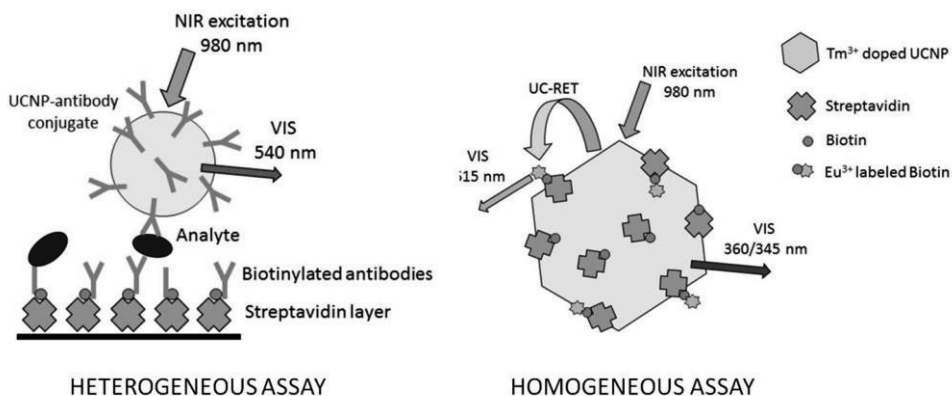


Figure 6. Simplified mechanisms of heterogeneous (left) and homogeneous assay principles using upconverting nanoparticles. (Modified from Sirkka et al.¹²⁶ (heterogeneous) and Lahtinen et al.¹²⁵ (homogeneous).)

The principle of the heterogeneous assay differs from that of homogeneous assay by involving captured molecules on a solid substrate, commonly a microtiter plate, where the analyte and labels are then subsequently bound (Figure 6.).¹¹⁹ The heterogeneous assay requires multiple steps in both the binding and washing off the excess of the reagents used. It is not as fast as the homogeneous assay but the detection limits are usually lower due to the removal of the interfering excess molecules by washing. UCNPs have been used for example in sensitive immunoassays for cardiac troponin I¹²⁶, the detection of diclofenac¹²⁷ and genotyping adenoviruses.¹²⁸ However, one problem arising from the small size of nanoparticles which limits the sensitivity of the assays is the non-specific binding to the solid support in addition to only binding to the desired linkers. The non-specific binding can be hindered by using blocking molecules such as bovine serum albumin (BSA)¹²⁹ or one can try to reduce it by surface modifications.¹³⁰ One recent discovery with UCNP based assays was that the sensitivity of the troponin I assay proposed by Sirkka et al¹²⁶ could be enhanced by adding poly(acrylic acid) to the assay which hindered the nonspecific binding of UCNPs.¹³¹

Lateral flow assays (LFAs) are a subdivision of heterogeneous assays which are widely used because of the inexpensiveness and suitability in point-of-care testing (e.g. pregnancy test). The assay is conducted on a test strip where the applied sample is directed through a matrix involving test and control lines to observe the desired analytes. UCNPs have been utilized for various schemes using LFAs ranging from the detection of tissue infections into potential biowarfare pathogens and viral infections.^{132–134}

The narrow emission lines of lanthanide upconversion luminescence and the possibility to change the observed color by selecting the doping ions while keeping the

nanoparticles similar in size and shape offers the possibility to perform multiplexed assays. The advantage of multiplexing is the much smaller amount of consumed time in the number of detected analytes. Printing an array-in-well type platform on a microtiter well offers a possibility to detect genotype-specific adenoviruses by imaging.¹³⁵ On the other hand, by coating different UCNPs with selected antibodies and utilizing array-in-well type printing it is possible to detect in both place- and color-dependent assay modes.¹³⁶ By changing the dopant ions and their concentration it is also possible to create color barcoded detection mechanism for detecting nuclei acids.¹³⁷

In the development of the varying types of biochemical assays using upconversion luminescence the construction of a well-functioning detection and reading system for upconversion luminescence has proven to be challenging. Soukka et al. first introduced a modified plate Chameleon reader in 2005 for their upconverting biomedical assays.¹³⁸ For the modification the Xenon flash lamp of a plate Chameleon reader was replaced with a continuous wavelength infrared laser diode. Similar modifications were later introduced into the detection of gel electrophoresis and lateral flow assay readouts by the collaboration of Tanke, Soukka and Gorris groups.¹³⁹ In addition to these custom house-built equipment two Finnish companies Kaivogen oy and Labrox oy joined forces in the middle of 2010s to create the first commercial upconversion nanoparticle system Upcon™ which involved a single mode plate reader manufactured by Labrox oy.¹⁴⁰ However, application research still relies mostly on in-house-built imaging and detection equipment.

2.3.2 Sensors

Because of the unique lanthanide upconversion luminescence emissions, the UCNPs are widely researched for use in many types of sensors in both solutions and in the solid state.⁴ In the solid state sensors the UCNPs are embedded into a desired matrix such as a hydrogel membrane¹⁴¹ or polystyrene¹⁴² with substances that change their properties with the desired detection scheme such as bromothymol blue (BTB) that changes color with changing pH. The detection is based on the so called inner filter effect where the emitted upconversion luminescence is affected by the change of the substance and thus the absorption properties of the counterpart. However, by using upconversion luminescence resonance energy transfer it is possible to create (bio)sensors that detect changes in the nanoscale and even within cells based on the changes in the upconversion luminescence (Figure 7.). In the next paragraphs only sensors based on NaYF₄ UCNPs and their RET-counterparts in liquid media are discussed.

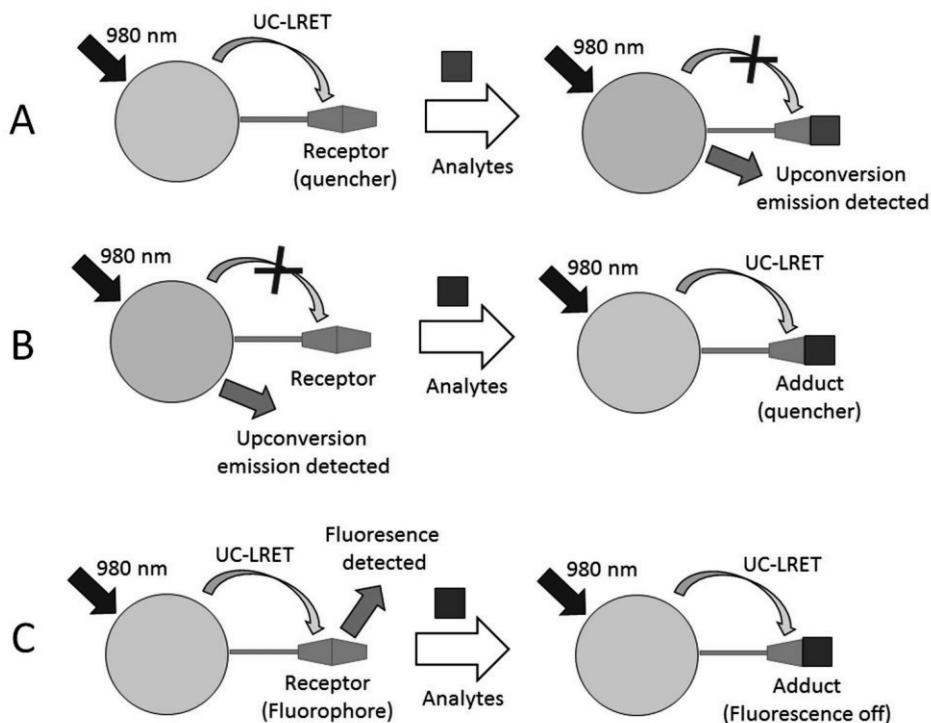


Figure 7. Simplified mechanisms of UC-LRET processes based on spectral overlap between the donor and acceptor. A) After the addition of the analytes, LRET is suppressed and upconversion emission is recovered; B) After the addition of the analytes, LRET is possible and the upconversion emission is quenched; C) If the receptor is highly emissive and is excited by the upconversion emission, then fluorescence is observed. After the addition of the analytes the adduct cannot be excited by the upconversion emission, fluorescence is not seen. (Modified from Zhou et al.⁴)

A possible *in vivo* pH probe of UCNPs coated with polyanionic tendrimers was suggested by Esipova et al. where the luminescence intensity ratio between green and red emission changed with the pH.¹⁴³ Arppe et al. introduced an intracellular pH probe which could be also imaged utilizing a resonance energy transfer between a UCNP donor and pH-sensitive pHrodo™ Red dye as an acceptor for the 550 nm emission of Er^{3+} .¹⁴⁴ Their probe and cellular uptake and distribution was further enhanced by coating the UCNPs with polyethylenimine.¹⁴⁵ A pH sensitive fluorescein isothiocyanate¹⁴⁶ has also been used with UCNPs as an intracellular pH probe acting as an acceptor to the 475 nm emission of Tm^{3+} with increasing pH and hemicyanine dye¹⁴⁷ has been suggested as a probe to see pH fluctuations within cells by blocking the green and blue upconversion luminescence with increasing pH. A core-shell approach with UCNP with a silica shell and BSA modification using BTB or rhodamine B (RhB) as a pH dyes produced even more sensitivity to the measurement

where the changes in the green upconversion luminescence were detected with pH change.¹⁴⁸ With BTB the green emission intensity was enhanced with increasing pH at the range of 6-8 and with RhB at pH range of 5-7 the green emission decreased with increasing pH.

The detection of metal ions and molecules is possible by using the resonance energy transfer method. The detection of Hg^{2+} using UCNPs can be done for example using a chromophoric Ru(II) complex¹⁴⁹ where the increase of Hg^{2+} concentration leads to the recovery of the green upconversion emission of Er^{3+} due to a loss of spectral overlap between the UCNPs and the Ru(II) complex. Also the use of rhodamine-derived molecules on the UCNPs surface results in enhanced energy transfer and thus increasing emission intensity of rhodamine with increased Hg^{2+} concentration.^{150,151} Modifying the UCNPs surface with glutathione the green upconversion emission is quenched with the addition of Hg^{2+} and Pb^{2+} .¹⁵² In addition a UCNPs-Gold nanoparticle connected with an aptamer has been developed for Hg^{2+} detection in food as the attachment of Hg into the aptamer chain results in the enhancement of the green upconversion luminescence intensity due to the removal of the green emission absorbing gold nanoparticle from the aptamer chain.¹⁵³ The use of Er^{3+} and Tm^{3+} doped UCNPs with cyanine modification the presence of MeHg^+ can be observed from the decrease in 800 nm (Tm^{3+}) and the increase in 670 nm (Er^{3+}) emission intensities.¹⁵⁴ For the detection of Cu^{2+} the UCNPs can be combined with tetraphenylporphyrin tetrasulfonic acid hydrate (TPPS)¹⁵⁵ or meso-tetra(4-sulfonatophenyl)porphine dihydrochloride (TSPP)¹⁵⁶ which both absorb the green upconversion emission of UCNPs. When the Cu^{2+} coordinates into the cavity of the molecules the UC-RET process is interfered resulting in the recovery of the green upconversion luminescence.

Modifying Er^{3+} -UCNPs with 4-((4-(2-aminoethylamino) naphthalen-1-yl)diazenyl) benzenesulfonic acid dihydrochloride (ANDBS) enables nitrite (NO_2^-) sensing by observing upconversion luminescence quenching when nitrite is attached.¹⁵⁷ Modifying UCNPs with NO-reactive rhodamine B-derived molecules enables nitric oxide (NO) detection as it reacts with the molecules opening the ring structure enabling strong rhodamine B absorption which absorbs the green upconversion luminescence.¹⁵⁸ Cyanide anions (CN^-) can be detected using Iridium(III) complexes on the Er^{3+} -UCNPs surfaces.¹⁵⁹ The energy transfer between the UCNPs and the complex is interfered with the addition of CN^- . This results in a change in the emitted color from yellow (from the iridium(III) complex) to green (from the UCNPs). Glutathione (GSH) molecules that are essential part of the cellular defense system can be monitored using Tm^{3+} doped UCNPs coated with MnO_2 nanosheets as the presence of GSH the MnO_2 is reduced to Mn^{2+} thus blocking the energy transfer between the UCNPs and the nanosheet resulting in increased blue 475 nm upconversion luminescence intensity.¹⁶⁰ In addition, a H_2O_2 sensor was suggested in the second near-infrared window combining a $\text{NaErF}_4:\text{Ho}^{3+}/\text{NaYF}_4$ core-shell structure coated with IR1061 molecules.¹⁶¹ With 1530 nm excitation the IR1061 on the surface absorbs the 980 nm emission leaving the 1180 nm emission intact. At the presence of OH^-

radicals formed from H₂O₂ the IR1061 molecules on the surface are destroyed resulting in the recovery of 980 nm emission.

Temperature sensing using UCNPs is based on emitting lanthanide ions and their emission intensity changes (luminescence intensity ratio, LIR) between specific energy levels. The green emissions of Er³⁺ at 525 and 545 nm is useful in this as the intensity ratio of the emissions change with temperature.^{162–164} The sensitivity and reliability of the obtained LIR ratios depends on the size and composition of the nanoparticles.¹⁶⁵ Also the laser irradiation conditions used affect the outcome as steady-state conditions have to be obtained and the laser power needs to be moderate not to heat the water in the sample as it affects the intensity ratios.¹⁶⁶ In addition to Er³⁺ other lanthanide ions such as Ho³⁺, Tb³⁺, Tm³⁺ and Nd³⁺ have been suggested as possible temperature sensing emitters due to their suitable energy levels that induce LIR changes in varying temperatures.^{167–170}

2.3.3 Bioimaging

The use of upconverting nanoparticles in bioimaging is driven by similar reasons as the use in biomedical assays such as lack of autofluorescence at the detection region and no photobleaching. However, the good penetration depth of the UCNPs' emission and their excitation is one benefit that is more useful in bioimaging than many other applications. Most of the research done with UCNPs in bioimaging consists of exploiting their luminescence properties, but by designing the UCNPs with selected ions it is possible to widen their use also into magnetic resonance imaging, X-ray computed tomography, positron emission tomography and single-photon emission computed tomography. It is also possible to create combinations from multiple methods.

The upconversion luminescence (UCL) can be used for imaging cells and their internal properties such as pH.^{144,171,172} Small animals and their desired parts such as lymph-nodes and tumors can be imaged, as well.^{173–176} The particle size for the used UCNPs is *ca.* 50 nm, while for the lymph-nodes bigger particles (100 nm) or more intense upconversion emission would be desirable. With photoluminescence imaging the NIR-to-visible upconversion emission of the Yb³⁺-Er³⁺ pair (ie. 980 to 660 nm) is widely used but also the NIR-to-NIR upconversion emission from Yb³⁺-Tm³⁺ (980 to 800 nm) is used when a deeper penetration depth is needed as both of the wavelengths used lie within the “optical biological window I” (700–1000 nm, Figure 8). Using 808 nm excitation absorbed by Nd³⁺ ions in the host material is also currently an interesting research topic due to the 808 nm excitation having less heating effects on the biological tissue and water than the 980 nm excitation used for Yb³⁺ excitation.^{177–179} In addition to upconversion luminescence imaging, the excitation of UCNPs results in downshifting luminescence at the optical biological window II (1000-1700 nm) which could enhance the image quality and signal-to background ratios even more.^{180–}

182

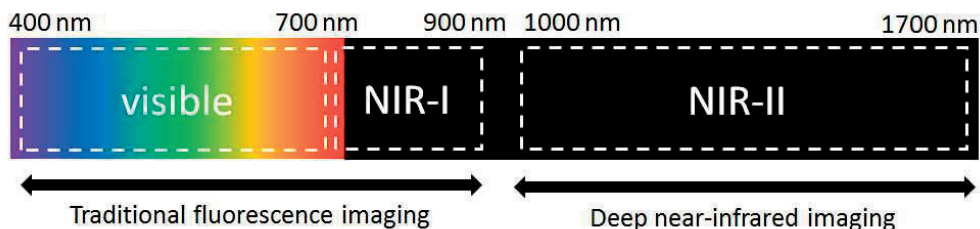


Figure 8. Wavelength regions of traditional fluorescence imaging and deep near-infrared imaging including the NIR-I and NIR-II biological window wavelengths.¹⁸⁰

By designing the composition of the UCNP it is possible to create multimodal imaging particles exploiting two or more imaging techniques. Using gadolinium in the host lattice or on the surface with a molecular antenna brings a possibility to use magnetic resonance imaging (MRI) along with the upconversion luminescence as Gd^{3+} can be used as a contrasting agent.^{183,184} Modifying UCNP with ^{18}F or ^{153}Sm the use of positron emission tomography (PET) and single-photon emission computed tomography (SPECT) bioimaging is possible.^{185–187} Also the rare earth ions in the UCNP have decent X-ray attenuation effect which makes them usable in X-ray computed tomography (CT)^{56,188–190} Combining these properties trimodal UCNP for UCL-CT-MRI^{191,192} and UCL-MRI-PET/SPECT^{185,193} have been studied and even a four-modal UCNP for UCL-MRI-CT-SPECT¹⁹⁴ has been proposed.

For the use of UCNP in bioimaging and especially in *in vivo* studies their toxicity has to be thoroughly studied and assessed both due to their nanosize as well as the unique physical and chemical properties of UCNP. Most concerns with UCNP arise from the possible aggregation in time course within tissues and cells. In addition, the disintegration of the UCNP and thus the release of lanthanides and fluoride as well as the possible interactions between the UCNP and the released ions with other compounds when used *in vivo*.^{195,196} The elimination time of UCNP used *in vivo* from the system is reported being from weeks to months as the size of the UCNP used has to be large enough for the luminescence intensity while ultrasmall particles would be faster eliminated.^{196,197} The toxicity is also widely influenced by the surface modifications and it seems that with some modifications such as PAA and SiO_2 the toxicity is relatively low^{197,198} while a possible threat can be with amphiphilic coatings that can detach from the UCNP surface.¹⁹⁹ However, while the possible toxicity seems to be dose dependent more detailed and long-term studies have to be made to fully understand it as there still is no standardized protocol for making cytotoxicity assessments for UCNP.

2.4 Surface properties of upconverting nanoparticles

The most used synthesis routes to produce UCNP result in surface capped UCNP with hydrophobic ligands. This creates a need for surface modifications as nearly all biomedical applications are conducted in aqueous environments where the as-prepared

UCNPs are not dispersible. In addition to creating water dispersible UCNPs another reason to modify their surface is the need of conjugative sites for biomolecules in biomedical applications.

As discussed previously with the upconversion luminescence properties, one recently arisen concern in the use of UCNPs in biomedical applications is the disintegration of the fluoride structured nanoparticles in aqueous environment.⁷⁸ Lisjak et al. further studied and proposed a mechanism which suggests that the dissolution of the outermost fluoride structure is imminent in aqueous environment and especially in phosphate based buffers already within the first minutes after the suspension is formed.⁵⁴ Lahtinen et al. published a similar study where they observed the disintegration of the hexagonal NaYF₄:Yb³⁺,Er³⁺ particles and that the disintegration was increased in low concentrations commonly used in biomedical applications and that using even a thick silica shell does not prevent the disintegration.⁸ This creates an urgent need for stable surface functions that prevent the disintegration process.

2.4.1 Surface modifications

As most of the UCNP syntheses result in hydrophobic nanoparticles, the first step of surface modifications with UCNPs is commonly the removal of the capping ligand used if the particles are needed in aqueous solutions. The most used protocols of removing capping ligands are derived from the publication of Bogdan et al. in 2011.²⁰⁰ The method is based on an acidic treatment of the UCNPs which detaches the oleic acid on the surface and creates a positively charged surface on which the water and OH⁻ are then coordinated. If the pH of the solution is increased the surface charge of the UCNPs can be changed due to deprotonation. The treatment renders the UCNPs water dispersible which then enables further modifications and use in the aqueous environments.

It is also possible to modify the hydrophobic ligands, in most cases the oleic acid (OA) chains, directly on the nanoparticle surface. As the OA chain involves a double bond, it can be oxidized by using the Lemieux-von Rudloff reagent into two carboxyl groups.^{201,202} The reagent is composed of permanganate (MnO₄⁻) and periodate (IO₄⁻) ions as they are both needed in reaction. Firstly, the permanganate oxidizes the double bond which is then reoxidized by periodate to produce separate two carboxyl acid ends. The resulting azelaic acid coated UCNPs are then dispersible in water but also in some polar solvents. A similar azelaic acid coating can be obtained by ozonolysis but it can also result in the formation of aldehydes on the surface, but they still make the particles dispersible in water.²⁰³

Ligand exchange

As the oleic acid capping is removed from the UCNP surface it leaves the surface free for H₂O and OH⁻ to attach to the surface atoms. To prevent this, a small and easily unattachable BF₄⁻ can be added on the surface before further modifications.^{42,204} The

ligand exchange is ensured by using an excess of the desired ligands and a suitable solvent and it can be accelerated by elevating the temperature.⁵⁹

Most often a carboxylic acid is used as an attaching group on the UCNP surface similarly to the oleic acid capping ligands. When citric acid^{42,205,206} and hexanedioic acid⁵⁹ are used also the gained outbound functional group is carboxylic acid. In addition, phosphate groups are good anchors on the nanoparticle surface and depending on the molecule used the outer functional group can be changed such as the amine in *O*-phospho- α -threonine and alendronate acid²⁰⁴ to hydroxyls in PEG-phosphates.^{42,204}

As polymers have repeating functional groups they offer possibilities for surface functionalizing while at the same time they have enough attaching sites also for the outer surface. Poly(acrylic acid) (PAA) is one of the most frequently used polymers in UCNP ligand exchange reactions as it produces carboxyl acid attaching sites both to the nanoparticle surface and the outer surface for further modifications.^{42,131,197} Polyvinylpyrrolidone (PVP) can be used as a surface modification polymer due to its carbonyl group in the pyrrolidone unit²⁰⁷ but the nanoparticles can also be synthesized using PVP as a stabilizer during the synthesis creating a PVP coating to the surface directly.⁶⁷ Photoinduced polymerization has been used in coating the upconversion nanomaterials either with the emission obtained from the core UCNPs²⁰⁸ or from an outside light source.²⁰⁹ In addition, co-polymers manufactured from oligo(ethylene glycol) methyl ether acrylate (OEGA) and acrylic acid (AA), monoacryloxyethyl phosphate (MAEP) and 1-acrylamido-2-methylpropane sulphonic acid (AMPS) and 2,2'-azobisisobutyronitrile (AIBN) have recently been studied as possible surface polymers and their attachment configurations with different functional groups on the UCNP surface have been studied.²¹⁰

Polyethylene glycol (PEG) is a widely used ligand in UCNP modifications due to its biocompatibility. It can be used in its diacid form allowing the carboxylic acids to attach to the nanoparticle surface but the more useful ones are the copolymer modifications of PEG such as PEG-phosphate^{42,204} and PEG-*b*-PAA²¹¹ where the functionality of the polymer is increased by combining it with another polymer. Especially when PAA is used the multiple carboxyl acids of PAA enhance the anchoring of the copolymers on the nanoparticle surface.

Amphiphilic coatings

Amphiphilic (original *amphi-* prefix meaning “both”) coatings are manufactured directly to the UCNP surface using ligand interactions when the hydrophobic ligands are still attached (Figure 9). Amphiphilic polymers and some detergents can be used as long as they have both hydrophobic and hydrophilic parts.^{42,79,212,213} The long alkyl chain interacts with the oleic acids alkyl chain by van der Waals interactions while the other end of the amphiphilic polymer used acts as a functional tool for the outer surface. Usually modified copolymers used are such as octylamine and/or

isopropylamine modified poly(acrylic acid)^{212,213} or poly(isobutylene-*alt*-maleic anhydride) modified with 4-(aminomethyl)pyridine or PEG.⁴² An amphiphilic coating consisting of poly(maleic anhydride-*alt*-1-octadecene) (PMAO) and bis(hexamethylene)triamine (BHMT) was recently reported to successfully hinder the disintegration of the core UCNPs in phosphate buffer.⁷⁹

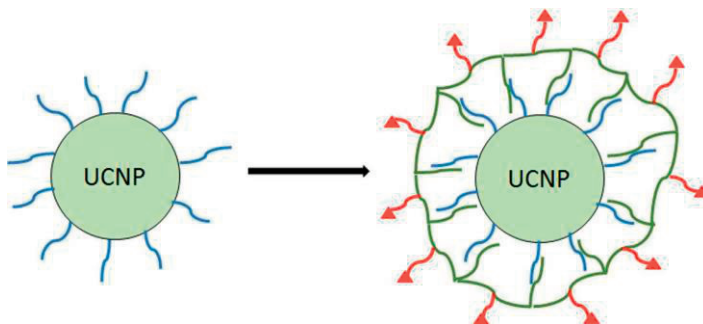


Figure 9. Simplified surface functionalization scheme of oleic acid capped upconverting nanoparticles via ligand interactions using amphiphilic polymers having hydrophobic and hydrophilic chains. (Modified from Sedlmeyer et al.²¹⁴)

Silica coating

In bioanalytical applications growing a silica shell on the surface of the particles is a widely used method due to its biocompatibility and minimal effect on the nanoparticles' optical properties (Figure 10).^{26,198,215,216} Silica is chemically inert and hydrophobic which helps dispersing the nanoparticles in aqueous environment.^{198,217} Also the rigidity of the silica layer can be altered by altering the functional groups used in growing the silica shell²⁶ and the thickness of the layer by varying the amount of used silicate (usually tetraethyl orthosilicate, TEOS) in the reaction.^{60,67}

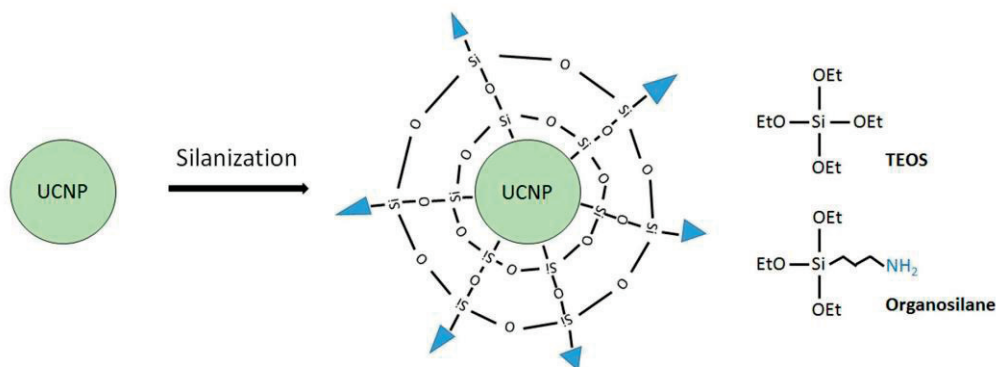


Figure 10. Simplified scheme of surface silanization of upconverting nanoparticles. (Modified from Wang et al.²⁶)

Both hydrophobic and hydrophilic particle surfaces can be modified with silica coating using different techniques. For hydrophilic surfaces the Stöber process is used where the silica shell is grown from tetraalkyl orthosilicate monomers and hydrolyzed in the presence of ammonia in an alcoholic solvent.²¹⁸ The method results in an inert silica shell which can then subsequently be activated by silanization reactions to produce binding sites for biomolecules with different functional groups depending on the protocol used.^{26,214} It is also possible to functionalize the silica shell simultaneously during the shell growth period.⁶⁰ For the hydrophobic particle surfaces a microemulsion method has to be applied. In this method reverse micelles are formed in the presence of a detergent in a nonpolar solvent containing UCNPs. The silica shell is grown on the particle surface inside the micelles and the reaction is started by adding ammonia.²¹⁹ Also the functionalization of the silica layer made by the microemulsion method can be made after the first shell growth or during it.

While there are many advantages in growing a silica shell on the particle surface there are limitations and things to consider when doing so.²¹⁴ Because of the shell growth methods, it is possible that multiple particles can be enclosed in one silica shell making them more polydisperse than anticipated. In addition, for each nanoparticle size range used the buffer system with pH and ionic strength have to be adjusted separately as the silica coating is able to induce agglomeration. Also the undesired non-specific binding to biomolecules can be enhanced using silica a shell. This produces false positives in biomedical applications.

Layer-by-layer deposition method

The layer-by-layer (LbL) method is based on self-assembled layers of polyanions and polycations which are attached to each other subsequently by electrostatic interactions.^{220–222} The manufacturing of the bilayers consists of simple cycles of introducing the desired template to an oppositely charged polyionic liquid. This is followed by washing steps before again introducing the subsequent polyionic liquid. The method is widely used for producing thin films on a flat surface but also nanoparticles have been used as a template for layer growth.^{223–225} Multiple parameters control the formation of the bilayer structure obtained from the LbL method such as pH and ionic strength of the solutions, deposition temperature and the counter ions used to adjust the ionic strength.^{221,226,227}

To be used in the surface modification of UCNPs the layer-by-layer method requires a charged surface where the layer deposition can take place. Positively charged poly(allylamine) hydrochloride (PAH) and negatively charged poly(sodium-4-styrenesulfonate) (PSS) have been studied with UCNPs for helping the bioconjugation through the amine groups of PAH¹¹⁸ as well as improving the use of UCNPs in aqueous environments by enhancing the dispersibility.⁴² While the use of different (co-)polymers on the UCNP surface has been researched widely the use of multiple layers and the layer-by-layer method has not gained that much attention.

2.4.2 Bioconjugation

In biomedical applications such as imaging, photodynamic therapy and different kind of assays bioconjugation is required between the luminescent label used and the specific biomolecules that are being detected. These kinds of biomolecules can be for example biotin, streptavidin, folic acid, different antibodies and DNA/RNA.²¹⁴ The biomolecules can attach to the UCNPs directly via non covalent forces like in the ligand exchange process. However, the indirect binding with functional groups through covalent bond creation is more used due to its better stability.

Direct binding

Some biomolecules are able to bind directly on the bare UCNP surface through electrostatic interactions with their charges. Folic acid has two carboxyl groups that are able to interact with the positive UCNP surface while leaving the folic acid receptor binding site free.¹⁸⁵ Also streptavidin is able to attach on the nanoparticle surface as its net charge is negative.²¹¹ If the streptavidin on the UCNP surface is accompanied with a PEG chain the non-specific binding and aggregation of the coated UCNPs is decreased. In addition, the hydrophobic oleic acid coated UCNP can be used in some cases, such as using DNA whose phosphate groups are able to attach on the lanthanides on the UCNP surface while the DNA strand remains free in close contact with the OA chain.²²⁸ The DNA is then able to attach on the desired target structures.

Indirect binding

The indirect binding refers to the binding of biomolecules on the surface modifications through covalent bonds. Many biomolecules such as antibodies, proteins or peptides, folic acid, streptavidin, and biotin can be bound to the UCNPs through their carboxylic and amine groups.²²⁹⁻²³¹ The binding is done through an EDC coupling reaction (where EDC is 1-ethyl-3-(3-dimethylaminopropyl)-carbodiimide) which activates the carboxyl group in the surface modifications and couples it to primary amines.²³² N-hydroxysulfosuccinimide (Sulfo-NHS) can then be used to form an amine bond with the desired biomolecule. Less common functional groups such as thiols can be used with maleimides for site specific labeling and using lectins as a component it is possible to bind selectively to carbohydrates.¹³⁹

A one-step approach using bispecific antibodies (BsAb) conjugating with methoxy polyethylene glycol (mPEG) on the nanoparticle surface was demonstrated by He et al.⁵¹ The BsAb preparation is more complicated than that of the widely used Immunoglobulin G (IgG) antibodies, but the conjugation time was shortened significantly (from two days to 30 min mixing). In addition, the binding efficiency between biomolecules was better because of the unblocked binding domains due to less steric interference.

3 AIMS OF THE STUDY

The overall aim of this thesis was to develop upconverting nanoparticles suitable for biomedical use. This meant optimizing the synthesis protocol to produce uniform nanoparticles with efficient upconversion luminescence. The purpose of introducing the layer-by-layer method for the surface modification of the NaYF₄ UCNPs was to study the manufacturing and formation of the bilayer coating on the surface and its effect on the UCNPs optical properties. Depending on the components used in the bilayer formation the method could enable shifting the excitation wavelength of the nanomaterials and/or enable less processing steps during the bioconjugation because of the attaching sites on the polyelectrolytes. Finally it was studied if the coating using bilayers could also protect the disintegration of UCNPs in the aqueous environment.

More specifically, the aims of the individual studies were:

- I** To produce upconverting nanoparticles with a desired size and shape with high upconversion luminescence intensity. To study how selected synthesis parameters affect the repeatability of the upconversion product.
- II** To study if the layer-by-layer method combining polyelectrolytes and metal ions could be used in the surface modification of upconverting nanoparticles. In addition the use of neodymium as metal ion was studied for the 808 nm excitation of the upconversion luminescence.
- III** To deepen the knowledge of the layer-by-layer method using polyelectrolytes and metal ions by studying the effect of polyelectrolyte length on the surface properties and the upconversion luminescence. In addition, optical detection of possible disintegration of the coated nanoparticles in aqueous environments was studied.
- IV** To study the manufacturing of poly(acrylic acid)/polyallylamide hydrochloride bilayers on the upconversion nanoparticle surface. The effect of the coating and their thermal crosslinking to upconversion luminescence intensity and to the disintegration of the coated nanoparticles in aqueous environments was studied.

4 SUMMARY OF MATERIALS AND METHODS

Full details of the materials and methods used in the thesis can be found in the original publications (I-IV). A brief summary of the materials and methods is described here.

4.1 Preparation of UCNPs

All materials in this thesis were prepared using the modified synthesis method obtained from Wang et al. to produce $\text{NaYF}_4:\text{Yb}^{3+},\text{Er}^{3+}$ nanoparticles ($x_{\text{Yb}}: 0.17, x_{\text{Er}}: 0.03$).⁴³ In this procedure (Figure 11) rare earth chlorides in methanol solutions were added in desired stoichiometry into a two-neck flask containing 1-octadecene and oleic acid. This solution was then heated to and maintained at 160 °C for 40 minutes in an inert atmosphere. After heating, the solution was cooled down to room temperature and a methanol solution containing the desired amounts of NH_4F and NaOH was added and the resulting solution was stirred for 30 min. The solution was then again heated to and maintained at 310 °C for 90 minutes before cooling down.

The obtained products were then precipitated with the addition of ethanol and collected after centrifuging. The products were washed multiple times with ethanol and dried at room temperature in a vacuum desiccator.

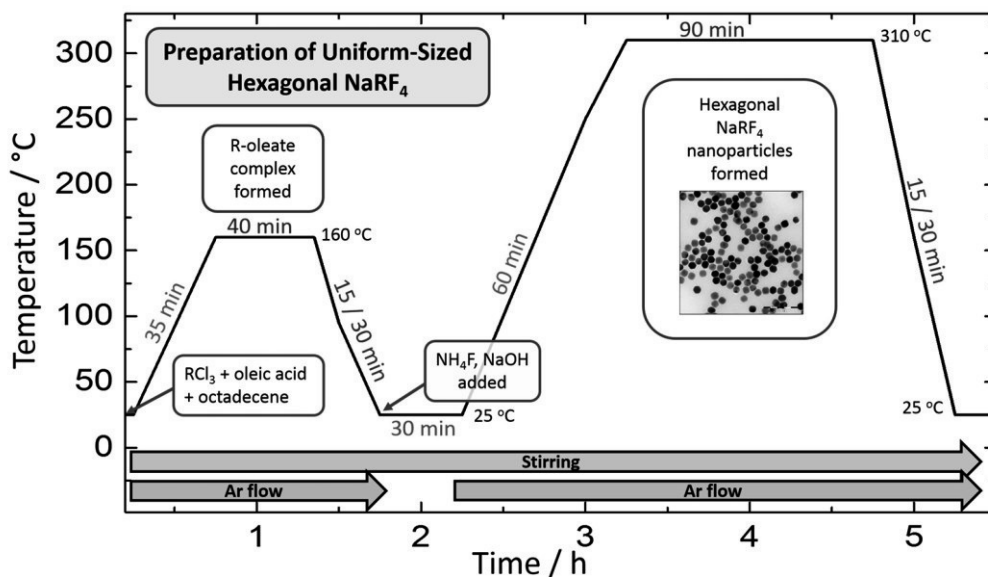


Figure 11. Schematic presentation of the synthesis protocol used in producing uniform hexagonal NaRF_4 (R: Y, Yb, Er) UCNPs (I).

The parameters of the synthesis were studied in a following manner. The inert argon flow was modified to be either 1, 2 or 3 dm^3h^{-1} , the cooling time was adjusted to 15 or

30 minutes and the stirring rate 125, 250, **375**, 500 or 625 rpm (**I**). When one of the parameters was changed the others were kept constant (**bold**). In other publications (**II-IV**) the parameters were kept constant (**bold**) when manufacturing the UCNPs.

4.1.1 Surface modifications of UCNPs

Removing the oleic acid surface

For surface modification the surface capping oleic acid ligands were removed with a procedure modified from Bogdan et al. and Mei et al.^{200,233} In the procedure the dried UCNPs were suspended in an ethanol solution whose pH was adjusted below 2 with HCl. This suspension was ultrasonicated and the UCNPs were collected via centrifugation. The procedure was repeated twice to ensure the removal of OA and the bare UCNP particles were dried for further use.

Layer-by-layer modification of the UCNP surface

A layer-by-layer coating cycle of the UCNPs involved introducing the dry core particles (*ca.* 50 mg) into the desired aqueous coating solution (total volume 1 ml). Poly(acrylic acid) or polyphosphate was used as the negatively charged component and either lanthanide ions as chlorides (neodymium, yttrium, ytterbium and erbium) or poly(allylamine hydrochloride) as the positive component. The ionic strength of the solution was adjusted with NaCl. The suspension containing the charged coating component was ultrasonicated and then collected via centrifuging. The products were then washed twice with water to remove the unattached material. All of the charged layers were deposited with a similar procedure until the desired number of bilayers was obtained. After the final layer the coated UCNPs were dried.

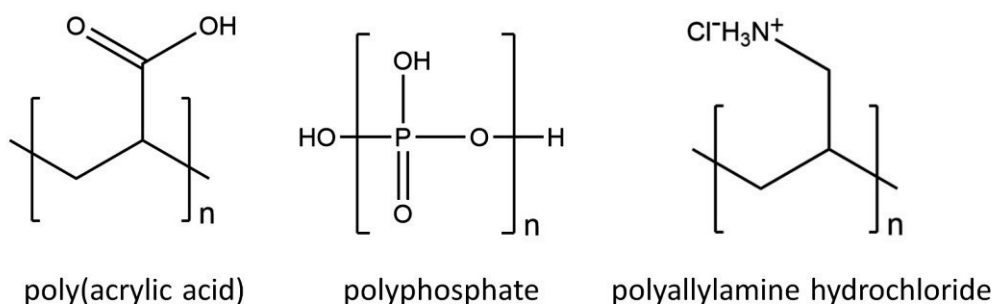


Figure 12. The polyelectrolytes used in the layer-by-layer modifications.

The coating process with long chain PAA and PP with varying ionic strength (0.05, 0.1 and 0.2 M NaCl) of the polyelectrolyte solution was studied in addition to varying the positive ion (Nd³⁺, Y³⁺, Yb³⁺ and Er³⁺) used in publication **II**. After that the coating process was studied with varying lengths of polyelectrolytes using Nd³⁺ as the positive ion (**III**).

The bilayer buildup using polyelectrolytes PAA and PAH was studied with two ionic strengths (0.1 and 0.2 M) of the polyelectrolyte solution in publication **IV**. When the coating was performed in the presence of additional fluoride with ionic concentration of 0.1 M NaCl the procedure was similar to that described earlier but 10 mM of NaF was added into all of the solutions used including the water used in washing (**IV**).

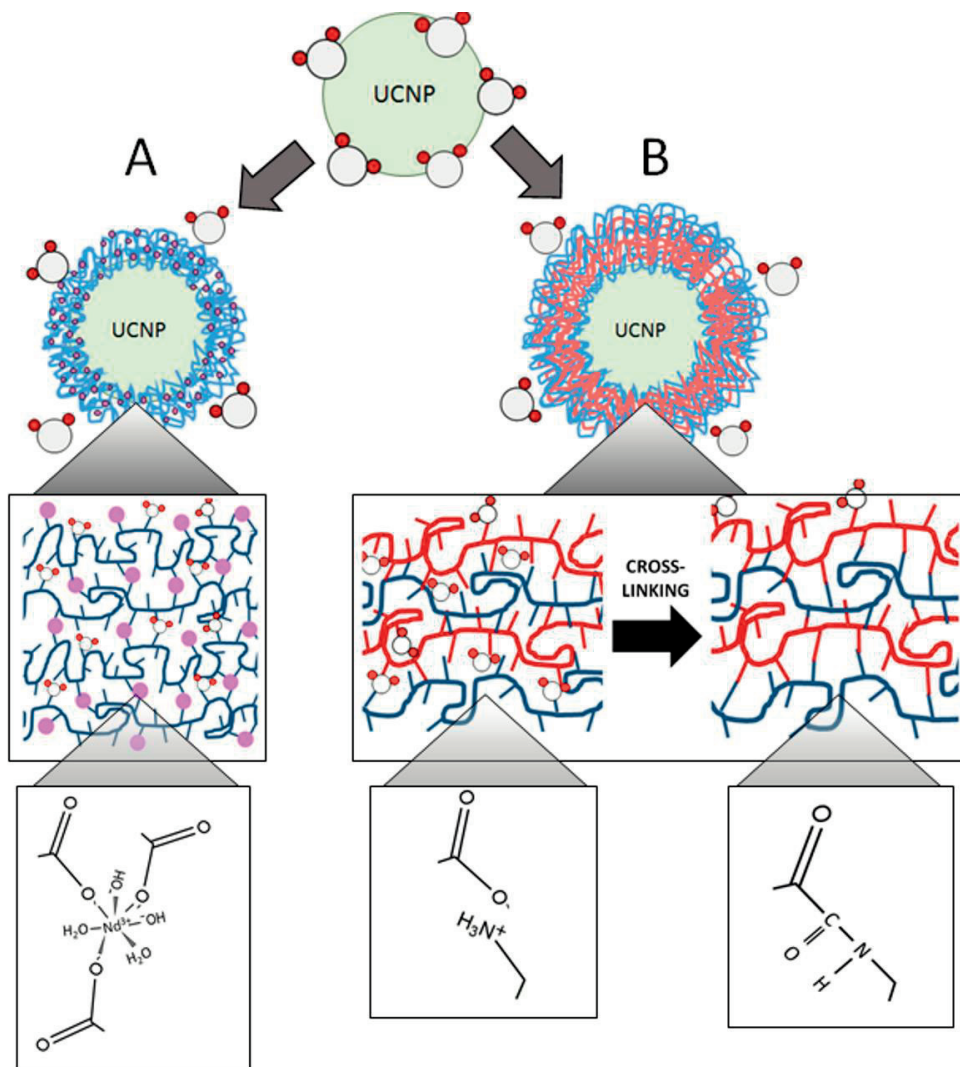


Figure 13. Schematic and not in scale presentation of the manufactured layer-by-layer assemblies of polyelectrolyte/metal ion (A) and polyelectrolyte/polyelectrolyte (B) combinations on the UCNPs with the presence of water molecules.

Crosslinking of the PAA/PAH bilayers

When PAA and PAH were used in coating the nanoparticles it was possible to further strengthen the bilayer formation by crosslinking the polyelectrolyte chains (**IV**). The crosslinking was performed in a nitrogen atmosphere at 180 °C (step 2 °C/min) for two hours to ensure the peptide bond between COOH and NH₂. The crosslinking between the polyelectrolytes used is expected to increase with increasing temperature but with the methods used here no specific degree of crosslinking can be estimated.^{234,235}

4.2 Characterization

4.2.1 Particle structure, size, morphology and uniformity

Transmission electron microscopy (TEM)

UCNPs were dispersed into diluted toluene (**I**) or ethanol (**II-IV**) and a drop of the suspension was dried on a copper grid when acceleration voltage of 120 kV was used. With low voltages a graphene oxide coated copper grid (40 kV) (**II**) or a laced carbon copper grid (60 kV) was used (**III-IV**). The grids were imaged with a Tecnai 12 Bio Twin transmission electron microscope equipped with a CCD camera (**I**) or with a JEM-1400 Plus transmission electron microscope using an OSIS Quemasa 11 Mpix bottom mounted digital camera. (**II-IV**)

Average particle diameters were calculated (**I-II**) and images processed using ImageJ software version 1.43s (<http://rsb.info.nih.gov/ij>).²³⁶

X-ray powder diffraction (XRD)

The UCNP particles' crystal structure was determined at room temperature using a Huber G670 image plate Guinier camera (Cu K_α radiation, 1.5406 Å) at 2θ range of 4-100° (step: 0.005°). Data was collected for 30 min and the image plate was read with 10 scans. The obtained diffraction data was compared with data of known NaRF₄ structures from the ICDD powder diffraction file (entry no. 28-1192 for the hexagonal and 06-0342 for the cubic structure).²³⁷

From the diffraction data the crystallite sizes of UCNPs were estimated using the Scherrer formula (Eq. 1).²³⁸ The reflections used for estimation were (002) and (200) for the crystallite thickness and the width of the hexagonal faces, respectively.

$$d = \frac{0.9\lambda}{\beta \cos\theta} \quad \beta^2 = \beta_s^2 - \beta_r^2 \quad (1)$$

In this equation, *d* is the mean crystallite size (m), *λ* is the X-ray wavelength (m), *β* (rad) the full width at half maximum (FWHM) of the chosen reflection and *θ* (°) half of the Bragg's angle (2θ). Instrument induced reflection broadening was eliminated

from the β_s value by using a micro crystalline reference (β_r (rad)) and the commercial microcrystalline PTIR 550/F material ($\text{NaYF}_4:\text{Yb}^{3+},\text{Er}^{3+}$) was used for this purpose.

4.2.2 Surface properties and elemental composition

FT-IR spectroscopy

The removal of oleic acid from the surface as well as the surface modifications with polyelectrolytes were studied using Fourier transform infrared spectra (FT-IR). The spectra were measured using a Bruker Vertex 70 with a MVP Star Diamond setup with the desired number of scans (32 or 256) at region 450–4000 cm^{-1} . The resolution of the measurements was 4 cm^{-1} .

Reflectance spectroscopy

Optically active ions (rare earths) present at the UCNPs surface were studied using reflectance spectra measured with an Avantes Avaspec 2048×14 fiber spectrometer. The spectra were measured at 350–1000 nm using an integration time of 400 ms and averaging 30 scans. An incandescent lamp of 60 W was used as a light source during the measurements.

Thermal analysis (TGA)

The thermal behavior of the UCNPs and their surface modifications were studied using a TA Instruments STD Q600 TGA-DSC apparatus. The measurements were made between 35–600 °C in a flowing air atmosphere using a heating rate of 10 °C/min.

X-ray fluorescence spectroscopy (XRF)

The elemental compositions of UCNPs were investigated using X-ray fluorescence spectroscopy (XRF) with the PANalytical Epsilon 1 apparatus using its internal Omnic calibration.

Zeta potential

The surface properties of the UCNPs were studied with zeta potential measurements using the Malvern Zetasizer Nano-ZS equipment. The concentration of the aqueous dispersions was 100 $\mu\text{g}/\text{ml}$ with pH *ca.* 6.

4.2.3 Luminescence properties

Upconversion luminescence

The upconversion luminescence spectra using 970 nm excitation were measured at room temperature. The dry nanomaterials were held inside a rotating capillary tube. After the excitation the desired band pass filters were used before and after the sample

and the emission was collected at a 90° angle and directed to the spectrometer with an optical fiber. The lasers and spectrometers used were Hamamatsu L9418-04 (976 nm) with Ocean Optics PC2000-CCD (I) and Optical Fiber Systems IFC-975-008-F (973 nm) or Wave spectrum WSLX-808-004-H (808 nm) with Avantes Avaspec HS-TEC (II-IV).

Downshifted luminescence

The downshifted luminescence emission and excitation spectra were collected with a Varian Cary Eclipse spectrofluorometer. Phosphorescence mode with a 0.1 ms delay and a 0.5 ms gate time was used to record the spectra.

Decay measurements for upconversion luminescence

For dry nanomaterials (I) the decay measurements for green and red upconversion luminescence were measured using a modular luminometer creating a square-wave excitation pulse profile for the laser (IFC-975-008-F, 973 nm). The obtained emission was collected to a PMT and amplified in a high-speed current amplifier and then collected with an A/D converter connected to a computer. The pulse profile consisted of a 20 ms excitation pulse followed by a 30 ms measurement time before the next pulse.

The measurements in aqueous media (III) were measured using 980 nm excitation and a lifetime measurement mode with a modified Plate Chameleon fluorometer.¹³⁸ The decays were measured after incubating the nanoparticles for 0, 4 or 24 h in pure water or phosphate buffer (pH 7.75) with or without KF in slow shaking. The concentration of the UCNPs in the measurement was 5 µg/ml and the measurements were made in Greiner polypropylene microtiter plates. The samples were exposed repeatedly to 2 ms pulsed excitation and the emissions were collected using a 535/40nm band-pass filter.

The data obtained from decay measurements was analyzed using two or three exponential decay components to obtain reasonable fits in Origin 2015 software (OriginLab, Northampton, MA).

4.2.4 Disintegration of the UCNPs

The disintegration of the nanoparticles was studied both with optical detection (III) and with a fluoride selective electrode method (IV). The optical detection from the nanoparticles suspended in aqueous media is described in the paragraph “*Decay measurements for upconversion luminescence*” in Section 4.2.3.

The fluoride ion selective measurements were carried out using a fluoride selective electrode and a reference electrode. A known amount of nanoparticles were suspended in 1 ml water (with or without additional fluoride) and sealed in a dialysis tube (MWCO 3500). Then the dialysis tube with its contents was introduced into an

Summary of materials and methods

aqueous solution of 0.1 M NaNO₃ (with or without additional fluoride, total volume 50 ml). The data was collected automatically in one minute intervals during the measurement period.

5 SUMMARY OF RESULTS AND DISCUSSION

5.1 Structure and uniformity of UCNPs

To fully exploit the use of the UCNPs in for example biomedical applications and imaging they have to be uniform in the desired size and shape in order to produce repeatable and similar binding sites to biomolecule conjugation. In addition they should produce efficient visible upconversion luminescence under near-infrared radiation. The synthesis method using oleic acid and 1-octadecene in high temperatures was chosen for this study because of its possibility to produce such desired uniform nanoparticles.

5.1.1 Crystal structure and phase purity

The crystal structure of the synthesis products was verified with XRD measurements and possible impurities remaining from the synthesis were identified. The products were distinguished between the hexagonal (β)- $\text{NaYF}_4\cdot\text{Yb}^{3+},\text{Er}^{3+}$ and the cubic (α) structure.²³⁷

Publication I is focused on the parameters of the synthesis procedure to obtain pure structured and uniform UCNPs. The crucial parameter in the synthesis affecting the crystal structure was found to be the flow rate of the inert gas (Figure 14). This suggested that when the gas flow was too slow it was unable to remove the evaporating gaseous products (H_2O , CO_2 , HCl) from the synthesis flask. This results in the formation of NaCl after the addition of the methanol solution containing the needed sodium and fluoride. However, when the sodium reacts to form NaCl it is unavailable for the formation of hexagonal UCNPs which needs more sodium in the structure than cubic one.²¹ The length of cooling period or the stirring rate did not have any effect on the obtained crystal structure.

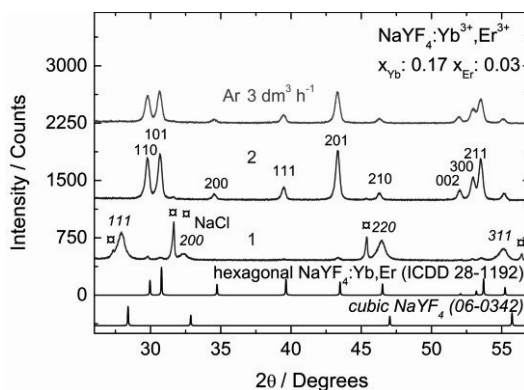


Figure 14. XRD patterns with hexagonal and cubic NaYF_4 reference patterns²³⁷ of the UCNPs prepared with argon flow of 1, 2 and 3 dm^3/h . (I)

The synthesis parameters that produced most efficient and uniform materials were used in the syntheses for the core materials of the publications **II-IV**. The parameters used are mentioned in the section 4.1. of this thesis. The obtained hexagonal NaYF₄:Yb³⁺,Er³⁺ UCNPs did not have any visible cubic impurities. However, regardless of the efficient gas flow, a small varying amount of NaCl could be found in some of the materials depending on the synthesis setup used.

5.1.2 Particle size and morphology

The particle size of the UCNPs was estimated from the XRD data with the help of the Scherrer equation.²³⁸ For the only cubic material the size estimation was 17 nm and for the large hexagonal prepared with 15 min cooling the size was 58 nm. For the rest of the hexagonal materials the average crystallite size was *ca.* 25±3 nm. **(I)** The particle size obtained from the TEM images in publication **I** was overall larger than that obtained from the XRD data. This was expected as the values from the Scherrer equation are based on the size of the diffracting domain instead of the actual particle size even though it gives a rough estimation of the size relations between materials when they are single crystals with a size of less than 100 nm. For the UCNPs used in other publications the average crystallite sizes calculated from the Scherrer equation were *ca.* 26±2 **(II)**, 24±2 **(III)** and 23±2 nm **(IV)**.

The morphology of the produced nanomaterials varied significantly when the synthesis parameters of gas flow and cooling period were modified as seen on the Figure 15 **(I)**. With the inert gas flow this is due to the structural differences of the nanomaterials but when the length of the cooling period is considered the reason for the wide range of size and morphology distribution is unclear. It could be that the faster cooling might interfere with the Ostwald ripening process producing a wider range of sizes as the β -NaYF₄ are formed from the α -NaYF₄ seeds formed during the first stages of second heating process.^{44,46,239}

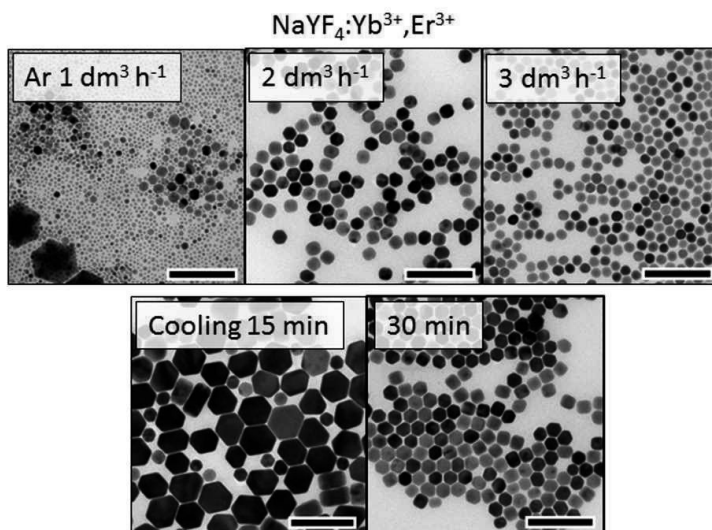


Figure 15. TEM images of the UCNP materials prepared with selected synthesis parameters argon flow of 1, 2 and 3 dm³/h and cooling of 15 and 30 minutes. The scale bar is 100 nm. (I)

When the synthesis parameters were held constant the obtained nanomaterials were uniform in morphology and their size in TEM was found to be slightly larger than obtained from the XRD calculations as expected (Figure 16).

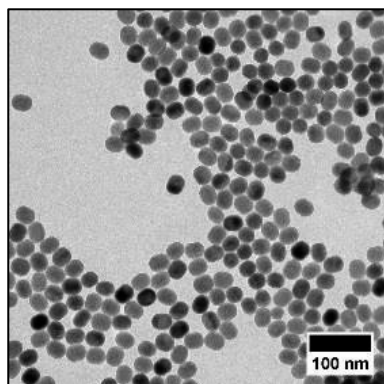


Figure 16. TEM image of the NaYF₄:Yb³⁺,Er³⁺ core material used in the publication II. The scale bar is 100 nm. (II)

5.2 Surface modification of UCNPs

The use of upconverting nanoparticles is greatly dependent on the possibility to modify their properties. The as-prepared UCNPs from the syntheses made in organic

solvents are commonly capped with oleic acid (OA) ligands and the UCNPs are not dispersible to water. For further use surface modifications must first be made to make the UCNPs dispersible in water and then to attach binding sites for biomolecules and linker molecules on the surface if and when they are needed for example in biomedical applications and assays. We studied the use of a simple layer-by-layer method and its behavior in the surface modification of UCNPs using negatively charged polyelectrolytes and positively charged metal ions. In addition layer formation was studied using only oppositely charged polyelectrolytes and their thermal crosslinking to see whether the shielding layers could be made more structured and rigid and thus shielding the particle even more.

5.2.1 Removal of OA capping ligands

The removal of the OA capping ligands from the as-prepared nanomaterials was confirmed by measuring the FT-IR spectra of the nanomaterials (Figure 17). The distinguishable vibrations arising from the surface-attached carboxyl groups ($1400\text{--}1500\text{ cm}^{-1}$) could be seen to disappear after the washing steps.²⁰⁰ Also the vibrations from the --CH groups have nearly vanished suggesting a successful removal of the OA capping ligands.

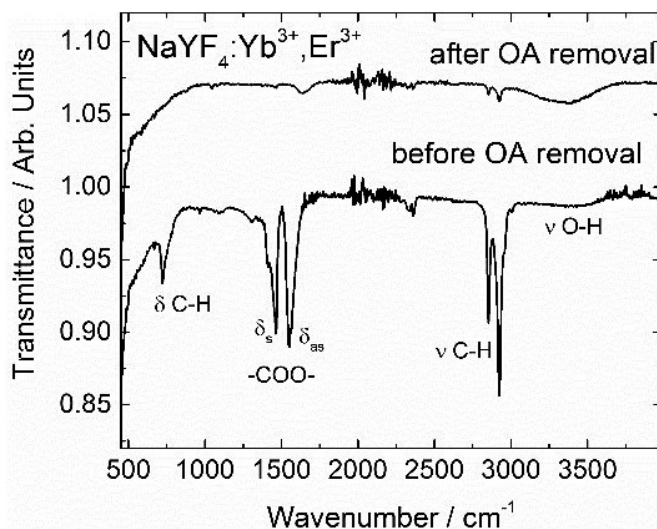


Figure 17. FT-IR spectra of the UCNP materials before and after removing the OA capping ligands from the surface. (II)

5.2.2 Layer-by-layer assembly on UCNP surface

To observe the layer formation in the layer-by-layer assembly various methods had to be utilized due to the varying properties of the layer counterparts that are not visible at the same time in the methods. For instance, the polyelectrolytes show clear vibrations

in the FT-IR spectra but the metal ions used are invisible. On the other hand, the optically active ions can be probed with the reflectance spectroscopy but the polyelectrolytes are invisible in that method.

Layer formation

The polyelectrolytes used in the coating process could be observed with FT-IR spectra because of their specific functional groups (Figure 18). With PAA and PAH the region from 1100 to 1750 cm^{-1} could be distinguished as vibrations arising from the carboxyl (PAA) and CH_2 groups. In addition, the same region should have vibrations from the amine in PAH but it is possible that they are hidden under these stronger vibrations from PAA.^{240,241} When bilayers of PAA/PAH were formed (IV) also an additional vibrational signal from the NH_2 of PAH was observed at 800-900 cm^{-1} in addition to those at the 1100–1750 cm^{-1} region. The vibrations arising from the $(\text{PO}_3)_n$ network in polyphosphate were clearly visible and distinguishable from those of PAA and bare core material vibrations.

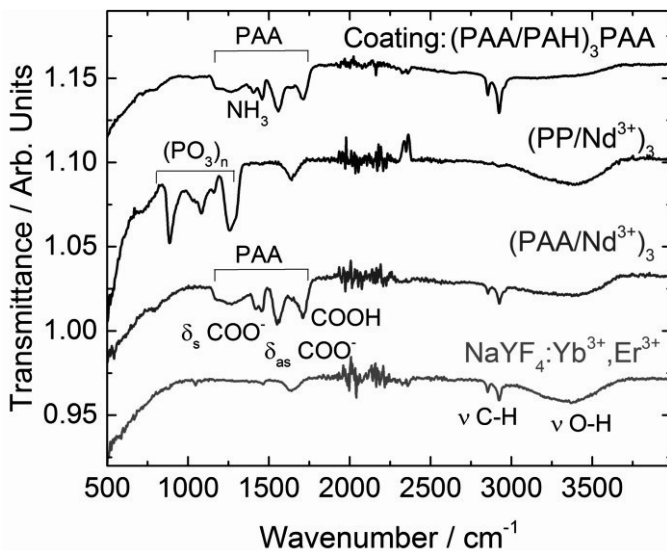


Figure 18. FT-IR spectra of the UCNP core material and UCNPs coated with three bilayers of PAA/PAH, PP/Nd^{3+} and PAA/Nd^{3+} .

Varying the ionic concentration (II) or the polyelectrolyte length (III) did not have a significant effect on the obtained FT-IR spectra. In some cases in the first bilayer no vibrations from the polyelectrolytes were present. With some materials the vibrations seemed to increase in intensity with the increasing number of bilayers. However, FT-IR measurements were made to distinguish the polyelectrolytes and were not quantitative so no clear conclusions could be drawn if the amount of polyelectrolyte was increasing with the number of bilayers.

One crucial method for observing layer formation was reflectance spectroscopy. It could be used to probe the surface of the nanomaterials when optically active ions were used. The ytterbium and erbium at the core are optically active and can be distinguished from each other due to their absorption at 980 nm and 490, 520, 540, 650 and 800 nm, respectively. After forming bilayers using neodymium ions a significant change could be observed in the reflectance spectra as the absorption from neodymium was seen at 575, 740, 975 and 870 nm. When the reflectance spectra were normalized to the ytterbium absorption (present only at the core) it could be observed that the neodymium absorptions are increasing in intensity with the increasing number of bilayers.

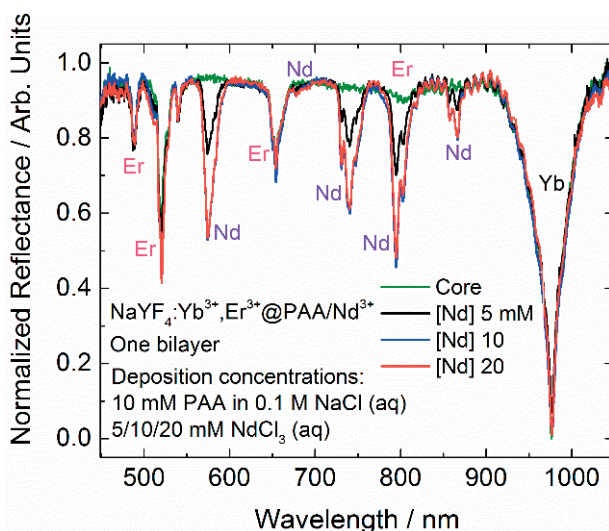


Figure 19. Reflectance spectra of the UCNPs coated with one bilayer of PAA/Nd³⁺ using different Nd³⁺ concentrations and M_w(PAA): 100,000. (II)

Differences could also be seen in the neodymium absorption when the coating was done with a varying concentration of neodymium and polyelectrolyte solutions (Figure 19, II). This is expected because the polyelectrolyte chain can only host a certain amount of positive ions and increasing the neodymium concentration does not increase the amount of ions attaching to the polyelectrolyte. This is due to the fact that the percentage of the open attaching sites is expected to be similar when the pH and ionic concentration of the polyelectrolyte solutions are held constant. A similar effect could be observed with the bilayers manufactured with varying lengths of polyelectrolytes (III).

Thermal analysis was used to study the layer formation as the PAA can be easily removed from the particle surface with heating and could be observed as an increasing mass loss in the process. PP however is not affected by heating in the range of the experiment and it was expected that the presence of PP on the nanoparticle surface

could be observed as a mass gain during the measurements (II). Especially with the materials having up to five bilayers the TGA showed an increase in the weight loss with the increasing number of bilayers (Figure 20). Thermal analysis was also performed to materials with half a bilayer and the structure of the weight loss curve suggested a successful buildup of the bilayer coating. The complementary neodymium layer to produce the bilayers was seen to slightly decrease the weight loss and the sequential PAA layer again increased the weight loss. With the lower number of bilayers the changes were not so clear suggesting that the layer formation might not be fully balanced and that the layers are formed in a step-like manner (III). In addition, the evaporation of the interlocked water molecules in the bilayer structure had a major influence on the shape of the TGA curves. With the materials coated using PAA/PAH up to 5.5 bilayers a similar formation with the interlocked water was observed from the TGA regardless of the ionic concentration of the polyelectrolyte solution used (IV).

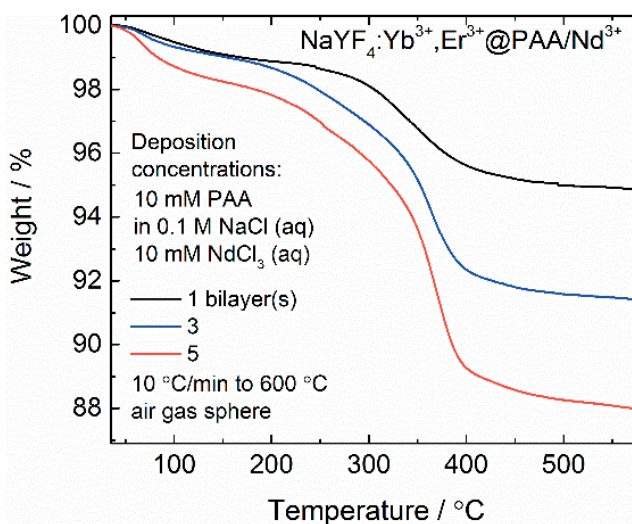


Figure 20. Thermal analysis curves of the coated UCNP materials prepared with $\text{PAA}/\text{Nd}^{3+}$ layers using $M_w(\text{PAA})$: 100,000. (II)

When the thermal behavior was studied between 200 and 500 °C with either $\text{PAA}/\text{Nd}^{3+}$ or PAA/PAH coating to remove the effect of interlocked water, it was observed that the bilayer is most probably formed in a step-like manner and not linearly within the first three bilayers. At five bilayers the mass drop was observed to be similar regardless of the deposition conditions used.

In addition to these methods also XRF analysis was used to study the increase of the concentrations of lanthanide ions and phosphorus in the materials where they were used. The obtained relative results from XRF agreed with other measurements confirming the successful bilayer formation. However, with a small number of

bilayers no phosphorus was observed even though FT-IR spectra show polyphosphate present in the materials, so the first bilayers might be too close to the equipment's detection limit with phosphorus as it is much a lighter element in comparison with the lanthanides.

Surface properties

Zeta potential measurements were used to observe changes in the core material surface after the bilayer formation and to confirm the buildup of the coating. The zeta potential of the core materials was positive varying from 10 to 30 mV depending on the core material used. The variation in the core materials' zeta potential suggests that there were varying amount of impurities such as OH^- on the surface on different core materials. When the bilayer was formed on the surface the zeta potential started decreasing. After three bilayers the decrease in the zeta potential was *ca.* 25–30 mV from the core material and with the materials having five bilayers *ca.* 35–40 mV (II-IV). The decrease and behavior of the zeta potential was similar regardless of the bilayer type.

From the zeta potentials measured with half a bilayer from the buildup of $\text{PAA}/\text{Nd}^{3+}$ layers on the UCNP surface the step-like increase in the coating is observed (Figure 21). The positive charge from neodymium ions is unable to overcome the full negative charge from PAA during the formation (II). However, there are enough attaching sites for the next negatively charged PAA to continue the layer formation. A similar step-like formation can be observed from the coatings manufactured with selected PAA lengths (III).

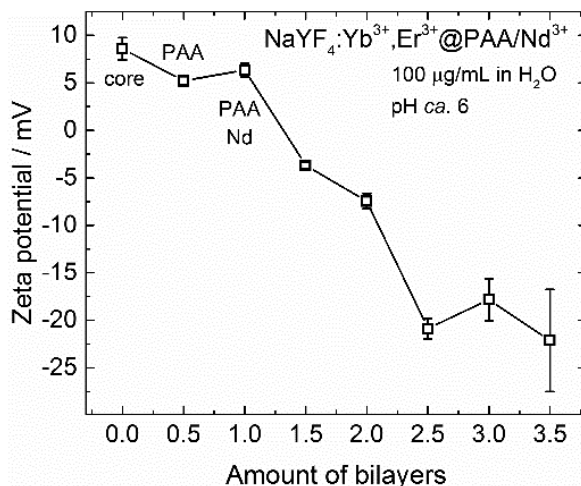


Figure 21. Development of zeta potential of $\text{NaYF}_4:\text{Yb}^{3+},\text{Er}^{3+}$ material coated with $\text{PAA}/\text{Nd}^{3+}$ bilayers ($M_w(\text{PAA}): 100,000$). (II)

In addition, TEM imaging was used to probe the particle surface to see if the coating can be observed (Figure 22). For this, the UCNPs were suspended into ethanol and dried on a graphene oxide grid (**II**) or a laced carbon grid (**III-IV**) instead of a copper grid to ensure a better contrast to probe the lighter organic structure on the surface. When these grids were imaged with a lower accelerating voltage the organic materials on the surface could be more distinguishable. From the TEM image it is clear, that some kind of changes have occurred on the particle surface, since it is becoming blurry and unstructured. Also especially with images taken with laced carbon grids some clear surface barrier can be seen from the coating.

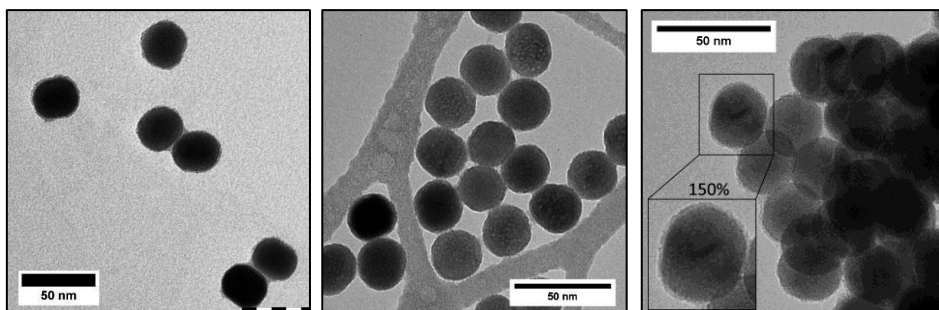


Figure 22. TEM images of the coated UCNPs with three (PAA/Nd³⁺) bilayers taken on graphene oxide grid with 40 kV (**II**, left $M_w(\text{PAA})$: 100,000) or laced carbon grid with 60 kV (**III**, center $M_w(\text{PAA})$: 2,000) and coated UCNPs with 5.5 bilayers of PAA/PAH (**IV**, right). Scale bars are 50 nm and the inset zoom 150 %.

Crosslinking of polyelectrolyte layers

The crosslinking of the PAA/PAH bilayers was tested with two temperatures (180 and 200 °C) and confirmed with FT-IR measurements. With both temperatures the crosslinking was successful but as the upconversion luminescence intensity was better with the 180 °C crosslinked material it was chosen as the crosslinking temperature for the studied materials. It was also considered that 200 °C might be too high of a temperature as the PAA starts to decompose already after that temperature.

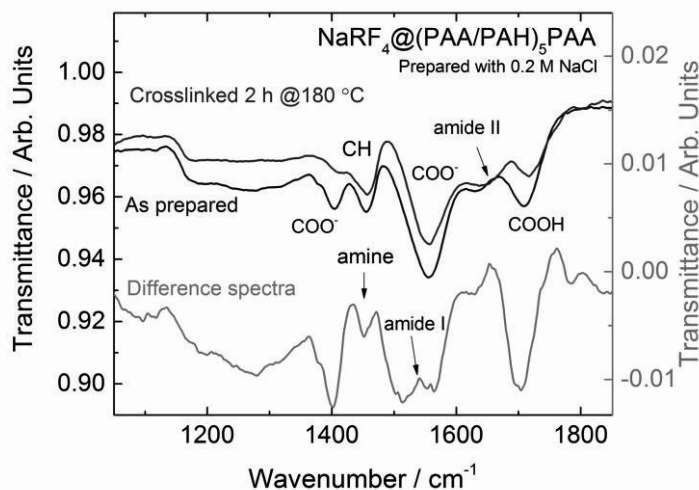


Figure 23. FT-IR spectra of the as-prepared and crosslinked coated nanomaterials prepared with ionic concentration of 0.2 M NaCl and their difference spectra. (IV)

With the different number of PAA/PAH bilayers the crosslinking was observed and the changes in the FT-IR spectra could be seen in the difference spectra as a reduction of the PAA-related COO^- and COOH vibrations as well as a slight increase in the amide peaks (Figure 23). However, as the outermost PAA layer is not taking part in the crosslinking its characteristic vibrations were clearly visible in the FTIR spectra even though they decreased.

The zeta-potential of the crosslinked materials was decreasing with the increasing number of bilayers. Also with the first bilayers the crosslinked zeta-potential is considerably lower than that of an unlinked material. With the increasing number of bilayers this difference becomes smaller. This suggests that crosslinking creates a more defined structure on the surface in comparison with the unlinked coating of the UCNPs by removing the positive charge inside the bilayers.

5.3 Upconversion luminescence properties of UCNPs

The most important property of the upconverting nanoparticles is, of course, their exceptional luminescence. The energy transfer upconversion process is delicate and prone to losing its efficiency due to intrinsic impurities as well as the impurities from the surface and the surrounding environment. In the current study the main focus was obtaining the most efficient upconversion luminescence from the small nanosized particles and then preserving the luminescence after the surface modifications. In

addition, measurements were made to see if the luminescence could be maintained after the UCNPs are introduced into aqueous environments.

5.3.1 As prepared UCNPs

All of the as prepared $\text{NaYF}_4:\text{Yb}^{3+},\text{Er}^{3+}$ nanoparticles had the desired upconversion luminescence from Er^{3+} in green ($515\text{--}560\text{ nm}$; $^2\text{H}_{11/2}, ^4\text{S}_{3/2}\rightarrow^4\text{I}_{15/2}$) and red ($640\text{--}685\text{ nm}$; $^4\text{F}_{9/2}\rightarrow^4\text{I}_{15/2}$).

As expected, the structure of the UCNPs was crucial for the upconversion luminescence intensity. The cubic UCNPs have poor upconversion luminescence in comparison to that obtained from hexagonal structured materials (Figure 24, I). In addition to the structure the size of the UCNPs had a significant effect on the upconversion luminescence intensity because of the larger surface area in the small nanoparticles. However, in some of the materials the upconversion luminescence intensity was not directly correlated on the size or structure. The higher upconversion luminescence intensity of the same-sized materials is possibly due to cation disordering and the possibility of optically active rare earth ions replacing Na^+ in the Na_2/R cation site of the hexagonal structure making the pathway for energy transfer to erbium ions more efficient.²³

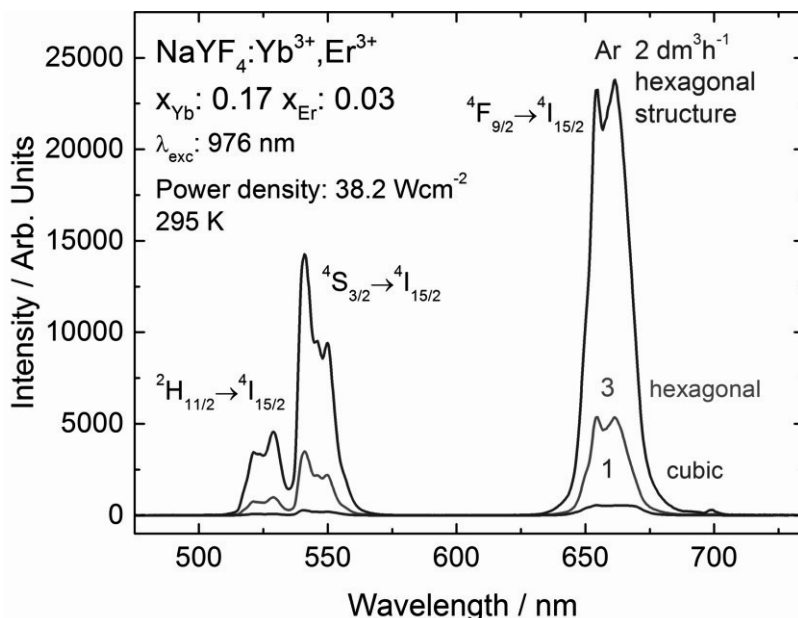


Figure 24. Up-conversion luminescence spectra of the $\text{NaYF}_4:\text{Yb}^{3+},\text{Er}^{3+}$ nanomaterials with argon flows of 1, 2 and $3\text{ dm}^3\text{h}^{-1}$ (I).

When the upconversion emission is plotted against excitation power density in log-log scale its linear fit gives information about the upconversion mechanism behind the

emissions. With the UCNPs having capped oleic acid on the surface (**I**) the obtained slopes for green emission were between 1.7–1.9 and for red emission 1.7–2.2. For the core materials without oleic acid surface the same slopes were 1.7–2.5 and 2.2–2.7 (**III-IV**). This suggests that the energy transfer requires more photons to produce the upconversion emission.

The upconversion decay measurements of the as prepared oleic acid capped UCNP powder samples were consistent with the emission intensity. The fitted lifetimes were the longest with the materials having the best upconversion luminescence intensity. Also it seemed, that the amplitudes shifted slightly to the second lifetime component with the best materials suggesting that more emission was obtained from the core erbium ions that are shielded more than those on the surface (**I**). The first lifetime component varied between 90 and 260 μs while the second remained close to 400 μs with the green upconversion emission. With the red emission, the corresponding lifetime components were *ca.* 400 and 1000-2000 μs , respectively.

In the publication **III** decay measurements were performed from bare core UCNPs suspended into pure water. The fitted green emission lifetimes obtained from these measurements (70 and 400-600 μs for the first and second component, respectively) correspond well with those obtained in the publication **I** when the probable quenching effect of the environment and the lack of surface protection from OA is taken into account.

5.3.2 Surface modified UCNPs

Materials coated using polyelectrolyte and metal ions

The upconversion luminescence of the surface modified UCNPs was studied in comparison with the core material used for the modifications. From all of the polyelectrolyte/metal coated UCNPs the green and red emissions of erbium ions were obtained regardless of the number of manufactured bilayers. Overall it seemed that the formed coatings were able to enhance the core upconversion luminescence up to a certain number of bilayers until the obtained luminescence intensity decreased again.

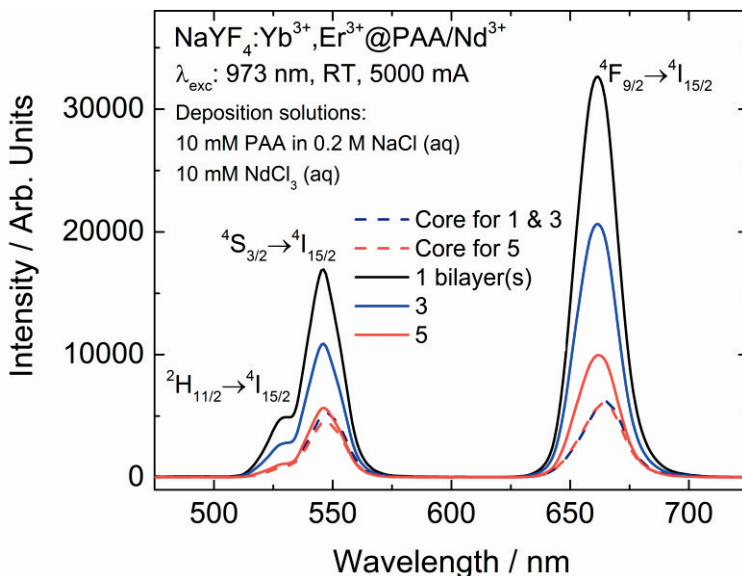


Figure 25. Upconversion luminescence spectra excited with 973 nm of the $\text{NaYF}_4:\text{Yb}^{3+},\text{Er}^{3+}$ nanoparticles coated with $\text{PAA}/\text{Nd}^{3+}$ bilayers prepared with deposition concentrations of 10 mM PAA in 0.2 M NaCl (aq) and 10 mM NdCl_3 (aq) (**II**).

When the ionic concentration of the polyelectrolyte solution was changed it brought differences on the surface coating because the concentration used affects the packing of the polyelectrolytes to a denser or looser structure (**II**). This makes differences in the upconversion luminescence intensity and for example the first bilayer of $\text{PAA}/\text{Nd}^{3+}$ with a 0.2 M ionic concentration of NaCl shields the nanoparticle very effectively and enhances the upconversion luminescence (Figure 25). However, with the increasing number of bilayers this enhancement is lost probably due to the higher amount of interlocked water within the layers. On the other hand, while the enhancement of the upconversion luminescence with $\text{PAA}/\text{Nd}^{3+}$ coating using a 0.1 M ionic concentration is not as strong in the first layers the decrease from the increased number of layers is not significant and the overall enhancement is good.

When the length (and thus M_w) of the polyelectrolyte was varied but the ionic effect and pH of the solutions were kept constant a similar effect was observed (Figure 26, **III**). The first bilayer provides a good shielding for the upconversion emission but with an increasing number of bilayers the water quenching and neodymium absorption are more relevant. However, the upconversion luminescence was also very dependent on the core materials luminescence. Weaker core luminescence was more easily shielded with the coating and if the core luminescence itself was already strong then the enhancement with the shielding was not as easily obtained.

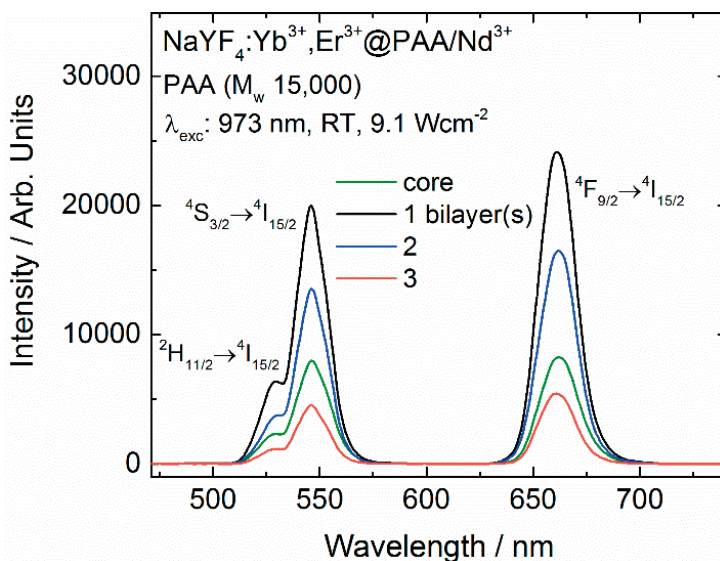


Figure 26. Upconversion luminescence spectra excited with 973 nm of the core and $\text{NaYF}_4:\text{Yb}^{3+},\text{Er}^{3+}@PAA/\text{Nd}^{3+}$ materials coated with PAA M_w : 15,000 (III).

The effect of the polyelectrolyte length and using neodymium in the bilayer structure on the upconversion process was studied with power dependent measurements using 973 nm excitation and powder samples (III). The fitted slopes for green upconversion emission obtained from the log-log presentation of the emission intensity and excitation power were similar to those obtained with oleic acid capping being 1.7–2.1. The slopes obtained for the red upconversion emission were slightly higher than those measured with capped oleic acid but lower than those obtained from bare UCNPs, 2.1–2.4. The increase in the slope of red upconversion luminescence suggests the presence of the three-photon process taking part in the upconversion emission.^{18,71}

The downshifted luminescence spectra showed that when the core and coated materials used were excited above the emitting levels (377 nm) the dominant emission is red (III). However, when the materials were excited directly to the green emitting levels (488 and 520 nm) red emission can also be obtained. From the excitation spectra it can be confirmed that the red emission is a product of the three-photon mechanism with the back transfer to ytterbium but also from the two-photon process from the green emitting levels. This can be seen as the red emission can be obtained regardless of the excitation wavelength in comparison with the results from Berry et al. and Hyppänen et al. where the red emission did not have a component from the green emitting levels of Er^{3+} (${}^2\text{H}_{11/2}$, ${}^4\text{S}_{3/2}$).^{18,69} This two-photon process is more dominant in the case of bare core materials.^{6,69}

The green upconversion emission decays were studied with the materials coated with varying length of polyelectrolytes (III) in aqueous environment. It could be observed that in comparison with their bare core counterparts both lifetime components were

smaller, but their ratio (amplitude i.e. the overall effect on the whole lifetime) shifted slightly to the second component (Table 1). With the materials coated with PAA/Nd³⁺ the increase in the number of bilayers did not have an effect on the first lifetime component and the effect on the second component was minimal (max. 40 μs). However, with the PP/Nd³⁺ coating the bilayers made with the short PP had a decreasing effect on both of the lifetime components. A similar decrease was observed also with the coating with the longer PP but the overall effect was smaller than that with the short PP.

Table 1. Upconversion luminescence lifetimes of the coated nanoparticles made with the longest polyelectrolyte lengths. The amplitude indicates the % effect in the total lifetime (III).

Sample	Polyelectrolyte	$\tau_1 / \mu\text{s}$	A / %	$\tau_2 / \mu\text{s}$	A / %
Core ^a		71±1	94	668±21	6
1 bilayer	PAA M _w : 100,000	69±1	93	683±22	7
2 bilayers	“	69±1	92	636±13	8
3 bilayers	“	66±1	92	654±15	8
1 bilayer	PP (long chain)	66±1	92	646±14	8
2 bilayers	“	64±1	91	617±16	9
3 bilayers	“	60±1	90	565±14	10

^a Core material for PAA M_w: 100,000 and PP (long chain) is the same

As the neodymium is currently widely studied for its use as a sensitizer to shift from the 970 nm to 808 nm excitation in applications also the upconversion luminescence with that excitation pathway was studied.^{17,75,242} However, with our polyelectrolyte/Nd³⁺ coated UCNPs materials no enhancement or energy transfer was observed with the materials coated with polyelectrolytes and neodymium ions (II). The only enhancement with this excitation was observed when the core lanthanides (Y, Yb, Er) were used on the coating suggesting that the neodymium was probably absorbing already the incoming excitation but not transferring it to ytterbium in the core materials. This could mean that the upconversion luminescence obtained from the 808 nm excitation is only due to absorption by the core material. Yb³⁺ has no closely matching energy levels for 808 nm excitation. Thus the absorption proceeds mostly through the ⁴I_{9/2} level of Er³⁺.

Materials coated and crosslinked using only polyelectrolytes

All of the UCNPs coated with PAA/PAH bilayers showed the upconversion luminescence expected from the core materials' Yb³⁺-Er³⁺ energy transfer when excited with 973 nm excitation. With all of the as prepared and unlinked materials the first bilayer was the most efficient in preserving the upconversion luminescence and the emission intensity started decreasing below the core particles' luminescence already at 3.5 bilayers of PAA/PAH. After crosslinking the PAA/PAH layers for 2

hours at 180 °C the behavior of the luminescence was similar with the materials prepared with both 0.1 and 0.2 M NaCl ionic concentration. However, the material prepared with additional 10 mM NaF during the coating protocol showed that all of the crosslinked materials had a stronger upconversion luminescence than the core material used (Figure 27). This suggested that some of the disintegration of the UCNPs already happens during the coating protocol and results in losing the upconversion luminescence intensity. In addition it suggested that the emission intensity loss with the increasing number of bilayers could be only due to the interlocked water molecules in the bilayer structure, as the intensity loss is similar with the as-prepared material prepared with or without the additional fluoride present.

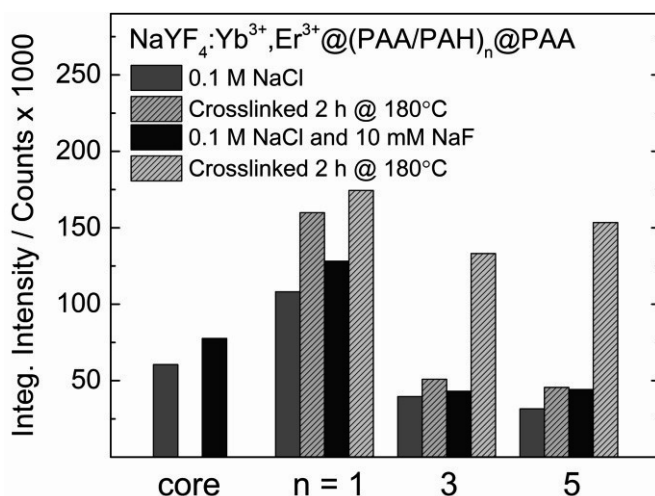


Figure 27. Integrated intensity of the upconversion luminescence of NaYF₄:Yb³⁺,Er³⁺ materials coated with (PAA/PAH)_nPAA bilayers prepared with or without additional fluoride (IV).

5.4 Disintegration studies of UCNPs

The majority of the research in biomedical assays and imaging is done in aqueous environments which makes preventing the disintegration of upconverting nanoparticles vital. For repetitive optical measurements, the emission intensity and its stability during the measurement period and even after storing the nanomaterials is crucial and the leakage of the fluoride ions into the surrounding environment while disintegrating can be detrimental depending on the purpose of the use of the UCNPs.

5.4.1 Optical detection

The optical detection of disintegration of the UCNPs in aqueous environments was carried out by observing the changes in the green upconversion emission decay profile (III). The incubation periods used were 0, 4 and 24 hours. The measurements were done in pure water and in the phosphate buffer with or without an additional 1 mM KF

that is supposed to prevent the UCNP disintegration in time course.⁸ Both the intensity of the upconversion emission and the lifetime components gave valuable information about the disintegration.

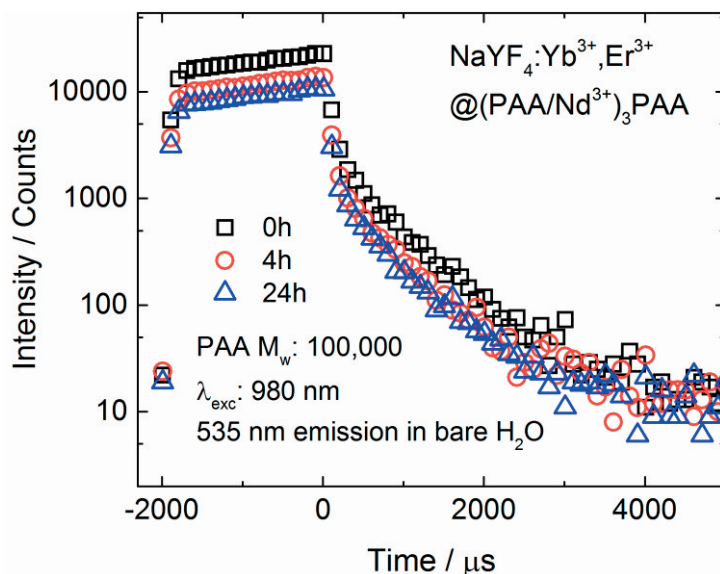


Figure 28. Upconversion luminescence decay curves excited with 980 nm and detected at 535 nm at time steps 0, 4 and 24 h for $\text{NaYF}_4:\text{Yb}^{3+},\text{Er}^{3+}$ material coated with $(\text{PAA}/\text{Nd}^{3+})_3\text{PAA}$ bilayers (M_w : 100,000) measured in pure water (III).

The green emission intensity of $\text{PAA}/\text{Nd}^{3+}$ coated UCNPs decreased over time when the measurements were made in pure water. In all of the materials the first 4 hours were the most crucial in the emission decrease but no significant decrease occurred before the 24 hour measurement. Only with 2 bilayers of $M_w(\text{PAA})$: 15,000 and 1 and 3 bilayers of $M_w(\text{PAA})$: 100,000 the emission remained strong during the whole measurement period (Figure 28). With the PP/Nd^{3+} coating the first bilayer the intensity decrease was small through the whole measurement period. However especially with the higher number of bilayers the decrease in the obtained emission was significant. With $\text{PAA}/\text{Nd}^{3+}$ layers the first lifetime component remained similar suggesting that the surface erbium ions are similarly affected by the environment, but changes in the second lifetime component are considered due to the disintegration of the UCNPs when the participating core erbium ions are forced into contact with the environment.^{8,69} With the coating using $M_w(\text{PAA})$: 2,000 and 15,000 the second lifetime component remained similar. The $\text{PAA}/\text{Nd}^{3+}$ coating that maintained the most intense emission after 24 hours also had the smallest decrease in the second lifetime component (*ca.* 50 μs) suggesting less disintegration (Table 2). With PP/Nd^{3+} coating the decrease in the second lifetime component was small with the first bilayer but significant with higher numbers of bilayers. When 1 mM KF was added into the measurement solutions the emission intensity and the lifetime components remained

similar for the whole measurement period as expected with both PAA and PP coatings.

Table 2. Upconversion luminescence lifetimes of the (PAA/Nd³⁺)₃PAA -coated nanoparticles (M_w(PAA): 100,000) at 5 µg/ml measured at 0, 4 and 24 hours in water, water and phosphate buffer. The amplitude indicates the % effect in the total lifetime (III).

		H ₂ O	A / %	Phosphate	A / %
0 h	τ ₁ / µs	66±1	92	67±1	92
	τ ₂	654±11	8	655±14	8
4	τ ₁	63±1	92	65±1	92
	τ ₂	590±12	8	611±11	8
24	τ ₁	62±1	92	91±1	92
	τ ₂	578±13	8	^a	

^a The phosphate buffer 24 h measurement could only be fitted reasonably with 1st order exponential decay.

When the decay measurements for the PAA/Nd³⁺ coated materials were made in the phosphate buffer it seemed, that the emission intensity was maintained for the first four hours and that it decreased only after that. In some cases the intensity was even enhanced a bit, but this is thought to arise from the possible aggregation of particles during the measurement. With PP/Nd³⁺ coating made with the longer PP the intensity behavior was similar for the first four hours to those measured with the PAA/Nd³⁺ layers. It seems that the short PP in the layer structure is greatly affected by the phosphate buffer and the intensity decrease is enormous. However, when the lifetime components of the PAA/Nd³⁺ layers are considered the second lifetime component decreases significantly (more than 100 µs) with all of the materials during the incubation period. The intensity of the green emission remained constant with the material coated with the shortest PAA (M_w: 2,000) during the whole incubation time. With the longer PAA lengths the intensity decreased slightly but remained strong. With PP/Nd³⁺ coating the second lifetime component decreases over time with all of the materials suggesting that the phosphate buffer is able to disintegrate the particle. The addition of 1 mM KF again made a difference in both the emission intensity as well as with the lifetime components of the PAA/Nd³⁺ coating. With the PP/Nd³⁺ coating only with the longer PP the additional fluoride is able to prevent the disintegration. The short PP coatings are not able to shield the particle even at this environment.

5.4.2 Fluoride ion selective detection

The disintegration of the upconverting nanoparticles and the release of fluoride ions from the nanoparticles were monitored for 24 hours using a fluoride ion selective electrode. The measurements were made in pure water using NaNO₃(aq) to increase

the ionic strength in the solution. Additional fluoride (10^{-5} M NaF) during the measurement was used to see if it affected the fluoride release as it has previously been seen to hinder the disintegration.⁸ From the obtained data a 1st order exponential fit was calculated to determine the amount of fluoride released at the equilibrium state. The disintegration of the PAA/PAH coated nanomaterials was monitored against the bare core materials used.

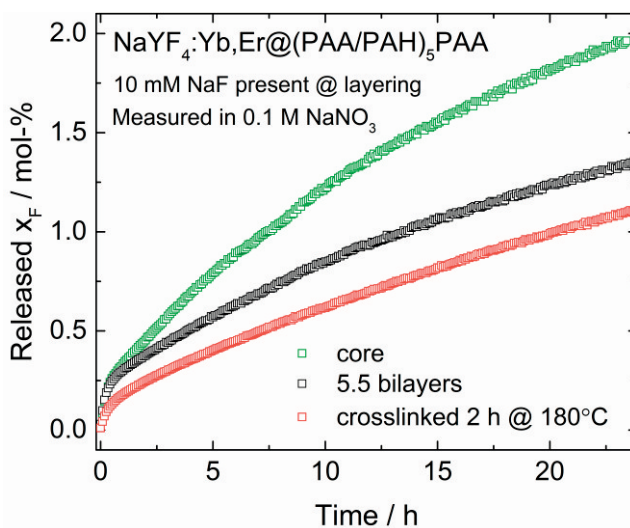


Figure 29. Released fluoride from the 5.5 (PAA/PAH) bilayer coated $\text{NaYF}_4:\text{Yb}^{3+},\text{Er}^{3+}$ nanomaterial and its core coated using 0.1M NaCl and additional 10 mM NaF (measured in 0.1 M NaNO_3) (IV).

The measurements confirmed the previous observation that the additional fluoride during the measurement is able to hinder the disintegration process with the core materials as well as the coated nanomaterials. All of the coated bilayers of PAA/PAH were able to hinder the disintegration of the fluoride ions in aqueous solution (Figure 29). Having the increasing number of bilayers on the nanoparticle surface seemed to enhance the shielding effect. This effect is thought to arise from the different concentration domains in the measurement system. The fluoride release seems to be dependent on the surrounding fluoride concentration, so it is expected that the fluoride concentration between the nanoparticle surface and the bilayer structure can become higher than that of the surrounding solution and bilayer structure and this might already decelerate the release of the fluoride ions from the nanoparticles. The crosslinking of the bilayers hindered the disintegration even further. This in agreement with the expectation that the crosslinking creates a denser structure on coating making it less permeable for molecules and ions.

From the derivative of the exponential fit the fluoride release rate and rate constants of the coated nanomaterials were obtained. This further confirmed that the crosslinking made the fluoride release slower. The slowest fluoride release was obtained from the

5.5 bilayers of PAA/PAH that were manufactured using the ionic concentration of 0.1 M NaCl with an additional 10 mM NaF present during the coating. When the measurements were made in the presence of an additional 10^{-5} M fluoride the derivative curves of the crosslinked materials were nearly flat when compared with the as prepared coated materials. This further confirmed that the release of the fluoride ions from the nanoparticle structure is driven by the fluoride concentration of the surrounding environment.

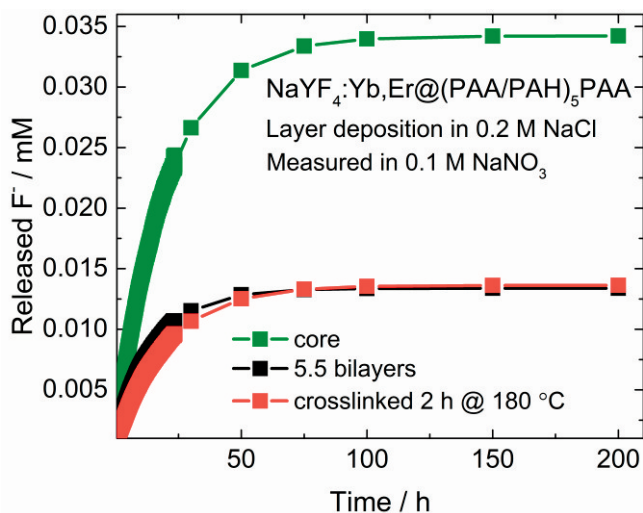


Figure 30. Extrapolated (30-200 h) equilibrium curves of fluoride release of 5.5 (PAA/PAH) bilayer coated $\text{NaYF}_4:\text{Yb}^{3+},\text{Er}^{3+}$ nanomaterial and its core prepared using 0.2 M NaCl (measured in 0.1 M $\text{NaNO}_3(\text{aq})$) (IV).

The equilibrium state of fluoride release was extrapolated from the obtained data. It was observed that with 5.5 bilayers of (PAA/PAH) coating made with a 0.2 M ionic concentration of NaCl (Figure 30) the equilibrium is reached fastest within 75 hours, while with other materials the disintegration continues past 100 hours.

While the disintegration of the UCNP's cannot be fully prevented it is efficiently decelerated with the (PAA/PAH) bilayer coating with or without crosslinking the layers. It seems that the deceleration in unlinked coating is due to fluoride ion concentration increasing on the bilayer structure and thus preventing the further disintegration. With the crosslinked materials, the decelerating is more likely to be arising from the more dense structure of the coating creating the high fluoride ion concentration between the surface of the UCNP and the bilayer structure.

6 CONCLUSIONS AND FUTURE PROSPECTS

The development of the detailed tailoring of upconverting nanoparticles with desired size, shape and optical properties has advanced during the last years creating even smaller nanoparticles. Simultaneously with the decrease in the UCNP size the need for controlling the negative effects of the environment on the particles has increased and created a branched field where the enhancement and shielding effects need to be adjusted for their biocompatibility for specific applications.

During my thesis research, we optimized a synthesis protocol to produce repeatedly uniform and spherical UCNPs for the needs of biomedical research. To minimize the negative effect from the nanoparticles' environment an easy and modifiable layer-by-layer method was incorporated into coating and surface modification of UCNPs. We studied the layer formation using both positively charged metal ions and negatively charged polyelectrolytes to introduce optically active ions as shell-like structure on the surface. In addition we used oppositely charged polyelectrolytes to prepare dense coating by crosslinking the layer structure. We studied the effect of these surface modifications and coatings on the upconversion luminescence of the core materials and if they minimize the disintegration of the UCNPs in aqueous environments.

The main conclusions based on the original publications are:

- I** A synthesis protocol for producing uniform and spherical UCNPs was modified from the existing literature and the crucial parameters affecting the UCNP formation and properties were identified. We learned that while the protocol yielded the desired UCNPs with good upconversion luminescence there are still uncontrollable parameters such as a possible cation reordering that affect the upconversion luminescence properties so that they can vary regardless of the similar shape and size.
- II** The layer-by-layer method using negatively charged polyelectrolytes and positively charged metal ions was successfully demonstrated in coating the UCNPs using both poly(acrylic acid) and polyphosphate as polyelectrolytes. It was observed that with a low number of bilayers the upconversion luminescence intensity of the core materials could be enhanced. However, the desired excitation path through the neodymium using 808 nm excitation was not observed.
- III** Upconversion luminescence properties of polyelectrolyte/metal ion coated UCNPs and the bilayer buildup were further studied by varying the length of the polyelectrolytes used. The coating enhanced the upconversion luminescence properties up to a certain number of bilayers. The loss of upconversion luminescence intensity is probably due to the presence of interlocked water molecules in the bilayer structure. Coatings made with poly(acrylic acid) were

the most resilient (24 hours) in aqueous environments and the upconversion luminescence intensity could be maintained for four hours even in a phosphate buffer.

- IV** Coating and crosslinking poly(acrylic acid)/polyallylamine hydrochloride onto UCNP surface was demonstrated. Using additional fluoride during the layer-by-layer coating the negative effect of aqueous coating solutions could be minimized for the core particles. Crosslinking of the bilayer coating resulted in more defined coating structure that was able to hinder the fluoride release from the UCNPs when introduced into aqueous environments. In addition, crosslinking the coating with materials prepared with additional fluoride present at the coating resulted in upconversion luminescence intensity enhancement that could be maintained with increasing the number of bilayers.

The research done in the scope of this thesis has given more insight in combining the layer-by-layer method with these unique luminescent materials in a way that has not yet been studied in detail previously. On the other hand, this study has widened the research done in the layer-by-layer method incorporating the use of metal ions as a positive component in the bilayer formation with small particles as templates. We have proved that the properties of upconverting nanoparticles can be enhanced using the layer-by-layer method and that it is a worthy research branch also in the field of upconversion luminescence and luminescent nanoparticles.

Albeit the work done in the scope of this thesis can be deemed as the much reviled *basic research* it defends its place in the world of upconverting nanoparticles where there are still a large variety of problems needing to be solved. The playground of layer-by-layer method and polymers is vast with a multitude of parameters affecting the outcome. The research in this thesis covers only a small fraction of what could still be done for both enhancing the UCNP properties as well as their surface functionalization. So the remaining question is, will the time drive past the upconversion phenomenon or not. Will they be good enough for applications or are they deemed only an interesting research field with no commercial applications because of their drawbacks that cannot be solved in reasonable time?

ACKNOWLEDGEMENTS

This research was carried out in the group of Inorganic Materials Chemistry at the Laboratory of Materials Chemistry and Chemical Analysis at the Department of Chemistry, University of Turku, during the years 2015–2019. Financial support from Nordic Energy Research (AquaFEED project), University of Turku joint research grant fund, Academy of Finland (NOMSEC project), Turku University Foundation and the Vilho, Yrjö and Kalle Väisälä Foundation are gratefully acknowledged for creating the possibility to venture through this project.

I would not be where I am today without my supervisor Adj. Prof. Mika Lastusaari. I am more than thankful for the insight, the knowledge and the music you have shared with me through the years even though I might have been a pain on your doorstep sometimes. Your humor has helped me along the years more than you know and I know that you always had my back. One of your greatest ideas was to introduce me and my research project to Adj. Prof. Mikko Salomäki who then became my other supervisor.

Mikko, to gain another supervisor who I already looked up to in a scientific way was great, but to have one with your personality and sense of humor is like winning a lottery. You have always been interested in my research with additional forward pushing comments and you have never turned me away with little problems have they been science related idiotic questions or, you know, the rest of the baggage. Three quarters of this thesis and probably the reason why it was so “easy” to finish is because of you. Thank you for always being there for me! If I ever gain half of your knowledge and the way you interact with your students, I would be happy.

I am very thankful for Prof. Carita Kvarnström for being my research director. Even though your position may have been more of a formal one I have always known that I could come to you with my problems. You have encouraged me with my ideas to arrange parties and celebrations to our laboratory. This has made me really happy as it sort of feels like I can give forward some of the love I have felt during my years here.

My other co-authors Dr. Iko Hyppänen, Prof. Jorma Hölsä, Satu Lahtinen, Dr. Henna Päckilä, Prof. Tero Soukka, Prof. Hendrik Swart, and Minnea Tuomisto are thanked for their input and invaluable comments regarding our publications, which turned out pretty well I think. I want to thank Ermei Mäkilä for teaching me how to use of zeta potential equipment and the company at the physics department during the measurements. Dr. Riikka Arppe and Dr. Markus Peurla are thanked for the TEM images in my publications.

None of the practical work done during the years would have been possible without the help of the best go-to people in the world: Kirsi Laaksonen, Kari Loikas, and Mauri Nauma. Kaisa Ketomäki is hugely appreciated for having an answer to basically

Acknowledgements

any question one might have regarding anything Department of Chemistry related. It turned out that whenever I saw any of you I ended up being a bit late from where I was going because you always had the time to chat with me.

I am grateful for Dr. Maria Sammalkorpi and Dr. Thomas Hirsch for carefully revising my thesis and for their kind comments and Prof. Darja Lisjak for agreeing to be my opponent in the disputation. Tiina Vistbacka and Henna Savela are honored for boldly going where many would not and proof-reading parts of this thesis.

There has not been a day during this thesis project that I have thought that I would not like to come to work. There have been days when working has been hard, but I have always enjoyed being here and being part of the Department of Chemistry. It feels home to me. Mostly this is due to the whole 3rd floor of Arcanum. I know the third floor is somewhat divided into four different research groups, but I have had the privilege to have friends in all of them. I have enjoyed chatting with you during the breaks and popping into your labs and asking “what is this?” and “why is this so colorful?”.

The Inorganic Materials Chemistry group (both the present and the past people in it) as a whole deserves a huge thank you for being my base camp. I want to thank Dr. Ari Lehtonen for our conversations about music and life in general and Milla Suominen for all the hugs I’ve received whenever I needed them. Pasi Salonen is thanked for being the ChemDraw wizard and always being eager to show me new kinds of colorful liquids in their lab. Everyone during the coffee breaks, afterwork drinks and all kinds of parties; Dr. Pia Damlin, Dr. Anssi Peuronen. Lauri Marttila, Rahul Yewale, Sachin Kochrekar, and Ville Eskonen to name only a few that I haven’t yet named.

Then there are the Powerpuff Girls in our office, Minnea Tuomisto and Isabella Norrbo. I have enjoyed our office and the time we have spent there “studying” so much. Thank you for your company during the working days and during the conference trips we’ve had. However, I am not sure why most of the evenings out with you tend to end up with headaches afterwards – but to clear one’s head every now and then is very important part of this journey!

I want to thank Dr. Maarit Karonen for agreeing to be my mentor during this last year. You know I value you highly as a scientist and basically “just being you”. Having discussions with you has forced me to analyze and organize my thoughts about my career and made them clearer.

The thing with growing up, having a family and a job and basically just “acting like an adult” that really bugs me is losing yourself and your friends to the treadmill of time. Suvi Ahvenainen, Riikka Arppe, Tiina Kamppikoski, Henna Savela, Risto Savela and Timo Valta, I have been fortunate that I got to know you during my student years and I am even more grateful that we have remained friends ever since. I want especially

Acknowledgements

thank Henna for our academic-mothers-need-a-break lunchbreaks, dinners and discussions. I can always count on you and I think you are an amazing scientist and a mother. My brother from another mother and a Brazilian uncle for Meeri, Lucas Rodrigues, who has time to visit use every time he is in Finland, I wish Brazil would not be so far away! There is also light in the abyss of the internet and I am happy that Tiina Vistbacka and Pirjo Merilahti have found their way into my life during the recent years. I find it weird that I feel like I have known you for ages.

I am forever grateful for my family for always being there for me. Even if I still don't know what dragged me towards chemistry and Turku you still encouraged me to come here. When I told you I would pursue doctoral studies you said "Yeah, we're sort of not surprised" (I was...). So mum and dad, Miika, Marjo, Milja and Riina, and Eeli and Alma, there is no better family to have – I am truly blessed! I am also grateful for my mother-in-law Vappu for coming to take care of Meeri when we have needed an extra hand due to daycare and two jobs, especially during my conference trips.

Then there is the home I always go to. I want to thank my husband Pekka and my one of a kind daughter Meeri for bringing my life so much more than I could have ever imagined. And let me tell you it is a quite a lot because she has a huge imagination and a reservoir of music already. I am not going to lie that combining family life with academic life is a walk in the park. It has proven to be one of the most difficult things I have ever done. For some reason I always felt guilty about the things I was not doing at the exact moment while being busy with the other. However, I would not change a day. If it weren't for you two I would probably end up covered in dust somewhere and forget to eat. Thank you for dragging me from my books to the real life. I love you.

Turku 13.2.2019



REFERENCES

- (1) Blasse, G.; Grabmaier, B. C. *Luminescent Materials*, 1st ed.; Springer-Verlag: Berlin, 1994.
- (2) Bünzli, J. G. Lanthanide Luminescence for Biomedical Analyses and Imaging. *Chem. Rev.* **2010**, *110*, 2729–2755.
- (3) Auzel, F. Upconversion and Anti-Stokes Processes with f and d Ions in Solids. *Chem. Rev.* **2004**, *104*, 139–173.
- (4) Zhou, J.; Liu, Q.; Feng, W.; Sun, Y.; Li, F. Upconversion Luminescent Materials: Advances and Applications. *Chem. Rev.* **2015**, *115*, 395–465.
- (5) Chen, G.; Qiu, H.; Prasad, P. N.; Chen, X. Upconversion Nanoparticles: Design, Nanochemistry, and Applications in Theranostics. *Chem. Rev.* **2014**, *114*, 5161–5214.
- (6) Arppe, R.; Hyppänen, I.; Perälä, N.; Peltomaa, R.; Kaiser, M.; Würth, C.; Christ, S.; Resch-Genger, U.; Schäferling, M.; Soukka, T. Quenching of the Upconversion Luminescence of NaYF₄:Yb³⁺,Er³⁺ and NaYF₄:Yb³⁺,Tm³⁺ Nanophosphors by Water: The Role of the Sensitizer Yb³⁺ in Non-Radiative Relaxation. *Nanoscale* **2015**, *7*, 11746–11757.
- (7) Plohl, O.; Kraft, M.; Kovac, J.; Belec, B.; Ponikvar-Svet, M.; Würth, C.; Lisjak, D.; Resch-Genger, U. Optically Detected Degradation of NaYF₄:Yb,Tm-Based Upconversion Nanoparticles in Phosphate Buffered Saline Solution. *Langmuir* **2017**, *33*, 553–560.
- (8) Lahtinen, S.; Lyytikäinen, A.; Pääkilä, H.; Hömppi, E.; Perälä, N.; Lastusaari, M.; Soukka, T. Disintegration of Hexagonal NaYF₄:Yb³⁺,Er³⁺ Upconverting Nanoparticles in Aqueous Media: The Role of Fluoride in Solubility Equilibrium. *J. Phys. Chem. C* **2017**, *121*, 656–665.
- (9) Hyppänen, I.; Lahtinen, S.; Ääritalo, T.; Mäkelä, J.; Kankare, J.; Soukka, T. Photon Upconversion in a Molecular Lanthanide Complex in Anhydrous Solution at Room Temperature. *ACS Photonics* **2014**, *1*, 394–397.
- (10) Nonat, A.; Chan, C. F.; Liu, T.; Platas-Iglesias, C.; Liu, Z.; Wong, W.; Wong, W.; Wong, K. Room Temperature Molecular up Conversion in Solution. *Nat. Commun.* **2016**, *7*, 11978.
- (11) Giedraityte, Z.; Tuomisto, M.; Lastusaari, M.; Karppinen, M. Three- and Two-Photon NIR-to-Vis (Yb, Er) Upconversion from ALD/MLD-Fabricated Molecular Hybrid Thin Films. *ACS Appl. Mater. Interfaces* **2018**, *10*, 8845–8852.
- (12) Dong, H.; Sun, L.; Yan, C. Energy Transfer in Lanthanide Upconverting Studies for Extended Optical Applications. *Chem. Soc. Rev.* **2015**, *44*, 1608–1634.
- (13) Streck, W.; Deren, P.; Bednarkiewicz, A. Cooperative Processes in KYb(WO₄)₂ Crystal Doped with Eu³⁺ and Tb³⁺ Ions. *J. Lumin.* **2000**, *87–89*, 999–1001.
- (14) Prorok, K.; Gnach, A.; Bednarkiewicz, A.; Streck, W. Energy Up-Conversion in Tb³⁺/Yb³⁺ Co-Doped Colloidal α -NaYF₄ Nanocrystals. *J. Lumin.* **2013**, *140*, 103–109.
- (15) Zhang, X.; Chen, Z.; Qiu, J. Mechanistic Investigation of Upconversion Luminescence in Er³⁺-Doped BaCl₂, BaF₂ and NaYF₄ Phosphors. *Mater. Chem. Phys.* **2015**, *162*, 76–81.
- (16) Zhong, Y.; Tian, G.; Gu, Z.; Yang, Y.; Gu, L.; Zhao, Y.; Ma, Y. Elimination of Photon Quenching by a Transition Layer to Fabricate a Quenching-Shield Sandwich Structure for 800 nm Excited Upconversion Luminescence of Nd³⁺-Sensitized Nanoparticles. *Adv. Mater.* **2014**, *26*, 2831–2837.

References

- (17) Prorok, K.; Bednarkiewicz, A. Energy Migration Up-Conversion of Tb^{3+} in Yb^{3+} and Nd^{3+} Codoped Active-Core/Active-Shell Colloidal Nanoparticles. *Chem. Mater.* **2016**, *28*, 2295–2300.
- (18) Berry, M. T.; May, P. S. Disputed Mechanism for NIR-to-Red Upconversion Luminescence in $NaYF_4:Yb^{3+},Er^{3+}$. *J. Phys. Chem. A* **2015**, *119*, 9805–9811.
- (19) Krämer, K. W.; Biner, D.; Frei, G.; Güdel, H. U.; Hehlen, M. P.; Lü, Thi, S. R. Hexagonal Sodium Yttrium Fluoride Based Green and Blue Emitting Upconversion Phosphors. *Chem. Mater.* **2004**, *16*, 1244–1251.
- (20) Suyver, J. F.; Grimm, J.; Veen, M. K. Van; Biner, D.; Krämer, K. W.; Güdel, H. U. Upconversion Spectroscopy and Properties of $NaYF_4$ Doped with Er^{3+} , Tm^{3+} and/or Yb^{3+} . *J. Lumin.* **2006**, *117*, 1–12.
- (21) Harju, E.; Hyppänen, I.; Hölsä, J.; Kankare, J.; Lahtinen, M.; Lastusaari, M.; Pihlgren, L.; Soukka, T. Polymorphism of $NaYF_4:Yb^{3+},Er^{3+}$ Up-Conversion Luminescence Materials. *Z. Krist. Proc.* **2011**, *1*, 381–387.
- (22) Aebischer, A.; Hostettler, M.; Hauser, J.; Krämer, K.; Weber, T.; Güdel, H. U.; Bürgi, H. Structural and Spectroscopic Characterization of Active Sites in a Family of Light-Emitting Sodium Lanthanide Tetrafluorides. *Angew. Chemie - Int. Ed.* **2006**, *45*, 2802–2806.
- (23) Brito, H. F.; Hölsä, J.; Laamanen, T.; Laihin, T.; Lastusaari, M.; Rodrigues, L. C. V.; Pihlgren, L.; Soukka, T. Rare Earth Distribution in $NaRF_4$: Effect on Up-Conversion Intensity. *Powder Diffr.* **2013**, *28*, S41–S50.
- (24) Brito, H. F.; Hölsä, J.; Laamanen, T.; Laihin, T.; Lastusaari, M.; Pihlgren, L.; Rodrigues, L. C. V.; Soukka, T. EXAFS Study of Cation Reordering in $NaYF_4:Yb^{3+}, Tb^{3+}$ up-Conversion Luminescence Materials. *J. Rare Earths* **2014**, *32*, 226–229.
- (25) Haase, M.; Schäfer, H. Upconverting Nanoparticles. *Angew. Chemie - Int. Ed.* **2011**, *50*, 5808–5829.
- (26) Wang, F.; Liu, X. Recent Advances in the Chemistry of Lanthanide-Doped Upconversion Nanocrystals. *Chem. Soc. Rev.* **2009**, *38*, 976–989.
- (27) Reddy, K. L.; Srinivas, V.; Shankar, K. R.; Kumar, S.; Sharma, V.; Kumar, A.; Bahuguna, A.; Bhattacharyya, K.; Krishnan, V. Enhancement of Luminescence Intensity in Red Emitting $NaYF_4:Yb/Ho/Mn$ Upconversion Nanophosphors by Variation of Reaction Parameters. *J. Phys. Chem. C* **2017**, *121*, 11783–11793.
- (28) Gerelkhuu, Z.; The, B.; Won, J.; Phan, T.; Conte, E.; Lee, Y. Influence of Cr^{3+} on Upconversion Luminescent and Magnetic Properties of $NaLu_{0.86-x}Gd_{0.12}F_4:Cr^{3+}/Er_{0.02}^{3+}$ (0 x 0.24) Material. *J. Lumin.* **2017**, *187*, 40–45.
- (29) Tuomisto, M.; Palo, E.; Laihin, T.; Hyppänen, I.; Lastusaari, M.; Swart, H. C.; Hölsä, J. Effect of Mn and Cr Doping on the Up-Conversion Luminescence from $NaYF_4:Yb^{3+},Er^{3+}$. *Opt. Mater.* **2016**, *59*, 115–119.
- (30) Martín-Rodríguez, R.; Valiente, R.; Polizzi, S.; Bettinelli, M.; Speghini, A.; Piccinelli, F. Upconversion Luminescence in Nanocrystals of $Gd_3Ga_5O_{12}$ and $Y_3Al_5O_{12}$ Doped with $Tb^{3+}-Yb^{3+}$ and $Eu^{3+}-Yb^{3+}$. *J. Phys. Chem. C* **2009**, *113*, 12195–12200.
- (31) Chen, X.; Jin, L.; Kong, W.; Sun, T.; Zhang, W.; Liu, X.; Fan, J.; Yu, S. F.; Wang, F. Confining Energy Migration in Upconversion Nanoparticles towards Deep Ultraviolet Lasing. *Nat. Commun.* **2016**, *7*, 10304.
- (32) Chen, D.; Liu, L.; Huang, P.; Ding, M.; Zhong, J.; Ji, Z. Nd^{3+} -Sensitized Ho^{3+} Single-Band Red Upconversion Luminescence in Core-Shell Nanoarchitecture. *J. Phys. Chem. Lett.* **2015**, *6*, 2833–2840.
- (33) Skripka, A.; Marin, R.; Benayas, A.;

References

- Canton, P.; Hemmer, E.; Vetrone, F. Covering the Optical Spectrum through Collective Rare-Earth Doping of NaGdF₄ Nanoparticles: 806 and 980 nm Excitation Routes. *Phys. Chem. Chem. Phys.* **2017**, *19*, 11825–11834.
- (34) Heer, S.; Kömpe, K.; Güdel, H.-U.; Haase, M. Highly Efficient Multicolour Upconversion Emission in Transparent Colloids of Lanthanide-Doped NaYF₄ Nanocrystals. *Adv. Mater.* **2004**, *23*, 2102–2105.
- (35) Yi, G.; Lu, H.; Zhao, S.; Ge, Y.; Yang, W. Synthesis, Characterization, and Biological Application of Size-Controlled Nanocrystalline NaYF₄:Yb,Er Infrared-to-Visible Up-Conversion Phosphors. *Nano Lett.* **2004**, *4*, 2191–2196.
- (36) Zeng, J.; Su, J.; Li, Z.; Yan, R.; Li, Y.-D. Synthesis and Upconversion Luminescence of Hexagonal-Phase NaYF₄:Yb,Er³⁺ Phosphors of Controlled Size and Morphology. *Adv. Mater.* **2005**, *17*, 2119–2123.
- (37) Zhang, Y.; Sun, X.; Si, R.; You, L.-P.; Yan, C. Single-Crystalline and Monodisperse LaF₃ Triangular Nanoplates from a Single-Source Precursor. *J. Am. Chem. Soc.* **2005**, *127*, 3260–3261.
- (38) Yi, G. S.; Chow, G. M. Synthesis of Hexagonal-Phase NaYF₄:Yb,Er and NaYF₄:Yb,Tm Nanocrystals with Efficient Up-Conversion Fluorescence. *Adv. Funct. Mater.* **2006**, *16*, 2324–2329.
- (39) Wisser, M. D.; Fischer, S.; Siefe, C.; Alivisatos, A. P.; Salleo, A.; Dionne, J. A. Improving Quantum Yield of Upconverting Nanoparticles in Aqueous Media via Emission Sensitization. *Nano Lett.* **2018**, *18*, 2689–2695.
- (40) Chan, E. M.; Han, G.; Goldberg, J. D.; Gargas, D. J.; Ostrowski, A. D.; Schuck, P. J.; Cohen, B. E.; Milliron, D. J. Combinatorial Discovery of Lanthanide-Doped Nanocrystals with Spectrally Pure Upconverted Emission. *Nano Lett.* **2012**, *12*, 3839–3845.
- (41) Han, S.; Qin, X.; An, Z.; Zhu, Y.; Liang, L.; Han, Y.; Huang, W.; Liu, X. Multicolour Synthesis in Lanthanide-Doped Nanocrystals through Cation Exchange in Water. *Nat. Commun.* **2016**, *7*, 13059.
- (42) Wilhelm, S.; Kaiser, M.; Würth, C.; Heiland, J.; Carrillo-Carrion, C.; Muhr, V.; Wolfbeis, O. S.; Parak, W. J.; Resch-Genger, U.; Hirsch, T. Water Dispersible Upconverting Nanoparticles: Effects of Surface Modification on Their Luminescence and Colloidal Stability. *Nanoscale* **2015**, *7*, 1403–1410.
- (43) Wang, F.; Han, Y.; Lim, C. S.; Lu, Y.; Wang, J.; Xu, J.; Chen, H.; Zhang, C.; Hong, M.; Liu, X. Simultaneous Phase and Size Control of Upconversion Nanocrystals through Lanthanide Doping. *Nature* **2010**, *463*, 1061–1065.
- (44) May, P. B.; Suter, J. D.; May, P. S.; Berry, M. T. The Dynamics of Nanoparticle Growth and Phase Change During Synthesis of B-NaYF₄. *J. Phys. Chem. C* **2016**, *120*, 9482–9489.
- (45) Gai, S.; Li, C.; Yang, P.; Lin, J. Recent Progress in Rare Earth Micro/Nanocrystals: Soft Chemical Synthesis, Luminescent Properties, and Biomedical Applications. *Chem. Rev.* **2014**, *114*, 2343–2389.
- (46) Rinkel, T.; Nordmann, J.; Raj, A. N.; Haase, M. Ostwald-Ripening and Particle Size Focussing of Sub-10 nm NaYF₄ Upconversion Nanocrystals. *Nanoscale* **2014**, *6*, 14523–14530.
- (47) Rinkel, T.; Raj, A. N.; Dühnen, S.; Haase, M. Synthesis of 10 nm β-NaYF₄:Yb,Er/NaYF₄ Core / Shell Upconversion Nanocrystals with 5 nm Particle Cores. *Angew. Chemie - Int. Ed.* **2016**, *55*, 1164–1167.
- (48) Ye, S.; Xiao, P.; Liao, H.; Li, S.; Wang, D. Fast Synthesis of Sub-10 nm β-NaYF₄:Yb³⁺, Er³⁺@NaYF₄ Core-Shell Upconversion Nanocrystals

References

- Mediated by Oleate Ligands. *Mater. Res. Bull.* **2018**, *103*, 279–284.
- (49) Homann, A. C.; Krukewitt, L.; Frenzel, F.; Würth, C.; Resch-Genger, U.; Haase, M. NaYF₄:Yb,Er/NaYF₄ Core/Shell Nanocrystals with High Upconversion Luminescence Quantum Yield. *Angew. Chemie - Int. Ed.* **2018**, *57*, 8765–8769.
- (50) Hesse, J.; Klier, D. T.; Sgarzi, M.; Nsubuga, A.; Bauer, C.; Grenzer, J.; Hübner, R.; Wislicenus, M.; Joshi, T.; Kumke, M. U.; et al. Rapid Synthesis of Sub-10 Nm Hexagonal NaYF₄ - Based Upconverting Nanoparticles Using Therminol® 66. *ChemistryOpen* **2018**, *7*, 159–168.
- (51) He, H.; Howard, C. B.; Chen, Y.; Wen, S.; Lin, G.; Zhou, J.; Thurecht, K. J.; Jin, D. Bispecific Antibody-Functionalized Upconversion Nanoprobe. *Anal. Chem.* **2018**, *90*, 3024–3029.
- (52) Liu, Y.; Zhang, C.; Liu, H.; Li, Y.; Xu, Z.; Li, L.; Whittaker, A. Controllable Synthesis of Up-Conversion Nanoparticles UCNPs@MIL-PEG for pH-Responsive Drug Delivery and Potential up-Conversion Luminescence/Magnetic Resonance Dual-Mode Imaging. *J. Alloys Compd.* **2018**, *749*, 939–947.
- (53) Li, C.; Quan, Z.; Yang, J.; Yang, P.; Lin, J. Highly Uniform and Monodisperse β-NaYF₄:Ln³⁺ (Ln = Eu, Tb, Yb/Er, and Yb/Tm) Hexagonal Microprism Crystals: Hydrothermal Synthesis and Luminescent Properties. *Inorg. Chem.* **2007**, *46*, 6329–6337.
- (54) Lisjak, D.; Plohl, O.; Vidmar, J.; Majaron, B.; Ponikvar-svet, M. Dissolution Mechanism of Upconverting AYF₄:Yb,Tm (A = Na or K) Nanoparticles in Aqueous Media. *Langmuir* **2016**, *32*, 8222–8229.
- (55) Laihinen, T.; Lastusaari, M.; Pihlgren, L.; Rodrigues, L. C. V.; Hölsä, J. Thermal Behaviour of the NaYF₄:Yb³⁺,R³⁺ Materials. *J. Therm. Anal. Calorim.* **2015**, *121*, 37–43.
- (56) He, M.; Huang, P.; Zhang, C.; Hu, H.; Bao, C.; Gao, G.; He, R.; Cui, D. Dual Phase-Controlled Synthesis of Uniform Lanthanide- Doped NaGdF₄ Upconversion Nanocrystals Via an OA/Ionic Liquid Two-Phase System for In Vivo Dual-Modality Imaging. *Adv. Funct. Mater.* **2011**, *21*, 4470–4477.
- (57) Du, P.; Luo, L.; Huang, X.; Su, J. Ultrafast Synthesis of Bifunctional Er³⁺/Yb³⁺-Codoped NaBiF₄ Upconverting Nanoparticles for Nanothermometer and Optical Heater. *J. Colloid Interface Sci.* **2018**, *514*, 172–181.
- (58) Resch-Genger, U.; Gorris, H. H. Perspectives and Challenges of Photon-Upconversion Nanoparticles — Part I: Routes to Brighter Particles and Quantitative Spectroscopic Studies. *Anal. Bioanal. Chem.* **2017**, *25*, 5855–5874.
- (59) Zhang, Q.; Song, K.; Zhao, J.; Kong, X.; Sun, Y.; Liu, X.; Zhang, Y.; Zeng, Q.; Zhang, H. Hexanedioic Acid Mediated Surface–ligand-Exchange Process for Transferring NaYF₄:Yb/Er (or Yb/Tm) up-converting Nanoparticles from Hydrophobic to Hydrophilic. *J. Colloid Interface Sci.* **2009**, *336*, 171–175.
- (60) Mader, H. S.; Link, M.; Achatz, D. E.; Uhlmann, K.; Li, X.; Wolfbeis, O. S. Surface-Modified Upconverting Microparticles and Nanoparticles for Use in Click Chemistries. *Chem. a Eur. J.* **2010**, *16*, 5416–5424.
- (61) Saleh, S. M.; Ali, R.; Hirsch, T.; Wolfbeis, O. S. Detection of Biotin-avidin Affinity Binding by Exploiting a Self-Referenced System Composed of Upconverting Luminescent Nanoparticles and Gold Nanoparticles. *J. Nanoparticle Res.* **2011**, *13*, 4603–4611.
- (62) Zhao, J.; Sun, Y.; Kong, X.; Tian, L.; Wang, Y.; Tu, L.; Zhao, J.; Zhang, H. Controlled Synthesis, Formation Mechanism, and Great Enhancement of Red Upconversion Luminescence of

References

- NaYF₄:Yb³⁺, Er³⁺
Nanocrystals/Submicroplates at Low Doping Level. *J. Phys. Chem. B* **2008**, *112*, 15666–15672.
- (63) Wang, Y.; Bao, L.; Liu, Z.; Pang, D. Aptamer Biosensor Based on Fluorescence Resonance Energy Transfer from Upconverting Phosphors to Carbon Nanoparticles for Thrombin Detection in Human Plasma. *Anal. Chem.* **2011**, *83*, 8130–8137.
- (64) Wang, L.; Zhang, Y.; Zhu, Y. One-Pot Synthesis and Strong Near-Infrared Upconversion Luminescence of Poly(Acrylic Acid)-Functionalized YF₃:Yb³⁺/Er³⁺ Nanocrystals. *Nano Res.* **2010**, *3*, 317–325.
- (65) Wang, F.; Liu, X. Upconversion Multicolor Fine-Tuning: Visible to Near-Infrared Emission from Lanthanide-Doped NaYF₄ Nanoparticles. *J. Am. Chem. Soc.* **2008**, *130*, 5642–5643.
- (66) Yu, X.; Li, M.; Xie, M.; Chen, L.; Li, Y.; Wang, Q. Dopant-Controlled Synthesis of Water-Soluble Hexagonal NaYF₄ Nanorods with Efficient Upconversion Fluorescence for Multicolor Bioimaging. *Nano Res.* **2010**, *3*, 51–60.
- (67) Li, Z.; Zhang, Y. Monodisperse Silica-Coated Polyvinylpyrrolidone/NaYF₄ Nanocrystals with Multicolor Upconversion Fluorescence Emission. *Angew. Chemie* **2006**, *118*, 7896–7899.
- (68) Kale, V.; Lastusaari, M.; Hölsä, J.; Soukka, T. Intense UV Upconversion through Highly Sensitized NaRF₄:Tm (R:Y,Yb) Crystals. *RSC Adv.* **2015**, *5*, 35858–35865.
- (69) Hyppänen, I.; Höysniemi, N.; Arppe, R.; Schäferling, M.; Soukka, T. Environmental Impact on the Excitation Path of the Red Upconversion Emission of Nanocrystalline NaYF₄:Yb³⁺,Er³⁺. *J. Phys. Chem. C* **2017**, *121*, 6924–6929.
- (70) Würth, C.; Kaiser, M.; Wilhelm, S.; Grauel, B.; Hirsch, T.; Resch-Genger, U. Excitation Power Dependent Population Pathways and Absolute Quantum Yields of Upconversion Nanoparticles in Different Solvents. *Nanoscale* **2017**, *9*, 4283–4294.
- (71) Anderson, R. B.; Smith, S. J.; May, P. S.; Berry, M. T. Revisiting the NIR-to-Visible Upconversion Mechanism in β-NaYF₄:Yb³⁺,Er³⁺. *J. Phys. Chem. Lett.* **2014**, *5*, 36–42.
- (72) Boyer, J. C.; van Veggel, F. C. Absolute Quantum Yield Measurements of Colloidal NaYF₄:Er³⁺,Yb³⁺ Upconverting Nanoparticles. *Nanoscale* **2010**, *2*, 1417–1419.
- (73) Kaiser, M.; Würth, C.; Kraft, M.; Hyppänen, I.; Soukka, T.; Resch-Genger, U. Power-Dependent Upconversion Quantum Yield of NaYF₄:Yb³⁺,Er³⁺ Nano- and Micrometer-Sized Particles - Measurements and Simulations. *Nanoscale* **2017**, *9*, 10051–10058.
- (74) Wilhelm, S. Perspectives for Upconverting Nanoparticles. *ACS Nano* **2017**, No. 11, 10644–10653.
- (75) Johnson, N. J. J.; He, S.; Diao, S.; Chan, E. M.; Dai, H.; Almutairi, A. Direct Evidence for Coupled Surface and Concentration Quenching Dynamics in Lanthanide-Doped Nanocrystals. *J. Am. Chem. Soc.* **2017**, *139*, 3275–3282.
- (76) Hossain, Y.; Hor, A.; Luu, Q.; Smith, S. J.; May, P. S.; Berry, M. T. Explaining the Nanoscale Effect in the Upconversion Dynamics of B-NaYF₄:Yb³⁺, Er³⁺ Core and Core-Shell Nanocrystals. *J. Phys. Chem. C* **2017**, *121*, 16592–16606.
- (77) Rabouw, F. T.; Prins, P. T.; Villanueva-delgado, P.; Castelijn, M.; Geitenbeek, R. G.; Meijerink, A. Quenching Pathways in NaYF₄:Er³⁺,Yb³⁺ Upconversion Nanocrystals. *ACS Nano* **2018**, *12*, 4812–4823.
- (78) Lisjak, D.; Plohl, O.; Ponikvar-Svet,

References

- M.; Majaron, B. Dissolution of Upconverting Fluoride Nanoparticles in Aqueous Suspensions. *RSC Adv.* **2015**, *5*, 27393–27397.
- (79) Plohl, O.; Kralj, S.; Majaron, B.; Fröhlich, E.; Ponikvar-svet, M.; Makovec, D.; Lisjak, D. Amphiphilic Coatings for the Protection of Upconverting Nanoparticles against Dissolution in Aqueous Media. *Dalt. Trans.* **2017**, *46*, 6975–6984.
- (80) Dukhno, O.; Przybilla, F.; Muhr, V.; Buchner, M.; Hirsch, T.; MELY, Y. Time-Dependent Luminescence Loss of Individual Upconversion Nanoparticles upon Dilution in Aqueous Solutions. *Nanoscale* **2018**, *10*, 15904–15910.
- (81) Kale, V.; Soukka, T.; Hölsä, J.; Lastusaari, M. Enhancement of Blue Upconversion Luminescence in Hexagonal NaYF₄:Yb,Tm by Using K and Sc Ions. *J. Nanoparticle Res.* **2013**, *15*, 1850.
- (82) Ding, M.; Ni, Y.; Song, Y.; Liu, X.; Cui, T.; Chen, D.; Ji, Z.; Xu, F.; Lu, C.; Xu, Z. Li⁺ Ions Doping Core-shell Nanostructures: An Approach to Significantly Enhance Upconversion Luminescence of Lanthanide-Doped Nanocrystals. *J. Alloys Compd.* **2015**, *623*, 42–48.
- (83) Chen, L.; Li, J.; Zhang, J.; Wang, X. Selectively Enhanced Red Upconversion Luminescence and Phase/Size Manipulation via Fe³⁺ Doping in NaYF₄:Yb,Er Nanocrystals. *Nanoscale* **2015**, *7*, 14752–14759.
- (84) Wu, Z.; Lin, M.; Liang, S.; Liu, Y.; Zhang, H.; Yang, B. Hot-Injection Synthesis of Manganese-Ion-Doped NaYF₄:Yb,Er Nanocrystals with Red Up-Converting Emission and Tunable Diameter. *Part. Part. Syst. Charact.* **2013**, *30*, 311–315.
- (85) Chen, X.; Peng, D.; Ju, Q.; Wang, F. Photon Upconversion in Core-shell Nanoparticles. *Chem. Soc. Rev.* **2015**, *44*, 1318–1330.
- (86) Johnson, N. J. J.; Korinek, A.; Dong, C.; Veggel, F. C. J. M. Van. Self-Focusing by Ostwald Ripening: A Strategy for Layer-by-Layer Epitaxial Growth on Upconverting Nanocrystals. *J. Am. Chem. Soc.* **2012**, *134*, 11068–11071.
- (87) Fischer, S.; Swabeck, J. K.; Alivisatos, A. P. Controlled Isotropic and Anisotropic Shell Growth in β-NaLnF₄ Nanocrystals Induced by Precursor Injection Rate. *J. Am. Chem. Soc.* **2017**, *139*, 12325–12332.
- (88) Li, D.; Liu, X.; Qiu, J. Probing Interaction Distance of Surface Quenchers in Lanthanide-Doped Upconversion Core-Shell Nanoparticles. *J. Phys. Chem. C* **2018**, *122*, 10278–10283.
- (89) Shell, C.; Fischer, S.; Bronstein, N. D.; Swabeck, J. K.; Chan, E. M.; Alivisatos, A. P. Precise Tuning of Surface Quenching for Luminescence Enhancement in Core - Shell Lanthanide-Doped Nanocrystals. *Nano Lett.* **2016**, *16*, 7241–7247.
- (90) Wang, Y.; Sun, L.; Xiao, J.; Feng, W.; Zhou, J.; Shen, J. Rare-Earth Nanoparticles with Enhanced Upconversion Emission and Suppressed Rare-Earth-Ion Leakage. *Chem. a Eur. J.* **2012**, *18*, 5558–5564.
- (91) Abel, K. A.; Boyer, J.; Veggel, F. C. J. M. Van. Hard Proof of the NaYF₄/NaGdF₄ Nanocrystal Core/Shell Structure. *J. Am. Chem. Soc.* **2009**, *131*, 14644–14645.
- (92) Johnson, N. J. J.; Veggel, F. C. J. M. Van. Lanthanide-Based Heteroepitaxial Compressive versus Tensile Strain Asymmetry. *ACS Nano* **2014**, *8*, 10517–10527.
- (93) Abel, K. A.; Boyer, J.-C.; Andrei, C. M.; Veggel, F. C. J. M. Van. Analysis of the Shell Thickness Distribution on NaYF₄/NaGdF₄ Core/Shell Nanocrystals by EELS and EDS. *J. Phys. Chem. Lett.* **2011**, *2*, 185–189.
- (94) Hudry, D.; Busko, D.; Popescu, R.; Gerthsen, D.; Abeykoon, A. M. M.; Kübel, C.; Bergfeldt, T.; Richards, B.

References

- S. Direct Evidence of Significant Cation Intermixing in Upconverting Core@Shell Nanocrystals: Toward a New Crystallochemical Model. *Chem. Mater.* **2017**, *29*, 9238–9246.
- (95) Pilch, A.; Würth, C.; Kaiser, M.; Wawrzyn, D. Shaping Luminescent Properties of Yb³⁺ and Ho³⁺ Co-Doped Upconverting Core–Shell β -NaYF₄ Nanoparticles by Dopant Distribution and Spacing. *Small* **2017**, *12*, 1701635.
- (96) Huang, K.; Liu, H.; Kraft, M.; Shikha, S.; Zheng, X.; Ågren, H.; Würth, C.; Resch-Genger, U.; Zhang, Y. A Protected Excitation-Energy Reservoir for Efficient Upconversion Luminescence. *Nanoscale* **2018**, *10*, 250–259.
- (97) Zuo, J.; Sun, D.; Tu, L.; Wu, Y.; Cao, Y.; Xue, B.; Zhang, Y.; Chang, Y.; Liu, X.; Kong, X.; et al. Precisely Tailoring Upconversion Dynamics via Energy Migration in Core-Shell Nanostructures. *Angew. Chemie - Int. Ed.* **2018**, *57*, 3054–3058.
- (98) Xie, X.; Gao, N.; Deng, R.; Sun, Q.; Xu, Q.; Liu, X. Mechanistic Investigation of Photon Upconversion in Nd³⁺-Sensitized Core-Shell Nanoparticles. *J. Am. Chem. Soc.* **2013**, *135*, 12608–12611.
- (99) Wang, X.; Valiev, R. R.; Ohulchanskyy, T. Y.; Ågren, H.; Chen, G. Dye-Sensitized Lanthanide-Doped Upconversion Nanoparticles. *Chem Soc Rev* **2017**, *46*, 4150–4167.
- (100) Zou, W.; Visser, C.; Maduro, J. A.; Pshenichnikov, M. S.; Hummelen, J. C. Broadband Dye-Sensitized Upconversion of near-Infrared Light. *Nat. Photonics* **2012**, *6*, 560–564.
- (101) Chen, G.; Damasco, J.; Qiu, H.; Shao, W.; Ohulchanskyy, T. Y.; Valiev, R. R.; Wu, X.; Han, G.; Wang, Y.; Yang, C.; et al. Energy-Cascaded Upconversion in an Organic Dye-Sensitized Core/ Shell Fluoride Nanocrystal. *Nano Lett.* **2015**, *15*, 7400–7407.
- (102) Zhao, F.; Yin, D.; Wu, C.; Liu, B.; Chen, T.; Guo, M.; Huang, K.; Chen, Z.; Zhang, Y. Huge Enhancement of Upconversion Luminescence by Dye/Nd³⁺ Sensitization of Quenching-Shield Sandwich Structured Upconversion Nanocrystals under 808 Nm Excitation. *Dalt. Trans.* **2017**, *46*, 16180–16189.
- (103) Muhr, V.; Würth, C.; Kraft, M.; Buchner, M.; Baeumner, A. J.; Resch-Genger, U.; Hirsch, T. Particle-Size-Dependent Förster Resonance Energy Transfer from Upconversion Nanoparticles to Organic Dyes. *Anal. Chem.* **2017**, *89*, 4868–4874.
- (104) Wu, D. M.; Garc, A.; Salleo, A.; Dionne, J. A. Plasmon-Enhanced Upconversion. *J. Phys. Chem. Lett.* **2014**, *5*, 4020–4031.
- (105) Hutter, B. E.; Fendler, J. H. Exploitation of Localized Surface Plasmon Resonance. *Adv. Mater.* **2004**, *16*, 1685–1706.
- (106) Feng, A. L.; You, M. L.; Tian, L.; Singamaneni, S.; Liu, M.; Duan, Z.; Lu, T. J.; Xu, F.; Lin, M. Distance-Dependent Plasmon-Enhanced Fluorescence of Upconversion Nanoparticles Using Polyelectrolyte Multilayers as Tunable Spacers. *Sci. Rep.* **2015**, *5*, 7779.
- (107) Lee, K.; Park, J.; Kwon, S. J.; Kwon, H.; Kyhm, J.; Kwak, K.; Jang, H. S.; Kim, S. Y.; Han, J. S.; Lee, S.; et al. Simultaneous Enhancement of Upconversion and Downshifting Luminescence via Plasmonic Structure. *Nano Lett.* **2015**, *15*, 2491–2497.
- (108) Chen, X.; Zhou, D.; Xu, W.; Zhu, J.; Pan, G.; Yin, Z.; Wang, H.; Zhu, Y.; Shaobo, C.; Song, H. Fabrication of Au-Ag Nanocage @ NaYF₄ @ NaYF₄:Yb,Er Core- Shell Hybrid and Its Tunable Upconversion Enhancement. *Sci. Rep.* **2017**, *7*, 41079.
- (109) Liu, Y.; Xia, Y.; Jiang, Y.; Zhang, M.; Sun, W.; Zhao, X.-Z. Coupling Effects of Au-Decorated Core-Shell β -NaYF₄:Er/Yb@SiO₂ Microprisms in

References

- Dye-Sensitized Solar Cells: Plasmon Resonance versus Upconversion. *Electrochim. Acta* **2015**, *180*, 394–400.
- (110) Chen, G.; Ding, C.; Wu, E.; Wu, B.; Chen, P.; Ci, X.; Liu, Y.; Qiu, J.; Zeng, H. Tip-Enhanced Upconversion Luminescence in Yb³⁺–Er³⁺ Codoped NaYF₄ Nanocrystals. *J. Phys. Chem. C* **2015**, *119*, 22604–22610.
- (111) Shang, Y.; Hao, S.; Yang, C.; Chen, G. Enhancing Solar Cell Efficiency Using Photon Upconversion Materials. *Nanomaterials* **2015**, *5*, 1782–1809.
- (112) Shan, G. Bin; Assaouidi, H.; Demopoulos, G. P. Enhanced Performance of Dye-Sensitized Solar Cells by Utilization of an External, Bifunctional Layer Consisting of Uniform β -NaYF₄:Er³⁺Yb³⁺ Nanoplatelets. *ACS Appl. Mater. Interfaces* **2011**, *3*, 3239–3243.
- (113) Liu, X.; Wang, Y.; Li, X.; Yi, Z.; Deng, R.; Liang, L.; Xie, X.; Loong, D. T. B.; Song, S.; Fan, D.; et al. Binary Temporal Upconversion Codes of Mn²⁺-Activated Nanoparticles for Multilevel Anti-Counterfeiting. *Nat. Commun.* **2017**, *8*, 889.
- (114) Liu, J.; Rijckaert, H.; Zeng, M.; Haustraete, K.; Laforce, B.; Vincze, L.; Driessche, I. Van; Kaczmarek, A. M.; Van Deun, R. Simultaneously Excited Downshifting/Upconversion Luminescence from Lanthanide-Doped Core/Shell Fluoride Nanoparticles for Multimode Anticounterfeiting. *Adv. Funct. Mater.* **2018**, *28*, 1707365.
- (115) Zijlmans, H. J. M. A. A.; Bonnet, J.; Burton, J.; Kardos, K.; Vail, T.; Niedbala, R. S.; Tanke, H. J. Detection of Cell and Tissue Surface Antigens Using Up-Converting Phosphors: A New Reporter Technology. *Anal. Biochem.* **1999**, *267*, 30–36.
- (116) Corstjens, P.; Zuiderwijk, M.; Brink, A.; Li, S.; Feindt, H.; Niedbala, R. S.; Tanke, H. Use of Up-Converting Phosphor Reporters in Lateral-Flow Assays to Detect Specific Nucleic Acid Sequences: A Rapid, Sensitive DNA Test to Identify Human Papillomavirus Type 16 Infection. *Clin. Chem.* **2001**, *47*, 1885–1893.
- (117) Kuningas, K.; Rantanen, T.; Ukonaho, T.; Lövgren, T.; Soukka, T. Homogeneous Assay Technology Based on Upconverting Phosphors. *Anal. Chem.* **2005**, *77*, 7348–7355.
- (118) Wang, L.; Yan, R.; Huo, Z.; Wang, L.; Zeng, J.; Bao, J.; Wang, X.; Peng, Q.; Li, Y. Fluorescence Resonant Energy Transfer Biosensor Based on Upconversion-Luminescent Nanoparticles. *Angew. Chemie - Int. Ed.* **2005**, *44*, 6054–6057.
- (119) Hemmilä, I. Fluoroimmunoassays and Immunofluorometric Assays. *Clin. Chem.* **1985**, *31*, 359–370.
- (120) Arppe, R.; Mattsson, L.; Korpi, K.; Blom, S.; Wang, Q.; Riuttamäki, T.; Soukka, T. Homogeneous Assay for Whole Blood Folate Using Photon Upconversion. *Anal. Chem.* **2015**, *87*, 1782–1788.
- (121) Kuningas, K.; Pääkkilä, H.; Ukonaho, T.; Rantanen, T.; Timo, L.; Tero, S. Upconversion Fluorescence Enables Homogeneous Immunoassay in Whole Blood. *Clin. Chem.* **2007**, *53*, 145–146.
- (122) Wang, Y.; Shen, P.; Li, C.; Wang, Y.; Liu, Z. Upconversion Fluorescence Resonance Energy Transfer Based Biosensor for Ultrasensitive Detection of Matrix Metalloproteinase-2 in Blood. *Anal. Chem.* **2012**, *84*, 1466–1473.
- (123) Wang, Y.; Liu, K.; Liu, X.; Gregorkiewicz, T.; Kong, X.; Aalders, M. C. G.; Buma, W. J.; Zhang, H. Critical Shell Thickness of Core/Shell Upconversion Luminescence NanoplatforM for FRET Application. *J. Phys. Chem. Lett.* **2011**, *2*, 2083–2088.
- (124) Drees, C.; Raj, A. N.; Kurre, R.; Busch, K. B.; Haase, M.; Piehler, J. Engineered Upconversion Nanoparticles for Resolving Protein Interactions inside Living Cells. *Angew. Chemie - Int. Ed.* **2016**, *55*,

References

- 11668–11672.
- (125) Lahtinen, S.; Wang, Q.; Soukka, T. Long-Lifetime Luminescent Europium(III) Complex as an Acceptor in an Upconversion Resonance Energy Transfer Based Homogeneous Assay. *Anal. Chem.* **2016**, *88*, 653–658.
- (126) Sirkka, N.; Lyytikäinen, A.; Savukoski, T.; Soukka, T. Upconverting Nanophosphors as Reporters in a Highly Sensitive Heterogeneous Immunoassay for Cardiac Troponin I. *Anal. Chim. Acta* **2016**, *925*, 82–87.
- (127) Hlaváček, A.; Farka, Z.; Hübner, M.; Horňáková, V.; Němeček, D.; Niessner, R.; Skládal, P.; Knopp, D.; Gorris, H. H. Competitive Upconversion-Linked Immunosorbent Assay for the Sensitive Detection of Diclofenac. *Anal. Chem.* **2016**, *88*, 6011–6017.
- (128) Ylihärsilä, M.; Harju, E.; Arppe, R.; Hattara, L.; Hölsä, J.; Saviranta, P.; Soukka, T.; Waris, M. Genotyping of Clinically Relevant Human Adenoviruses by Array-in-Well Hybridization Assay. *Clin. Microbiol. Infect.* **2013**, *19*, 551–557.
- (129) Jeyachandran, Y. L.; Mielczarski, J. A.; Mielczarski, E.; Rai, B. Efficiency of Blocking of Non-Specific Interaction of Different Proteins by BSA Adsorbed on Hydrophobic and Hydrophilic Surfaces. *J. Colloid Interface Sci.* **2010**, *341*, 136–142.
- (130) Bentzen, E. L.; Tomlinson, I. D.; Mason, J.; Gresch, P.; Warnement, M. R.; Wright, D.; Sanders-bush, E.; Blakely, R.; Rosenthal, S. J. Surface Modification To Reduce Nonspecific Binding of Quantum Dots in Live Cell Assays. *Bioconjug. Chem.* **2005**, *16*, 1488–1494.
- (131) Lahtinen, S.; Lyytikäinen, A.; Sirkka, N.; Päckilä, H.; Soukka, T. Improving the Sensitivity of Immunoassays by Reducing Non-Specific Binding of Poly(Acrylic Acid) Coated Upconverting Nanoparticles by Adding Free Poly(Acrylic Acid). *Microchim. Acta* **2018**, *185*, 220.
- (132) Corstjens, P. L. A. M.; Dood, C. J. De; Priest, J. W.; Tanke, H. J.; Handali, S. Feasibility of a Lateral Flow Test for Neurocysticercosis Using Novel Up-Converting Nanomaterials and a Lightweight Strip Analyzer. *PLoS Negl. Trop D.* **2014**, *8*, e2944.
- (133) Hua, F.; Zhang, P.; Zhang, F.; Zhao, Y.; Li, C.; Sun, C.; Wang, X.; Yang, R.; Wang, C.; Yu, A.; et al. Development and Evaluation of an Up-Converting Phosphor Technology-Based Lateral Flow Assay for Rapid Detection of Francisella Tularensis. *Sci. Rep.* **2015**, *5*, 17178.
- (134) Juntunen, E.; Salminen, T.; Talha, S. M.; Martiskainen, I.; Soukka, T.; Pettersson, K.; Waris, M. Lateral Flow Immunoassay With Upconverting Nanoparticle-Based Detection for Indirect Measurement of Interferon Response by the Level of MxA. *J. Med. Virol.* **2017**, *89*, 598–605.
- (135) Ylihärsilä, M.; Valta, T.; Karp, M.; Hattara, L.; Harju, E.; Hölsä, J.; Saviranta, P.; Waris, M.; Soukka, T. Oligonucleotide Array-in-Well Platform for Detection and Genotyping Human Adenoviruses by Utilizing Upconverting Phosphor Label Technology. *Anal. Chem.* **2011**, *83*, 1456–1461.
- (136) Kale, V.; Päckilä, H.; Vainio, J.; Ahomaa, A.; Sirkka, N.; Lyytikäinen, A.; Talha, S. M.; Kutsaya, A.; Waris, M.; Julkunen, I.; et al. Spectrally and Spatially Multiplexed Serological Array-in-Well Assay Utilizing Two-Color Upconversion Luminescence Imaging. *Anal. Chem.* **2016**, *88*, 4470–4477.
- (137) Zhang, F.; Shi, Q.; Zhang, Y.; Shi, Y.; Ding, K.; Zhao, D.; Stucky, G. D. Fluorescence Upconversion Microbarcodes for Multiplexed Biological Detection: Nucleic Acid Encoding. *Adv. Mater.* **2011**, *23*, 3775–3779.
- (138) Soukka, T.; Kuningas, K.; Rantanen,

References

- T.; Haaslahti, V.; Lövgren, T. Photochemical Characterization of Up-Converting Inorganic Lanthanide Phosphors as Potential Labels. *J. Fluoresc.* **2005**, *15*, 513–528.
- (139) Sedlmeier, A.; Hlaváček, A.; Birner, L.; Mickert, M. J.; Muhr, V.; Hirsch, T.; Corstjens, P. L. A. M.; Tanke, H. J.; Soukka, T.; Gorris, H. H. Highly Sensitive Laser Scanning of Photon-Upconverting Nanoparticles on a Macroscopic Scale. *Anal. Chem.* **2016**, *88*, 1835–1841.
- (140) UpconTM, Kaivogen oy, Labrox oy, <http://www.upcon.fi> 18.6.2018.
- (141) Sun, L.; Peng, H.; Stich, M. I. J.; Achatz, D.; Wolfbeis, O. S. PH Sensor Based on Upconverting Luminescent Lanthanide Nanorods. *Chem. Commun.* **2009**, *0*, 5000–5002.
- (142) Mader, H. S.; Wolfbeis, O. S. Optical Ammonia Sensor Based on Upconverting Luminescent Nanoparticles. *Anal. Chem.* **2010**, *82*, 5002–5004.
- (143) Esipova, T. V.; Ye, X.; Collins, J. E.; Sakadžić, S.; Mandeville, E. T.; Murray, C. B.; Vinogradov, S. A. Dendritic Upconverting Nanoparticles Enable in Vivo Multiphoton Microscopy with Low-Power Continuous Wave Sources. *PNAS* **2012**, *109*, 20826–20831.
- (144) Arppe, R.; Näreoja, T.; Sami, N.; Mattson, L.; Koho, S.; Rosenholm, J. M.; Soukka, T.; Schäferling, M. Photon Upconversion Sensitized Nanoprobes for Sensing and Imaging of pH Sensing and Imaging of pH. *Nanoscale* **2014**, *6*, 6837–6843.
- (145) Näreoja, T.; Deguchi, T.; Chirist, S.; Peltomaa, R.; Prabhakar, N.; Fazeli, E.; Perälä, N.; Rosenholm, J. M.; Arppe, R.; Soukka, T. Ratiometric Sensing and Imaging of Intracellular pH Using Polyethylenimine-Coated Photon Upconversion Nanoprobes. *Anal. Chem.* **2017**, *89*, 1501–1508.
- (146) Li, C.; Zuo, J.; Zhang, L.; Chang, Y.; Zhang, Y.; Tu, L.; Liu, X.; Xue, B.; Li, Q.; Zhao, H.; et al. Accurate Quantitative Sensing of Intracellular pH Based on Self-Ratiometric Upconversion Luminescent Nanoprobe. *Sci. Rep.* **2016**, *6*, 38617.
- (147) Li, H.; Dong, H.; Yu, M.; Liu, C.; Li, Z.; Wei, L.; Sun, L.; Zhang, H. NIR Ratiometric Luminescence Detection of pH Fluctuation in Living Cells with Hemicyanine Derivative-Assembled Upconversion Nanophosphors. *Anal. Chem.* **2017**, *89*, 8863–5569.
- (148) Liu, X.; Zhang, S.; Wei, X.; Yang, T.; Chen, M.; Wang, J. A Novel “Modularized” Optical Sensor for pH Monitoring in Biological Matrixes. *Biosens. Bioelectron.* **2018**, *109*, 150–155.
- (149) Liu, Q.; Peng, J.; Li, F. High-Efficiency Upconversion Luminescent Sensing and Bioimaging of Hg(II) by Chromophoric Ruthenium Complex-Assembled Nanophosphors. *ACS Nano* **2011**, *5*, 8040–8048.
- (150) Li, S.; Zhao, X.; Tao, D.; Zhang, W.; Zhang, K. Hg(II)-Activated Emission “Turn-on” Chemosensors Excited by up-Conversion Nanocrystals: Synthesis, Characterization and Sensing Performance. *Spectrochim. Acta Part A Mol. Biomol. Spectrosc.* **2015**, *137*, 581–588.
- (151) Song, K.; Mo, J.; Lu, C. Hg(II) Sensing Platforms with Improved Photostability: The Combination of Rhodamine Derived Chemosensors and up-conversion Nanocrystals. *Spectrochim. Acta Part A Mol. Biomol. Spectrosc.* **2017**, *179*, 125–131.
- (152) Chatti, M.; Sarkar, S.; Mahalingam, V. Glutathione-Modified Ultrasmall Ce³⁺ and Tb³⁺-Doped SrF₂ Nanocrystals for Fluorescent Determination of Hg(II) and Pb(II) Ions. *Microchim. Acta* **2016**, *186*, 133–140.
- (153) Liu, Y.; Ouyang, Q.; Li, H.; Chen, M.; Zhang, Z.; Chen, Q. Turn-On Fluorescence Sensor for Hg²⁺ in Food Based on FRET between Aptamers-Functionalized Upconversion

References

- Nanoparticles and Gold Nanoparticles. *J. Agric. Food Chem.* **2018**, *66*, 6188–6195.
- (154) Liu, Y.; Chen, M.; Cao, T.; Sun, Y.; Li, C.; Liu, Q.; Yang, T.; Yao, L.; Feng, W.; Li, F. A Cyanine-Modified Nanosystem for *in Vivo* Upconversion Luminescence Bioimaging of Methylmercury. *J. Am. Chem. Soc.* **2013**, *135*, 9869–9876.
- (155) Yan, Q.; Chen, Z.; Xue, S.; Han, X.; Lin, Z.; Zhang, S.; Shi, G.; Zhang, M. Lanthanide-Doped Nanoparticles Encountering Porphyrin Hydrate: Boosting a Dual-Mode Optical Nanokit for Cu²⁺ Sensing. *Sensors Actuators B Chem.* **2018**, *268*, 108–114.
- (156) Huang, X.; Wang, L.; Zhang, X.; Yin, X.; Bin, N.; Zhong, F.; Liu, Y.; Cai, Q. Dye-Assembled Nanocomposites for Rapid Upconversion Luminescence Sensing of Cu²⁺. *Sensors Actuators B Chem.* **2017**, *248*, 1–8.
- (157) Chen, J.; Chen, H.; Zhou, C.; Xu, J.; Yuan, F.; Wang, L. An Efficient Upconversion Luminescence Energy Transfer System for Determination of Trace Amounts of Nitrite Based on NaYF₄:Yb³⁺,Er³⁺ as Donor. *Anal. Chim. Acta* **2012**, *713*, 111–114.
- (158) Wang, N.; Yu, X.; Zhang, K.; Mirkin, C. A.; Li, J. Upconversion Nanoprobes for the Ratiometric Luminescent Sensing of Nitric Oxide. *J. Am. Chem. Soc.* **2017**, *139*, 12354–12357.
- (159) Liu, J.; Liu, Y.; Liu, Q.; Li, C.; Sun, L.; Li, F. Iridium(III) Complex-Coated Nanosystem for Ratiometric Upconversion Luminescence Bioimaging of Cyanide Anions. **2011**, *1*, 15276–15279.
- (160) Deng, R.; Xie, X.; Vendrell, M.; Chang, Y.; Liu, X. Intracellular Glutathione Detection Using MnO₂ - Nanosheet-Modified Upconversion Nanoparticles. *J. Am. Chem. Soc.* **2011**, *135*, 20168–20171.
- (161) Liu, L.; Wang, S.; Zhao, B.; Pei, P.; Fan, Y.; Li, X.; Zhang, F. Er³⁺ Sensitized 1530 nm to 1180 nm Second Near-Infrared Window Upconversion Nanocrystals for *In Vivo* Biosensing. *Angew. Chemie - Int. Ed.* **2018**, *57*, 7518–7522.
- (162) Wang, X.; Kong, X.; Yu, Y.; Sun, Y.; Zhang, H. Effect of Annealing on Upconversion Luminescence of ZnO:Er³⁺ Nanocrystals and High Thermal Sensitivity. *J. Phys. Chem. C* **2007**, *111*, 15119–15124.
- (163) Vetrone, F.; Naccache, R.; Zamarro, A.; Juarranz, A.; Fuente, D.; Sanz-rodri, F.; Maestro, L. M.; Marti, E.; Jaque, D.; Capobianco, J. A. Temperature Sensing Using Fluorescent Nanothermometers. *ACS Nano* **2010**, *4*, 3254–3258.
- (164) Balabhadra, S.; Debasu, M. L.; Brites, C. D. S.; Ferreira, R. A. S.; Carlos, D. Upconverting Nanoparticles Working As Primary Thermometers In Different Media. *J. Phys. Chem. C* **2017**, *121*, 13962–13968.
- (165) Marciniak, L.; Prorok, K.; Bednarkiewicz, A. Size Dependent Sensitivity of Yb³⁺,Er³⁺ Upconverting Luminescent Nano-Thermometers. *J. Mater. Chem. C* **2017**, *5*, 7890–7897.
- (166) Hyppänen, I.; Perälä, N.; Arppe, R.; Schäferling, M.; Tero, S. Environmental and Excitation Power Effects on the Ratiometric Upconversion Luminescence Based Temperature Sensing Using Nanocrystalline NaYF₄:Yb³⁺,Er³⁺. *ChemPhysChem* **2017**, *18*, 692–701.
- (167) Zhou, S.; Jiang, S.; Wei, X.; Chen, Y.; Duan, C.; Yin, M. Optical Thermometry Based on Upconversion Luminescence in Yb³⁺/Ho³⁺ Co-Doped NaLuF₄. *J. Alloys Compd.* **2014**, *588*, 654–657.
- (168) Wei, J.; Wei, H.; Ji, X.; Ren, S.; Dai, H.; Cheng, L.; Zhang, J. Temperature Sensing Behavior in Yb³⁺-Tb³⁺ and Eu³⁺ Doped Ca₂Gd₈(SiO₄)₆O₂ Phosphors Based on Upconversion and Downshifting Luminescence. *J. Mater. Sci. Mater. Electron.* **2018**, *29*, 12061–12066.

References

- (169) Tong, L.; Li, X.; Hua, R.; Cheng, L.; Sun, J.; Zhang, J. Optical Temperature Sensing Properties of Yb³⁺/Tm³⁺ Co-Doped NaLuF₄ Crystals. *Curr. Appl. Phys.* **2017**, *17*, 999–1004.
- (170) Balabhadra, S.; Debasu, M. L.; Brites, C. D. S.; Nunes, L. A. O.; Rocha, J.; Bettinelli, M.; Carlos, L. D. Boosting the Sensitivity of Nd³⁺-Based Luminescent Nanothermometers. *Nanoscale* **2015**, *7*, 17261–17267.
- (171) Kostiv, U.; Kotelnikov, I.; Proks, V.; Šlouf, M.; Kučka, J.; Engstová, H.; Ježek, P.; Horák, D. RGDS- and TAT-Conjugated Upconversion of NaYF₄:Yb³⁺/Er³⁺&SiO₂ Nanoparticles: In Vitro Human Epithelioid Cervix Carcinoma Cellular Uptake, Imaging, and Targeting. *ACS Appl. Mater. Interfaces* **2016**, *8*, 20422–20431.
- (172) Liang, L.; Care, A.; Zhang, R.; Lu, Y.; Packer, N. H.; Sunna, A.; Qian, Y.; Zvyagin, A. V. Facile Assembly of Functional Upconversion Nanoparticles for Targeted Cancer Imaging and Photodynamic Therapy. *ACS Appl. Mater. Interfaces* **2016**, *8*, 11945–11953.
- (173) Xue, Z.; Yi, Z.; Li, X.; Li, Y.; Jiang, M.; Liu, H.; Zeng, S. Upconversion Optical/Magnetic Resonance Imaging-Guided Small Tumor Detection and *in Vivo* Tri-Modal Bioimaging Based on High-Performance Luminescent Nanorods. *Biomaterials* **2017**, *115*, 90–103.
- (174) Zhou, J.; Zhu, X.; Chen, M.; Sun, Y.; Li, F. Water-Stable NaLuF₄-Based Upconversion Nanophosphors with Long-Term Validity for Multimodal Lymphatic Imaging. *Biomaterials* **2012**, *33*, 6201–6210.
- (175) Rao, L.; Bu, L.-L.; Cai, B.; Xu, J.-H.; Li, A.; Zhang, W.-F.; Sun, Z.-J.; Guo, S.-S.; Liu, W.; Wang, T.-H.; et al. Cancer Cell Membrane-Coated Upconversion Nanoprobes for Highly Specific Tumor Imaging. *Adv. Mater.* **2016**, *28*, 3460–3466.
- (176) Zeng, S.; Wang, H.; Lu, W.; Yi, Z.; Rao, L.; Liu, H.; Hao, J. Dual-Modal Upconversion Fluorescent/X-Ray Imaging Using Ligand-Free Hexagonal Phase NaLuF₄:Gd/Yb/Er Nanorods for Blood Vessel Visualization. *Biomaterials* **2014**, *35*, 2934–2941.
- (177) Chen, X.; Tang, Y.; Liu, A.; Zhu, Y.; Gao, D.; Yang, Y.; Sun, J.; Fan, H.; Zhang, X. NIR-to-Red Upconversion Nanoparticles with Minimized Heating Effect for Synchronous Multidrug Resistance Tumor Imaging and Therapy. *ACS Appl. Mater. Interfaces* **2018**, *10*, 14378–14388.
- (178) Hong, A.; Kim, Y.; Lee, T. S.; Kim, S.; Lee, K.; Kim, G.; Jang, H. S. Intense Red-Emitting Upconversion Nanophosphors (800 nm-Driven) with a Core/Double-Shell Structure for Dual-Modal Upconversion Luminescence and Magnetic Resonance *in Vivo* Imaging Applications. *ACS Appl. Mater. Interfaces* **2018**, *10*, 12331–12340.
- (179) Rocha, U.; Kumar, K. U.; Jacinto, C.; Villa, I.; Sanz-Rodríguez, F.; de la Cruz, M. del C. I.; Juarranz, A.; Carrasco, E.; Veggel, F. C. J. M. Van; Bovero, E.; et al. Neodymium-Doped LaF₃ Nanoparticles for Fluorescence Bioimaging in the Second Biological Window. *Small* **2014**, *10*, 1141–1154.
- (180) Ding, F.; Zhan, Y.; Lu, X.; Sun, Y. Recent Advances in Near-Infrared II Fluorophores for Multifunctional Biomedical Imaging. *Chem. Sci.* **2018**, *9*, 4370–4380.
- (181) Naczynski, D. J.; Tan, M. C.; Zevon, M.; Wall, B.; Kohl, J.; Kulesa, A.; Chen, S.; Roth, C. M.; Riman, R. E.; Moghe, P. V. Rare-Earth-Doped Biological Composites as *in Vivo* Shortwave Infrared Reporters. *Nat. Commun.* **2013**, *4*, 2199.
- (182) Zhong, Y.; Ma, Z.; Zhu, S.; Yue, J.; Zhang, M.; Antaris, A. L.; Yuan, J.; Cui, R.; Wan, H.; Zhou, Y.; et al. Boosting the Down-Shifting Luminescence of Rare-Earth Nanocrystals for Biological Imaging beyond 1500 nm. *Nat. Commun.* **2017**,

References

- 8, 737.
- (183) Zhou, J.; Lu, Z.; Shan, G.; Wang, S.; Liao, Y. Gadolinium Complex and Phosphorescent Probe-Modified NaDyF₄ Nanorods for T₁- and T₂-Weighted MRI/CT/Phosphorescence Multimodality Imaging. *Biomaterials* **2014**, *35*, 368–377.
- (184) Dash, A.; Blasiak, B.; Tomanek, B.; Veggel, F. C. J. M. Van. Validation of Inner, Second, and Outer Sphere Contributions to T₁ and T₂ Relaxation in Gd³⁺-Based Nanoparticles Using Eu³⁺ Lifetime Decay as a Probe. *J. Phys. Chem. C* **2018**, *122*, 11557–11569.
- (185) Liu, Q.; Sun, Y.; Li, C.; Zhou, J.; Li, C.; Yang, T.; Zhang, X.; Yi, T.; Wu, D.; Li, F. ¹⁸F-Labeled Magnetic-Upconversion Nanophosphors via Rare-Earth Cation-Assisted Ligand Assembly. *ACS Nano* **2011**, *5*, 3146–3157.
- (186) Sun, Y.; Yu, M.; Liang, S.; Zhang, Y.; Li, C.; Mou, T.; Yang, W.; Zhang, X.; Li, B.; Huang, C.; et al. Fluorine-18 Labeled Rare-Earth Nanoparticles for Positron Emission Tomography (PET) Imaging of Sentinel Lymph Node. *Biomaterials* **2011**, *32*, 2999–3007.
- (187) Yang, Y.; Sun, Y.; Cao, T.; Peng, J.; Liu, Y.; Wu, Y.; Feng, W.; Zhang, Y.; Li, F. Hydrothermal Synthesis of NaLuF₄:¹⁵³Sm,Yb,Tm Nanoparticles and Their Application in Dual-Modality Upconversion Luminescence and SPECT Bioimaging. *Biomaterials* **2013**, *34*, 774–783.
- (188) Lee, N.; Choi, S. H.; Hyeon, T. Nano-Sized CT Contrast Agents. *Adv. Mater.* **2013**, *25*, 2641–2660.
- (189) Liu, Z.; Li, Z.; Liu, J.; Gu, S.; Yuan, Q.; Ren, J.; Qu, X. Long-Circulating Er³⁺-Doped Yb₂O₃ up-Conversion Nanoparticle as an in Vivo X-Ray CT Imaging Contrast Agent. *Biomaterials* **2012**, *33*, 6748–6757.
- (190) Ma, J.; Huang, P.; He, M.; Pan, L.; Zhou, Z.; Feng, L.; Gao, G.; Cui, D. Folic Acid-Conjugated LaF₃:Yb,Tm@SiO₂ Nanoprobes for Targeting Dual-Modality Imaging of Upconversion Luminescence and X-ray Computed Tomography. *J. Phys. Chem. B* **2012**, *116*, 14062–14070.
- (191) Chen, C.; Liu, J.; Chen, Y.; Li, C.; Liu, X.; Huang, H.; Liang, C.; Lou, Y.; Shi, Z.; Feng, S. Sub-10 Nm Sr₂LuF₇:Yb/Er@Sr₂GdF₇@SrF₂ Up-Conversion Nanocrystals for Up-Conversion Luminescence–Magnetic Resonance–Computed Tomography Trimodal Bioimaging. *ACS Appl. Mater. Interfaces* **2017**, *9*, 5748–5756.
- (192) Zhang, P.; He, Y.; Liu, J.; Feng, J.; Sun, Z.; Lei, P.; Yan, Q.; Zhang, H. Core-shell BaYbF₅:Tm@BaGdF₅:Yb,Tm Nanocrystals for in Vivo Trimodal UCL/CT/MR Imaging. *RSC Adv.* **2016**, *6*, 14283–14289.
- (193) Cui, X.; Mathe, D.; Kovács, N.; Horváth, I.; Jauregui-Osoro, M.; Rosales, R. T. M. De; Mullen, G. E. D.; Wong, W.; Yan, Y.; Krüger, D.; et al. Synthesis, Characterization, and Application of Core-Shell Co_{0.16}Fe_{2.84}O₄@NaYF₄(Yb, Er) and Fe₃O₄@NaYF₄(Yb, Tm) Nanoparticle as Trimodal (MRI, PET/SPECT, and Optical) Imaging Age. *Bioconjug. Chem.* **2016**, *27*, 319–328.
- (194) Sun, Y.; Zhu, X.; Peng, J.; Li, F. Core-Shell Lanthanide Upconversion Nanophosphors as Four-Modal Probes for Tumor Angiogenesis Imaging. *ACS Nano* **2013**, *7*, 11290–11300.
- (195) Gnach, A.; Lipinski, T.; Bednarkiewicz, A.; Capobianco, J. A. Upconverting Nanoparticles: Assessing the Toxicity. *Chem. Soc. Rev.* **2015**, *44*, 1561–1584.
- (196) Sun, Y.; Feng, W.; Yang, P.; Huang, C.; Li, F. The Biosafety of Lanthanide Upconversion Nanomaterials. *Chem Soc Rev* **2015**, *44*, 1509–1525.
- (197) Xiong, L.; Yang, T.; Yang, Y.; Xu, C.; Li, F. Long-Term in Vivo Biodistribution Imaging and Toxicity of Polyacrylic Acid-Coated

References

- Upconversion Nanophosphors. *Biomaterials* **2010**, *31*, 7078–7085.
- (198) Abdul, R. J.; Zhang, Y. Biocompatibility of Silica Coated NaYF₄ Upconversion Fluorescent Nanocrystals. *Biomaterials* **2008**, *29*, 4122–4128.
- (199) Das, G. K.; Stark, D. T.; Kennedy, I. M. Potential Toxicity of Up-Converting Nanoparticles Encapsulated with a Bilayer Formed by Ligand Attraction. *Langmuir* **2014**, *30*, 8167–8176.
- (200) Bogdan, N.; Vetrone, F.; Ozin, G. A.; Capobianco, J. A. Synthesis of Ligand-Free Colloidally Stable Water Dispersible Brightly Luminescent Lanthanide-Doped Upconverting Nanoparticles. *Nano Lett.* **2011**, *11*, 835–840.
- (201) Chen, Z.; Chen, H.; Hu, H.; Yu, M.; Li, F.; Zhang, Q.; Zhou, Z.; Yi, T.; Huang, C. Versatile Synthesis Strategy for Carboxylic Acid - Functionalized Upconverting Nanophosphors as Biological Labels. *J. Am. Chem. Soc.* **2008**, *130*, 3023–3029.
- (202) Naccache, R.; Vetrone, F.; Mahalingam, V.; Cuccia, L. A.; Capobianco, J. A. Controlled Synthesis and Water Dispersibility of Hexagonal Phase NaGdF₄:Ho³⁺/Yb³⁺ Nanoparticles. *Chem. Mater.* **2009**, *21*, 717–723.
- (203) Zhou, B. H.; Xu, C.; Sun, W.; Yan, C. Clean and Flexible Modification Strategy for Carboxyl/Aldehyde-Functionalized Upconversion Nanoparticles and Their Optical Applications. *Adv. Funct. Mater.* **2009**, *19*, 3892–3900.
- (204) Nsubuga, A.; Sgarzi, M.; Zarschler, K.; Kubeil, M.; Hübner, R.; Steudtner, R.; Graham, B.; Joshi, T.; Stephan, H. Facile Preparation of Multifunctionalisable ‘Stealth’ Upconverting Nanoparticles for Biomedical Applications. *Dalt. Trans.* **2018**, *47*, 8595–8604.
- (205) Cao, T.; Yang, T.; Gao, Y.; Yang, Y.; Hu, H.; Li, F. Water-Soluble NaYF₄:Yb/Er Upconversion Nanophosphors: Synthesis, Characteristics and Application in Bioimaging. *Inorg. Chem. Commun.* **2010**, *13*, 392–394.
- (206) Liu, Q.; Sun, Y.; Yang, T.; Feng, W.; Li, C.; Li, F. Sub-10 nm Hexagonal Lanthanide-Doped NaLuF₄ Upconversion Nanocrystals for Sensitive Bioimaging in Vivo. *J. Am. Chem. Soc.* **2011**, *133*, 17122–17125.
- (207) Jin, J.; Gu, Y.; Man, C. W.; Cheng, J.; Xu, Z.; Zhang, Y. Polymer-Coated NaYF₄:Yb³⁺, Er³⁺ Upconversion Nanoparticles for Charge-Dependent Cellular Imaging. *ACS Nano* **2011**, No. 10, 7838–7847.
- (208) Beyazit, S.; Ambrosini, S.; Marchyk, N.; Palo, E.; Kale, V.; Soukka, T.; Tse Sum Bui, B.; Haupt, K. Versatile Synthetic Strategy for Coating Upconverting Nanoparticles with Polymer Shells through Localized Photopolymerization by Using the Particles as Internal Light Sources. *Angew. Chemie - Int. Ed.* **2014**, *53*, 8919–8923.
- (209) Bagheri, A.; Arandiyani, H.; Adnan, N. N. M.; Boyer, C.; Lim, M. Controlled Direct Growth of Polymer Shell on Upconversion Nanoparticle Surface via Visible Light Regulated Polymerization. *Macromolecules* **2017**, *50*, 7137–7147.
- (210) Duong, H. T. T.; Chen, Y.; Tawfik, S. A.; Wen, S.; Parviz, M.; Shimoni, O.; Jin, D. Systematic Investigation of Functional Ligands for Colloidal Stable Upconversion Nanoparticles. *RSC Adv.* **2018**, *8*, 4842–4849.
- (211) Kamimura, M.; Miyamoto, D.; Saito, Y.; Soga, K.; Nagasaki, Y. Design of Poly(Ethylene Glycol)/Streptavidin Coimmobilized Upconversion Nanophosphors and Their Application to Fluorescence Biolabeling. *Langmuir* **2018**, *24*, 8864–8870.
- (212) Wu, S.; Han, G.; Milliron, D. J.; Aloni, S.; Altoe, V.; Talapin, D. V.; Cohen, B. E.; Schuck, P. J. Non-Blinking and

References

- Photostable Upconverted Luminescence from Single Lanthanide-Doped Nanocrystals. *PNAS* **2009**, *106*, 10917–10921.
- (213) Yi, G.; Chow, G. Water-Soluble NaYF₄Yb,Er(Tm)/NaYF₄/Polymer Core Shell/Shell Nanoparticles with Significant Enhancement of Upconversion Fluorescence. *Chem. Mater.* **2007**, *19*, 341–343.
- (214) Sedlmeier, A.; Gorris, H. H. Surface Modification and Characterization of Photon-Upconverting Nanoparticles for Bioanalytical Applications. *Chem. Soc. Rev.* **2014**, *44*, 1526–1560.
- (215) Nann, T.; Mulvaney, P. Single Quantum Dots in Spherical Silica Particles. *Angew. Chemie - Int. Ed.* **2004**, *43*, 5393–5396.
- (216) Li, Z.; Zhang, Y.; Jiang, S. Multicolor Core/Shell-Structured Upconversion Fluorescent Nanoparticles. *Adv. Mater.* **2008**, *20*, 4765–4769.
- (217) Idris, N. M.; Li, Z.; Ye, L.; Sim, E. K. W.; Mahendran, R.; Ho, P. C.; Zhang, Y. Tracking Transplanted Cells in Live Animal Using Upconversion Fluorescent Nanoparticles. *Biomaterials* **2009**, *30*, 5104–5113.
- (218) Stober, W.; Fink, A.; Bohn, E. Controlled Growth of Monodisperse Silica Spheres in the Micron Size Range. *J. Colloid Interface Sci.* **1968**, *26*, 62–69.
- (219) Darbandi, M.; Nann, T. One-Pot Synthesis of YF₃@silica Core/Shell Nanoparticles. *Chem. Commun.* **2006**, No. 7, 776–778.
- (220) Decher, G. Fuzzy Nanoassemblies: Toward Layered Polymeric Multicomposites. *Science* **1997**, *277*, 1232–1237.
- (221) Borges, J.; Mano, J. F. Molecular Interactions Driving the Layer-by-Layer Assembly of Multilayers. *Chem. Rev.* **2014**, *114*, 8883–8942.
- (222) De Villiers, M. M.; Otto, D. P.; Strydom, S. J.; Lvov, Y. M. Introduction to Nanocoatings Produced by Layer-by-Layer (LbL) Self-Assembly. *Adv. Drug Deliv. Rev.* **2011**, *63*, 701–715.
- (223) Schneider, G.; Decher, G. Functional Core/Shell Nanoparticles via Layer-by-Layer Assembly. Investigation of the Experimental Parameters for Controlling Particle Aggregation and for Enhancing Dispersion Stability. *Langmuir* **2008**, *24*, 1778–1789.
- (224) Yan, Y.; Bjo, M.; Caruso, F. Assembly of Layer-by-Layer Particles and Their Interactions with Biological Systems. *Chem. Mater.* **2014**, *26*, 452–460.
- (225) Wang, Y.; Angelatos, A. S.; Caruso, F. Template Synthesis of Nanostructured Materials via Layer-by-Layer Assembly. *Chem. Mater.* **2008**, *20*, 848–858.
- (226) Dubas, S. T.; Schlenoff, J. B. Factors Controlling the Growth of Polyelectrolyte Multilayers. *Macromolecules* **1999**, *32*, 8153–8160.
- (227) Salomäki, M.; Kankare, J. Specific Anion Effect in Swelling of Polyelectrolyte Multilayers. *Macromolecules* **2008**, *41*, 4423–4428.
- (228) Li, L.; Wu, P.; Hwang, K.; Lu, Y. An Exceptionally Simple Strategy for DNA-Functionalized Up-Conversion Nanoparticles as Biocompatible Agents for Nanoassembly, DNA Delivery, and Imaging. *J. Am. Chem. Soc.* **2013**, *135*, 2411–2414.
- (229) Xiong, L.; Chen, Z.; Yu, M.; Li, F.; Liu, C.; Huang, C. Synthesis, Characterization, and *in Vivo* Targeted Imaging of Amine-Functionalized Rare-Earth up-converting Nanophosphors. *Biomaterials* **2009**, *30*, 5592–5600.
- (230) Zhang, P.; Steelant, W.; Kumar, M.; Scholfield, M. Versatile Photosensitizers for Photodynamic Therapy at Infrared Excitation. *J. Am. Chem. Soc.* **2007**, *129*, 4526–4527.
- (231) Xiong, L.; Chen, Z.; Tian, Q.; Cao, T.; Xu, C.; Li, F. High Contrast Upconversion Luminescence Targeted

References

- Imaging in Vivo Using Peptide-Labeled Nanophosphors. *Anal. Chem.* **2009**, *81*, 8687–8694.
- (232) Conde, J.; Dias, J. T.; Grazú, V.; Moros, M.; Baptista, P. V; de la Fuente, J. M. Revisiting 30 Years of Biofunctionalization and Surface Chemistry of Inorganic Nanoparticles for Nanomedicine. *Front. Chem.* **2014**, *2*, 1–27.
- (233) Mei, Q.; Jing, H.; Li, Y.; Yisibashaer, W.; Chen, J.; Nan, B. Biosensors and Bioelectronics Smartphone Based Visual and Quantitative Assays on Upconversion Paper Sensor. *Biosens. Bioelectron.* **2016**, *75*, 427–432.
- (234) Harris, J. J.; Derose, P. M.; Bruening, M. L. Synthesis of Passivating, Nylon-Like Coatings through Cross-Linking of Ultrathin Polyelectrolyte Films. *J. Am. Chem. Soc.* **1999**, *121*, 1978–1979.
- (235) Balachandra, A. M.; Dai, J.; Bruening, M. L. Enhancing the Anion-Transport Selectivity of Multilayer Polyelectrolyte Membranes by Templating with Cu²⁺. *Macromolecules* **2002**, *35*, 3171–3178.
- (236) Rasband, W. S. *U.S. ImageJ, National Institutes of Health, Bethesda, Maryland, USA, (Http://Imagej.Nih.Gov/Ij/), 1997-2016.*
- (237) PCPDFWIN v 1.30, Powder Diffraction File, 1997, International Centre for Diffraction Data, Entries 06-0342 (Cubic NaYF₄) and 28-1192 (Hexagonal Na(Y_{0.57}Yb_{0.39}Er_{0.04})F₄). International Centre for Diffraction Data.
- (238) Klug, H. P.; Alexander, L. E. *X-Ray Powder Diffraction Procedures*; Wiley: New York, 1959.
- (239) Voss, B.; Haase, M. Intrinsic Focusing of the Particle Size Distribution in Colloids Containing Nanocrystals of Two Different Crystal Phases. *ACS Nano* **2013**, *7*, 11242–11254.
- (240) Workman, Jerry, J. *The Handbook of Organic Compounds: NIR, IR, Raman and UV-VIS Spectra Featuring Polymers and Surfactants*; Academic Press, 2001.
- (241) Li, H.; Zheng, H.; Tong, W.; Gao, C. Non-Covalent Assembly of Poly (Allylamine Hydrochloride)/ Triethylamine Microcapsules with Ionic Strength-Responsiveness and Auto-Fluorescence. *J. Colloid Interface Sci.* **2017**, *496*, 228–234.
- (242) Liu, B.; Chen, Y.; Li, C.; He, F.; Hou, Z.; Huang, S.; Zhu, H.; Chen, X.; Lin, J. Poly(Acrylic Acid) Modification of Nd³⁺-Sensitized Upconversion Nanophosphors for Highly Efficient UCL Imaging and pH-Responsive Drug Delivery. *Adv. Funct. Mater.* **2015**, *25*, 4717–4729.

Annales Universitatis Turkuensis



**UNIVERSITY
OF TURKU**

ISBN 978-951-29-7572-3 (PRINT)
ISBN 978-951-29-7573-0 (PDF)
ISSN 0082-7002 (Print)
ISSN 2343-3175 (Online)